

THE MELTING BEHAVIOR OF COAL ORE COMPOSITES

**THE MELTING BEHAVIOR
OF
COAL ORE COMPOSITES**

By

MAHSHID FATHI ROODSARI, BSc.

A Thesis

Submitted to the School of Graduate Studies

in Partial Fulfilment of the Requirments

for the Degree

Master of Science

McMaster University

© Copyright by Mahshid Fathi Roodsari, April 2005

MASTER OF SCIENCE (2005)

materials Science and Engineering

McMaster University

Hamilton, Ontario

TITLE: The Melting Behavior of Coal Ore Composites

AUTHOR: Mahshid Fathi Roodsari, B.Sc.

SUPERVISOR: Dr. David Conochie

NUMBER OF PAGES: ii-x, 143

Abstract

A breakthrough ironmaking technology (ITmk3) produces iron separated from slag by heating coal-iron ore composite pellets at temperatures as low as 1325C in about 10 minutes. Other researchers have studied the melting behavior, including the formation of a dense metallic shell separated from slag but the mechanism has not been yet fully understood. Exploring this knowledge gap was targeted in this study.

The initial experiments included heating of composite samples at different temperatures and time intervals. Three coal types and two coal/ore ratios were investigated. By these experiments slag free iron production at low temperature and short time was confirmed. Coal type and coal/ore ratio were found to have a significant effect on melting behavior.

The main series of experiments focused on the effect of slag composition mainly CaO and SiO₂, slag content and reaction time on the melting behavior. The main characterization methods included Optical Microscopy, Energy Dispersed X-ray Analysis (EDX), and simultaneous Differential Thermal Analysis (DTA), and Thermo Gravimetric Analysis (TGA).

Despite most of the obtained results being qualitative, this study was successful in exploring some of the most important reasons behind the melting behavior of coal ore composites.

It was revealed that the formation of a low melting point slag containing FeO in the core of the pellet and its exudation to the iron shell is responsible for the formation of a dense metallic shell. Densification of iron occurs by reduction of FeO in slag. The rate and extent of reduction is related to the physical properties of slag that in turn is influenced by slag composition. More basic slags tend to have higher rate of FeO reduction in slag. By reduction of FeO in slag, the interfacial tension of the remaining slag with iron increases and slag is separated from iron.

Acknowledgment

I would like to acknowledge my supervisor Dr. David Conochie for all his assistance and helpful suggestions during the course of my thesis and all his support over the last two years.

This thesis would have never been completed without financial support; therefore I would like to acknowledge the Steel Research Center.

I would like to thank the Materials Science and Engineering department and its staff whom all work very hard to keep things running, especially Ed McCaffery, John Rodda, Doug Colley, Chris Butcher, Betty Petro and Jane Mah .

I would also like to thank my husband Mansoor Barati for all the support he has given me through the time of my project and writing thesis.

Table of Contents

Terminology.....	1
Chapter 1	2
1.Literature Review	2
1.1. Introduction.....	2
1.2. Blast Furnace Ironmaking Technologies.....	3
1.3. Direct Ironmaking Technologies.....	3
1.3.1. Natural Gas Based Processes	3
1.3.2. Coal based direct reduction.....	5
1.4. Melting Behavior of Coal Ore Composite Pellets.....	13
1.4.1. Reaction sequence from single pellet studies	13
1.4.2. Result of reduction and melting test	14
1.4.3. Modeling of the melting behavior	18
1.5. Melting steps	20
1.5.1. Formation of initial dispersed liquid slag from ash and gangue minerals	20
1.5.2. Liquid penetration	21
1.5.3. Change in inter-particle distances	22
1.5.4. Rearrangement.....	23
1.5.5. Pore size change.....	24
1.5.6. Contact increase.....	25
1.5.7. Formation of slag percolations (coalescence of dispersed liquid slag).....	25
1.6. Carburization and local melting of iron.....	27
1.6.1. Carburizing by CO gas	30
1.6.2. Iron melting by solid carbon	30
1.6.3. Carbon Content Analysis in Iron Rod	33
1.7. Densification of Iron.....	35
1.8. Melting of iron shell and phase separation	37
1.8.1. Settling of Iron Droplets through Slag (Application of Stock's Equation) ..	37
1.8.2. Surface Tension of Liquid Iron	38
1.8.3. Surface Tension of Slag	38
1.8.4. Interfacial Tension between Iron and slag.....	39
1.9. Review Summary	40
1.10. Focusing questions	41
 Chapter 2	 42
2.Initial Experiments – Effects of Furnace Temperature, Time, Coal Type and Coal/Ore ratio	42
2.1. Assumptions.....	42
2.2. Material Preparation.....	43
2.3. Screening	44
2.4. Mixing	44
2.4.1. Mixing Method	44
2.4.2. Final Samples	45
2.5. Heating	45

2.6.	Cooling	46
2.7.	Characterization	47
2.7.1.	Primary Characterization-(Weighing- Optical Scanning).....	47
2.7.2.	Mounting and Cutting	50
2.7.3.	Observation of Microstructure	51
2.8.	Conclusions from Initial Experiments	56
2.9.	Sources of Error	58
Chapter 3		60
3.	Main Series of Experiments: Changing Slag Composition and Content.....	60
3.1.	Experiments	60
3.1.1.	SiO ₂ -CaO- Al ₂ O ₃ System.....	61
3.1.2.	Material Preparation	62
3.1.3.	Mixing	66
3.1.4.	Pellet Making	66
3.1.5.	Heating	67
3.1.6.	Cooling.....	67
Chapter 4		68
4.	Results and Discussion	68
4.1.	Low Magnification Microscopy	68
4.1.1.	Higher Magnification Optical Microscopy-Polished Cross Section and Energy Dispersed X-Ray Analysis (EDX)	74
4.2.	Leco Carbon and Sulfur Analysis.....	110
4.3.	Simultaneous Differential Thermal Analysis and Thermo -Gravimetric Analysis (DTA/TGA)	112
4.4.	Current Understanding.....	124
Chapter 5		126
5.	Summary, Conclusions and Recommendations for future work	126
5.1.	Summary	126
5.2.	Conclusions.....	127
5.3.	Recommendations for future work	129
6.	References	130
7.	Appendix	132

List of Figures

Figure 1- 1-Schematic diagram of the Midrex process	4
Figure 1- 2- Schematic diagram of the HYL process	4
Figure 1- 3.SL/RN process flow	5
Figure 1- 4-Inmetco Process Flow.....	6
Figure 1- 5-Fastmet process flow diagram	7
Figure 1- 6- Increasing productivity and energy efficiency in Lu's process	8
Figure 1- 7-IDI Process Flow Diagram	9
Figure 1- 8.Corex Process Flow Diagram	10
Figure 1- 9.Hismelt Process flow diagram	11
Figure 1- 10.Itmk3 Process Flow Diagram	12
Figure 1- 11- schematic view of the apparatus	13
Figure 1-12-Cross sectional view of the reduced pellets	14
Figure 1- 13-Overall and cross- sectional view of time sampled pellets	15
Figure 1- 14-Variation of pellet temperature and CO, CO ₂	16
Figure 1- 15-Reduction degree and pellet temperature	17
Figure 1- 16-species and phases as a function of time in the pellet	19
Figure 1-17- Pellet microstructure schematic – initial formation of liquid slag from gangue and ash and remaining unreduced particles of FeO	21
Figure 1- 18-A schematic diagram of penetration and fragmentation of particles	22
Figure 1- 19-Rearrangement of particles in the presence of liquid	23
Figure 1- 20-Schematics showing the rearrangement and fragmentation in a simple model of one type particles and one type liquid	24
Figure 1- 21-Geometry of the particle and liquid menisci around a spherical pore	25
Figure 1- 22-Schematic of the coalescence of liquid droplets	26
Figure 1- 23-A schematic of the pellet microstructure with slag percolations	27
Figure 1- 24-A schematic of the pellet microstructure with a network of slag	27
Figure 1- 25- Fe-C phase diagram, Itmk3 operational area is shown	28
Figure 1- 26-A schematic of the microscopic pellet structure after melting of iron	28
Figure 1- 27-Variation of carbon content in metallic iron and whole of the pellet	29
Figure 1- 28-Calculated liquid phase thickness of iron by graphite (Murakami et al) and 100% CO gas (Sasaki et al) as a function of carburization time	31
Figure 1- 29-Schematic sketch of sample set up	32
Figure 1- 30-Image of sample observed using laser microscope	32
Figure 1- 31-Schematic sketch of carburization mechanism during the smelting reduction	33
Figure 1- 32-Line analysis of carbon concentration distribution in iron rod determined by EPMA	34
Figure 1- 33-The three mechanisms of shape accommodation and neck growth during the intermediate stage (a) contact flattening, (b) dissolution of fine grains, and (c) solid-state diffusion [21]	35
Figure 1- 34-A schematic diagram of the steps leading to grain growth by coalescence	36
Figure 1- 35- The contrast between an isolated and skeletal microstructure	36

Figure 2- 1- (a)Schematic of the box furnace , (b) The alumina crucibles on zirconia tray ,(b) graphite caps on the alumina crucibles with semi-porous zirconia tray	45
Figure 2- 2-Cooling the samples	46
Figure 2- 3- Scanned images, samples with sub-stoichiometric coal at 1300C.....	48
Figure 2- 4- Scanned images, samples with stoichiometric coal at 1300C.....	49
Figure 2- 5- Scanned images, samples with stoichiometric coal at 1350C.....	50
Figure 2- 6- Samples reacted at 1300C for 5min	52
Figure 2- 7- Samples reacted at 1300C for 10min	53
Figure 2- 8- Samples reacted at 1300C for 15min	54
Figure 2- 9-Schematic showing the times required for the furnace to reach the desired temperature	58
Figure 3- 1-Ternary phase diagram of $\text{SiO}_2\text{-CaO-Al}_2\text{O}_3$ system	62
Figure 3- 2-Particle Size distribution of iron ore	63
Figure 3- 3-Cumulative probability diagram of iron ore particle size	63
Figure 3- 4- Particle size distribution of coal	64
Figure 3- 5- Cumulative probability diagram of coal particle size.....	64
Figure 4- 1-Images of pellets heated for 6 minutes.....	69
Figure 4- 2- Images of pellets heated for 8 minutes.....	70
Figure 4- 3- Images of pellets heated for 10 minutes.....	71
Figure 4- 4- Cross sectional images of pellets heated for 8 minutes	72
Figure 4- 5- Cross sectional images of pellets heated for 10 minutes	73
Figure 4- 6- Pellet 1, $\text{CaO/SiO}_2=0.13$, 5Wt% gangue and ash, 1310C, 8min	75
Figure 4- 7- Pellet 1, $\text{CaO/SiO}_2=0.13$, 5Wt% gangue and ash, 1310C, 10min.....	76
Figure 4- 8-Pellet 2, $\text{CaO/SiO}_2=0.55$, 5Wt% gangue and ash, 1310C, 8min	78
Figure 4- 9- Pellet 2, $\text{CaO/SiO}_2=0.55$, 5Wt% gangue and ash, 1310C, 10min.....	80
Figure 4- 10-Schematic showing the steps occurring in pellet 2.....	82
Figure 4- 11- Pellet 3, $\text{CaO/SiO}_2=1.42$, 5Wt% gangue and ash, 1310C, 8min.....	83
Figure 4- 12- Pellet 3, $\text{CaO/SiO}_2=1.42$, 5Wt% gangue and ash, 1310C, 10min.....	85
Figure 4- 13-General effect of variation in FeO content of various $\text{Al}_2\text{O}_3\text{-CaO-SiO}_2$ slags on the interfacial tension with Iron	86
Figure 4- 14-Viscosities of $\text{CaO-SiO}_2\text{-Al}_2\text{O}_3\text{-FeO}$ slag systems	87
Figure 4- 15-Schematic showing the steps occurring in pellet 3.....	87
Figure 4- 16- Pellet 4, $\text{CaO/SiO}_2=0.13$, 10Wt% gangue and ash, 1310C, 8min.....	88
Figure 4- 17- Pellet 4, $\text{CaO/SiO}_2=0.13$, 10Wt% gangue and ash, 1310C, 10min.....	89
Figure 4- 18- Interfacial tension between liquid iron and liquid $\text{CaO-Al}_2\text{O}_3\text{-SiO}_2$ slags (mN/m) at 1550C,	90
Figure 4- 19- Schematic showing the steps occurring in pellet 4.....	91
Figure 4- 20-Pellet 5, $\text{CaO/SiO}_2=0.55$, 10Wt% gangue and ash, 1310C, 8min.....	92
Figure 4- 21- Pellet 5, $\text{CaO/SiO}_2=0.55$, 10Wt% gangue and ash, 1310C, 10min.....	94
Figure 4- 22-Pellet 6, $\text{CaO/SiO}_2=1.42$, 10Wt% gangue and ash, 1310C, 8min.....	95
Figure 4- 23- Pellet 6, $\text{CaO/SiO}_2=1.42$, 10Wt% gangue and ash, 1310C, 10min.....	97
Figure 4- 24-Pellet 7, $\text{CaO/SiO}_2=0.13$, 15Wt% gangue and ash, 1310C, 8min.....	98
Figure 4- 25- Pellet 7, $\text{CaO/SiO}_2=0.13$, 15Wt% gangue and ash, 1310C, 10min.....	100
Figure 4- 26-Pellet 8, $\text{CaO/SiO}_2=0.55$, 15Wt% gangue and ash, 1310C, 8min.....	101
Figure 4- 27- Pellet 8, $\text{CaO/SiO}_2=0.55$, 15Wt% gangue and ash, 1310C, 10min.....	103
Figure 4- 28-Pellet 9, $\text{CaO/SiO}_2=1.42$, 15Wt% gangue and ash, 1310C, 8min.....	104

Figure 4- 29- Pellet 9, CaO/SiO ₂ =1.42, 15Wt% gangue and ash, 1310C, 10min.....	105
Figure 4- 30- Pellet 10, CaO/SiO ₂ =0.26, 3.17Wt% gangue and ash, 1310C, 8min.....	107
Figure 4- 31- Pellet 10, CaO/SiO ₂ =0.26, 3.17Wt% gangue and ash, 1310C, 10min.....	108
Figure 4- 32- Carbon content of the final melted iron versus CaO/SiO ₂ in slag for different slag weight percents.....	110
Figure 4- 33- Sulfur content of the final melted iron versus CaO/SiO ₂ in slag for different slag weight percents.....	111
Figure 4- 34- Superimposed DTA curves of samples 1-3 and 10 as reference.....	113
Figure 4- 35- Superimposed DTA curves of samples 4-6 and 10 as reference.....	113
Figure 4- 36- Superimposed DTA curves of samples 7-9 and 10 as reference.....	114
Figure 4- 37- Simultaneous DTA/TGA curves for sample 1 with CaO/SiO ₂ =0.13, 5Wt% Slag.....	115
Figure 4- 38- Simultaneous DTA/TGA curves for sample 2 with CaO/SiO ₂ =0.55, 5Wt% gangue and ash.....	116
Figure 4- 39- Simultaneous DTA/TGA curves for sample 3 with CaO/SiO ₂ =1.42, 5Wt% gangue and ash.....	117
Figure 4- 40- Simultaneous DTA/TGA curves for sample 4 with CaO/SiO ₂ =0.13, 10Wt% gangue and ash.....	117
Figure 4- 41- Simultaneous DTA/TGA curves for sample 5 with CaO/SiO ₂ =0.55, 10Wt% gangue and ash.....	118
Figure 4- 42- Simultaneous DTA/TGA curves for sample 6 with CaO/SiO ₂ =1.42, 10Wt% gangue and ash.....	118
Figure 4- 43- Simultaneous DTA/TGA curves for sample 7 with CaO/SiO ₂ =0.13, 15Wt% gangue and ash.....	119
Figure 4- 44- Simultaneous DTA/TGA curves for sample 8 with CaO/SiO ₂ =0.55, 15Wt% gangue and ash.....	119
Figure 4- 45- Simultaneous DTA/TGA curves for sample 9 with CaO/SiO ₂ =1.42, 15Wt% gangue and ash.....	120
Figure 4- 46- Simultaneous DTA/TGA curves for no addition sample with CaO/SiO ₂ =0.26, 15Wt% gangue and ash.....	120
Figure 4- 47- TGA curves for samples 1-3.....	121
Figure 4- 48- TGA curves for samples 4-6.....	122
Figure 4- 49- TGA curves for samples 7-9.....	122
Figure 7- 1- Scanned images, samples with sub-stoichiometric coal at 1325C.....	134
Figure 7- 2- Scanned images, samples with sub-stoichiometric coal at 1350C.....	135
Figure 7- 3- Scanned images, samples with stoichiometric coal at 1325C.....	136
Figure 7- 4- Samples reacted at 1325C for 5 min.....	137
Figure 7- 5- Samples reacted at 1325C for 10 min.....	138
Figure 7- 6- Samples reacted at 1325C for 15 min.....	139
Figure 7- 7- Samples reacted at 1350C for 5 min.....	140
Figure 7- 8- Samples reacted at 1350C for 10 min.....	141
Figure 7- 9- Samples reacted at 1350C for 15 min.....	142

List of Tables

Table 1- 1- the chemical compositions of raw materials (wt %)[2]	14
Table 2- 1-Ore chemical composition as analyzed in Actalabs No.m10703	43
Table 2- 2-Coal composition	43
Table 2- 3-Ash composition in weight percent	44
Table 3- 1- Change in melting points of the CaO-SiO ₂ -15%Al ₂ O ₃ slag with composition	61
Table 3- 2-Composition of ore used in the second series of experiments	63
Table 3- 3-Composition of Coal A used	64
Table 3- 4-Composition of Ash in coal used in the second series of experiments.....	65
Table 3- 5- Composition of composite gangue and ash.....	65
Table 3- 6- Samples	65
Table 3- 7-The weight percent of additional CaO, SiO ₂ and Al ₂ O ₃ in 100grams of each composite batch	66
Table 4- 1-EDX-results, pellet 1, CaO/SiO ₂ =0.13, 5Wt% gangue and ash, heated at 1310C	77
Table 4- 2- EDX-results –pellet 2, CaO/SiO ₂ =0.55, 5Wt% gangue and ash, heated at 1310C.....	81
Table 4- 3- EDX-results - pellet 3, CaO/SiO ₂ =1.42, 5Wt% gangue and ash, heated at 1310C.....	84
Table 4- 4- EDX-results - pellet 4, CaO/SiO ₂ =0.13, 10Wt% gangue and ash, heated at 1310C...	89
Table 4- 5- EDX-results - pellet 5, CaO/SiO ₂ =0.55, 10Wt% gangue and ash, heated at 1310C...	93
Table 4- 6- EDX-results - pellet 6, CaO/SiO ₂ =1.42, 10Wt% gangue and ash, heated at 1310C...	96
Table 4- 7- EDX-results - pellet 7, CaO/SiO ₂ =0.13, 15Wt% gangue and ash, heated at 1310C...	99
Table 4- 8- EDX-results - pellet 8, CaO/SiO ₂ =0.55, 15Wt% gangue and ash, heated at 1310C.	102
Table 4- 9- EDX-results - pellet 9, CaO/SiO ₂ =1.42, 15Wt% gangue and ash, heated at 1310C.	106
Table 4- 10- EDX-results - pellet 10 (with no addition), CaO/SiO ₂ =0.26, 3.17Wt% gangue and ash, heated at 1310C	109
Table 4- 11-The results of leco Carbon and Sulfur test on the final melted iron	110
Table 4- 12-Relative reduction degrees at 1200C, 1300C and 1400C derived from DTA/TGA curves	123
Table 7- 1-Experimental conditions, final weights in primary series of experiments.....	132
Table 7- 2- Experimental conditions, final weights, second series of experiments.....	143

Terminology

The system being studied is a complex multiphase system involving solids, liquids and gas. The following terms have been used to assist with the descriptions of the microstructures and processes occurring during melting.

Dispersed particles or drops: Separated particles or droplets, distributed in different regions of the pellet (May be minerals, metal or slag).

Filament: An irregular elongated body of liquid or liquid with solid which may form a planar or a three dimensional network.

Continuous structure: A liquid or liquid with solid or solid phase in which a closed path can connect all parts of it.

Coalesced slag: A big droplet of liquid slag formed after smaller dispersed slag droplets join to reduce the total surface energy

Densification: Decrease of the porosity from the microstructure

Exudation: The escape of liquid droplets from inside to the surface of a partly densified structure which may be liquid, liquid with solid or solid.

Percolation: Drainage of a liquid through bed of solids, leading to phase separation and coalescence. Percolation may also be driven by gas flow.

Slag melting: Initial melting of ash particles and gangue minerals from solid particles to liquid slag which may occur over a range of temperatures

Iron melting: Transformation of solid reduced iron particles to liquid iron:

- By temperature increase to melting point
- By carbon diffusion which lowers the melting point

Chapter 1

1. Literature Review

1.1. Introduction

The Blast Furnace is currently the most important process as it is a productive and efficient ironmaking method. However blast furnace is being replaced by new processes with lower capital and operational costs which are able to use more available raw materials and meet the new environmental regulations.

In addition, there is a growing demand for Direct Reduced Iron (DRI) in recent years as demand for high quality steel has increased and electric furnace ironmaking has remarkably developed. There are various direct ironmaking technologies which are generally divided in natural gas based and coal based processes. As there are abundant sources of coal in North American countries, coal based processes are preferred to natural gas based processes in these countries.

The most efficient coal based direct ironmaking processes are those reducing coal iron ore composite pellets in a Rotary Hearth Furnace (RHF) such as Fastmet with very fast reduction rate and low fuel ratio.[1]

In a recent development of the Fastmet process (ITmk3 process), it was found that by a slight increase in the reduction temperature to (1325-1350C), pellets were melted by the time of reduction completion, slag was separated from iron and clean iron nuggets produced in a very short period of about 10 minutes.[2]

Such clean and dense iron would be an excellent feed for the Electric Arc Furnace as there would be less need for slag melting and energy and flux consumptions would also be decreased. [2]

The mechanism of coal ore composite reduction has been studied up to now by many researchers, including Lu and co-workers([3] to[8]), but the mechanism of melting of coal ore composite pellets and iron-slag separation during rapid heating has not yet been revealed and is the focus of this study. It is considered that the molten slag among carbon and reduced iron is strongly influential in the phenomena.

1.2. Blast Furnace Ironmaking Technologies

The Blast furnace is a tall shaft type furnace which is based on moving bed reduction. Iron ore pellets or sinter, coke and flux are charged into the top of the shaft. A blast of heated air is introduced at the bottom of the shaft which burns the injected fuel and most of the coke to produce heat and reducing gas that removes the oxygen from the ore. The total process time is 6-8 hours.

In the Blast furnace softening and melting of ferrous burden occurs in the cohesive zone. The liquid phase formed, can lead to loss in permeability and increase the pressure drop. Therefore in most blast furnaces, before the burden reaches the softening temperature, most reduction has taken place. After melting, the reduced iron runs down to the bottom of the hearth. The slag which forms from flux and gangue melts and accumulates on top of the liquid iron in the hearth [9].

1.3. Direct Ironmaking Technologies

Direct ironmaking methods can be divided into two major groups; gas based ironmaking and coal based ironmaking.

1.3.1. Natural Gas Based Processes

Natural gas based processes rely on natural gas as their reductant. The most famous natural gas processes are Midrex and HYL. These processes are beneficial only in areas with abundant sources of natural gas.

- Midrex

The Midrex process uses a shaft furnace in which iron oxide is charged in form of pellets or lump. In the shaft of the furnace while the iron ore burden moves down the furnace, counter flow gases including H_2 and CO reduce the iron ore and convert it to sponge iron. The DRI produced can be sent for Hot Briquette Iron (HBI) production or directly to the Electric Arc Furnace (EAF) for melting.

It should be noted that the amounts of SiO_2 and Al_2O_3 should be very low in the charge from iron ore feed to the end of DRI production as the ore gangue is not separated prior to steelmaking.[9]

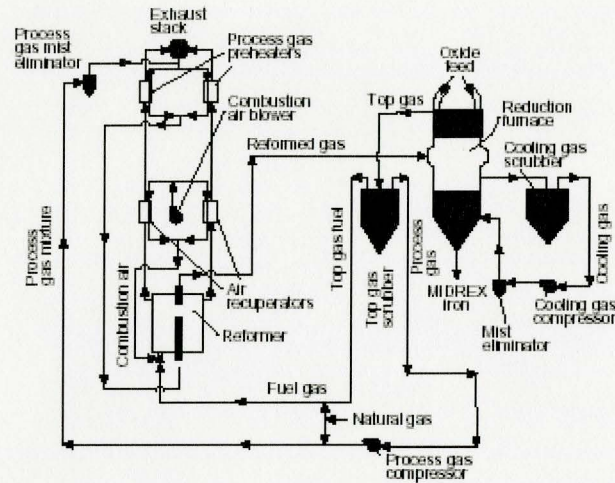


Figure 1- 1-Schematic diagram of the Midrex process [9]

- HYL

The HYL process is based on a moving bed shaft furnace which reduces iron ore pellets and lump ore. The reducing gas is generated in a reformer which reforms natural gas to H₂ and CO. The products of this process can be in the form of DRI or HBI. Hot discharged DRI can be transported directly to an Electric Arc Furnace for melting and production of so-called HYTemp iron.

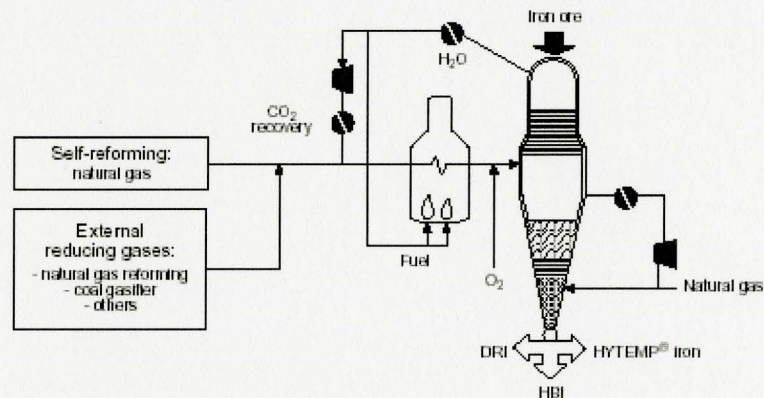


Figure 1- 2- Schematic diagram of the HYL process [9]

1.3.2. Coal based direct reduction

Due to limited and localized supply of natural gas, gas-based processes are not suitable for most North American regions. The other option is coal based DRI processes, because an abundant supply of coal is available world wide. Therefore various coal based processes have recently been developed. In this section some of the more important coal based ironmaking processes are described.

- SL/RN

The SL/RN process is a kiln based process. The ore feed can be in the form of iron ore, lump or pellet and the reductant used is non-coking coal. Typical retention times are around 10 hours. The kiln has two regions; preheat and reduction. In the preheat region, the charge is heated to about 1000C, then devolatilization and reduction to wustite takes place. Part of the gas is burned in the freeboard above the bed by the air injected into the kiln. The heat generated is transferred to the charge by radiation and conductive heat transfer from the lining which is first exposed to the flame and heated before contacting the charge. The charge then enters the reduction zone where the temperature is about 1000C to 1100C [9].

Softening and melting of the ore gangue and coal ash in the kiln is very problematic and form accretions, rings and blockages. For this reason the melting point of gangue in ore and ash in coal should be relatively high. This in turn would mean higher flux and energy consumption in steelmaking.

The DRI produced in the SL/RN process can be transferred to Electric Arc Furnace, (EAF), for melting.

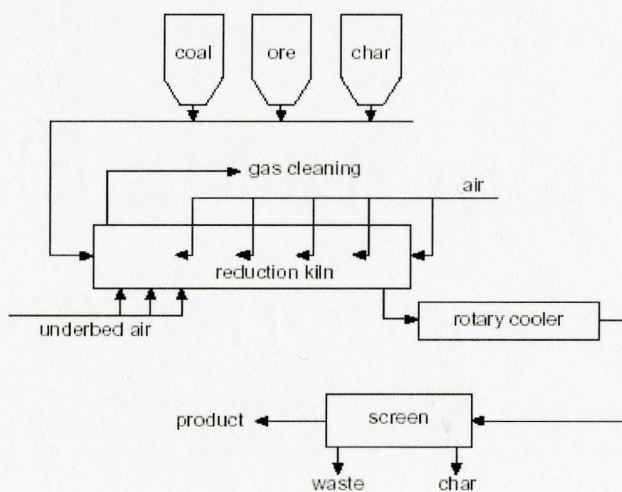


Figure 1- 3.SL/RN process flow [9]

- Inmetco Process

Inmetco process uses a Rotary Hearth Furnace (RHF). The raw materials for the Inmetco furnace is in the form of disk pellets which are made of iron ore fines, waste iron bearing materials and coal.

The pellets which are distributed on the RHF are heated for 10-15 minutes to produce sponge direct reduced iron. The furnace consists of the heating and reduction zones. The products DRI can be cooled or directly charged to the EAF for melting. [10]

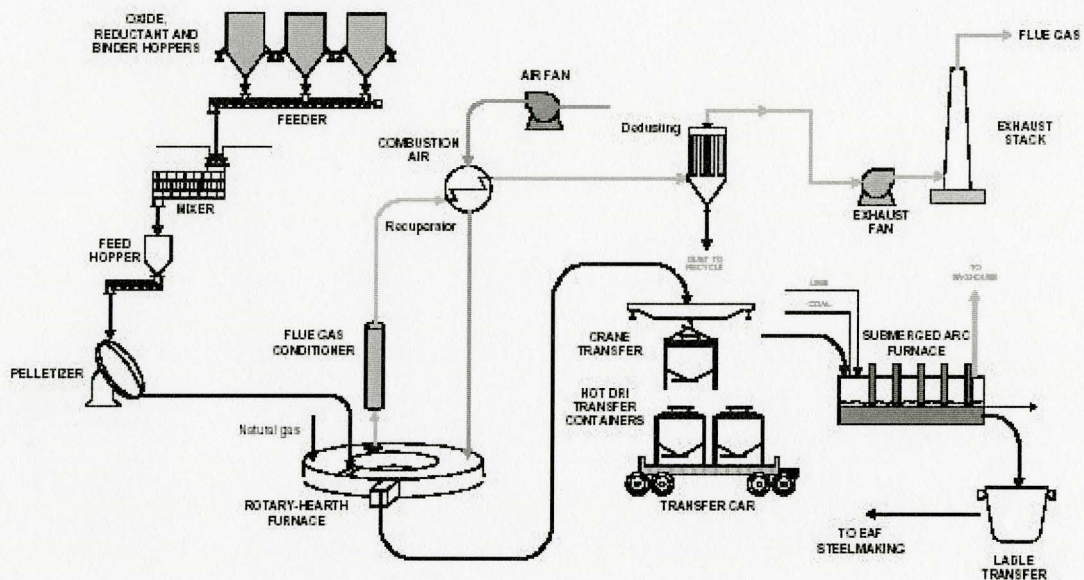


Figure 1-4-Inmetco Process Flow [10]

- Fastmet Process

The Fastmet Process has been developed by the Midrex Company. This process is a solid carbon based reduction technology.

First, pellets are made from concentrates and reductant. Pellets are dried before being sent to the RHF. The materials are then fed to the furnace in a single layer. Inside the furnace, pellets are heated by radiation from RHF zone temperatures of more than 1300C, and iron oxide is reduced to metallic iron.

Residence time on the hearth is typically 6 -10 minutes. During this time, 85 - 95 percent of the iron oxide is converted to metallic iron [1], [9], [11].

The final product, direct reduced iron, can be hot briquetted, be cooled or directly charged to the specially designed electric furnace (FASTMELT) for melting.

The melter is required to remove ironmaking slag before the metal is sent to steelmaking. If only small quantities of DRI are to be used in steelmaking, then the melting step may be omitted.

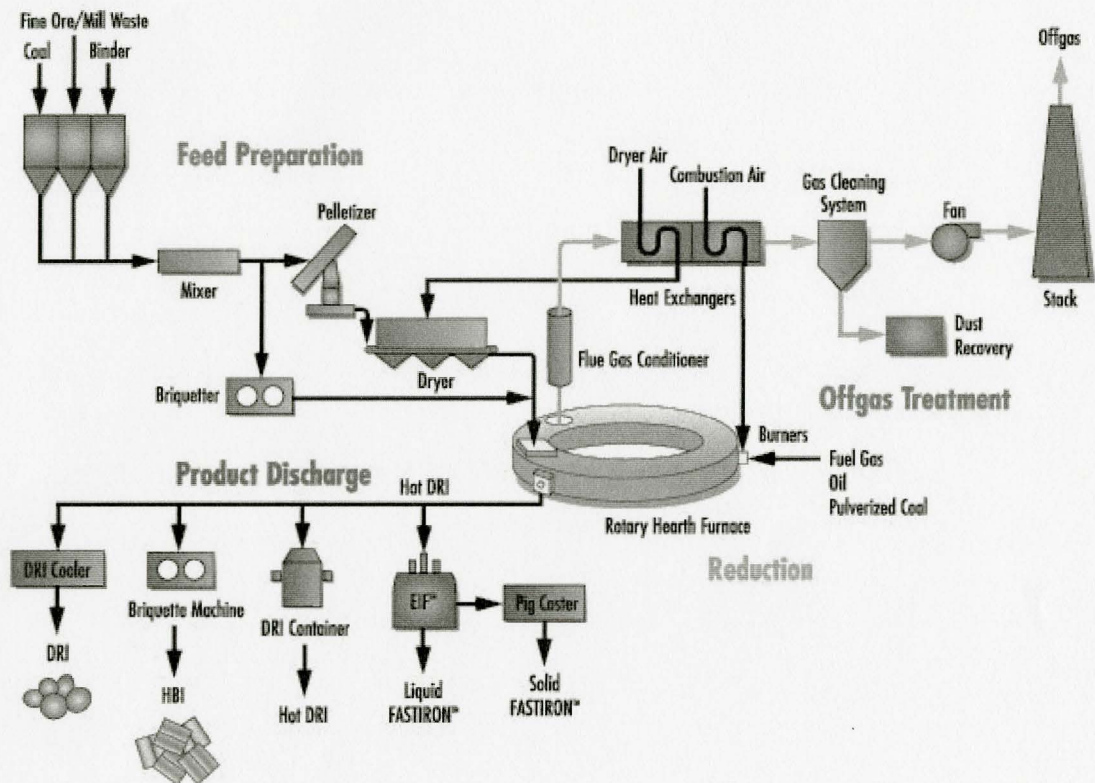


Figure 1- 5-Fastmet process flow diagram [12]

- Dr. Lu's process

The reduction kinetics in coal iron ore composites is dependent on temperature as strongly endothermic reactions are involved in the process. In addition, newly reduced iron can be re-oxidized by CO_2 and/or O_2 in high temperature combustion flame. An optimal combination of reaction temperature, volatile matter in coal, and bed height leads to the creation of a self-protective atmosphere and effective heat transfer outside and inside the bed of agglomerates to produce high quality DRI from iron ore/coal mixtures. Dr.Lu has developed an RHF based ironmaking method using coal ore composites which

uses a high CO/CO_2 ratio (greater than 2) and multiple layers of pellets instead of 1 layer which presents increased energy efficiency and productivity of RHF. Preliminary tests of the project have been carried out at McMaster University and pilot plant work was completed in Italy. The product is sponge reduced iron which can be melted in the Electric Arc Furnace. [13]

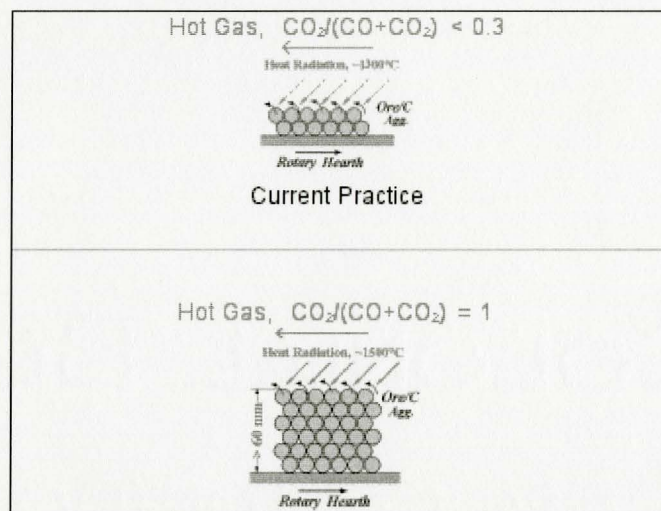


Figure 1- 6- Increasing productivity and energy efficiency in Lu's process [13]

- Iron Dynamics

The Iron Dynamics process is a rotary hearth furnace type process and uses natural gas for heat generation. In this process, first raw materials including iron ore and coal are ground and pelletized. Pellets after being dried are distributed onto the furnace hearth. Temperature, gas flow and gas composition are controlled to properly heat, reduce and protect the pellets. The DRI produced falls into the slag layer of the Submerged Arc Furnace (SAF) by gravity where smelting takes place. [10], [14]

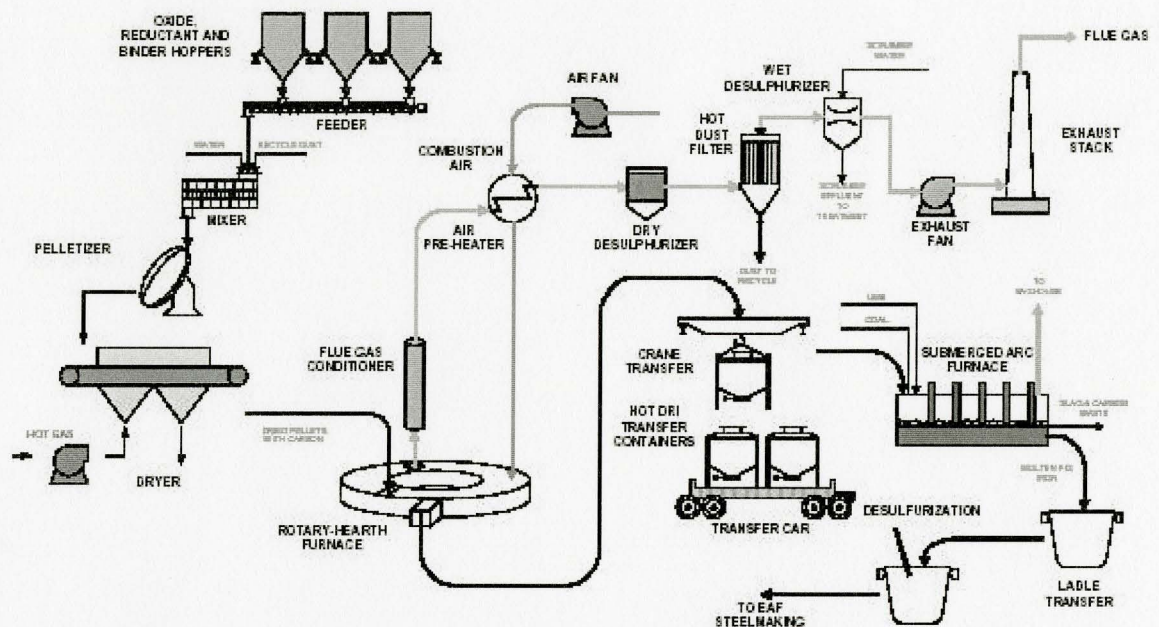


Figure 1- 7-IDI Process Flow Diagram [10]

- Corex

The Corex process is a shaft furnace process. The raw materials for this ironmaking method are iron ore in the form of pellets or lump ore and non coking coal.

Similar to Blast Furnace the reduction gas moves in counter flow to the descending burden. The reduced iron is then discharged from the reduction shaft into the melter gasifier where hot metal is produced. The gas which contains mainly of CO and H₂ which is produced by the gasification of coal with oxygen leaves the melter gasifier at temperatures between 1000 -1050 C. [9]

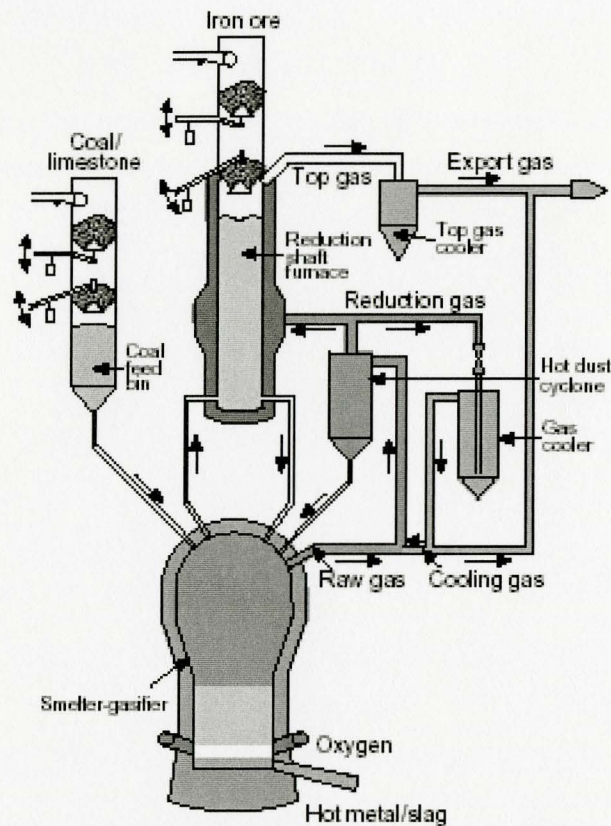


Figure 1- 8. Corex Process Flow Diagram [9]

- Hismelt

Hismelt is an air based direct smelting technology. In this process a vertical vessel is used which is located within the hearth and contains molten iron bath and slag layer above the metal bath.

Iron ore fines, coal and fluxes are injected directly into the melt. Carbon is dissolved by contacting the iron melt and reacts with the iron oxide in the slag and forms CO gas. Rapid heating of the coal also results in cracking of the coal volatiles which releases hydrogen.

A fountain of molten material is projected into the top space by the formation of CO and H₂ gas. Hot air at 1200C is blasted into the top space through a water-cooled lance. The carbon monoxide and hydrogen is post combusted with oxygen (from the hot air blast). The metal and slag which are heated in the top space fall back into the bath and provide energy for direct smelting of the iron ore. [9]

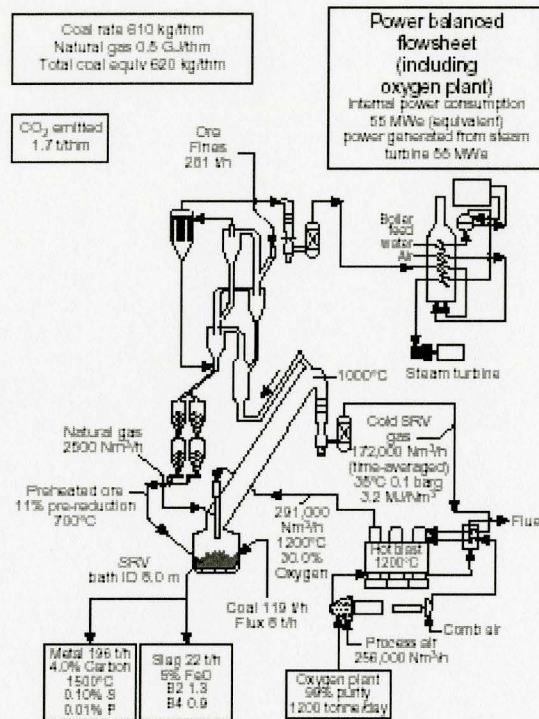


Figure 1-9. Hismelt Process flow diagram [9]

- ITmk3 (Iron Technology mark 3)

ITmk3 is the most recent ironmaking process developed by Kobe Steel Company which uses RHF. The raw material for this process is coal-ore composite pellets. In this process carbon containing pellets are heated such that reduction and gas generation occur simultaneously. This technology is the development of the Fastmet process in which by increasing the temperature to about 1350°C, formation of liquid iron and slag phases takes place.

The pellets after reduction can be melted and slag and metal be cleanly separated in a very short period of time of about 10 minutes. The product is an excellent feed for the EAF which can be rapidly melted and no additional energy would be consumed for slag melting [15] to [18].

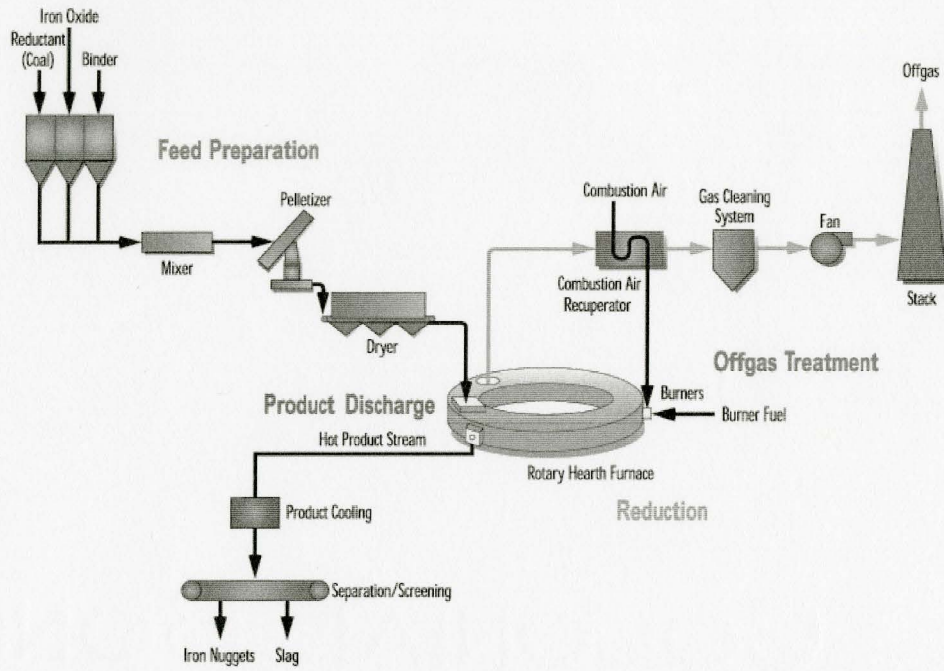


Figure 1- 10.Itmk3 Process Flow Diagram [12]

1.4. Melting Behavior of Coal Ore Composite Pellets

1.4.1. Reaction sequence from single pellet studies

Kobayashi et al, [2], investigated the reduction behavior of carbon composite iron ore pellets on the Fastmet process; they used a bench scale reactor. The microstructure of the Fastmet pellet can be described as sintered metallic iron in close contact with coal, which had transformed by heating and softening and formed char.

Kobayashi and Matsumura et al then developed the preliminary studies of rapid reduction of coal ore composites followed by melting and phase separation. In their experimental work, they heated carbon composite iron ore pellets at temperatures above 1300C in a small electric resistance furnace.

The tube furnace used had the inner diameter of 50 mm and a length of 1500mm in all tests to investigate both reduction and melting behavior of composite pellets. Figure 1- 11 provides a schematic view of the apparatus.

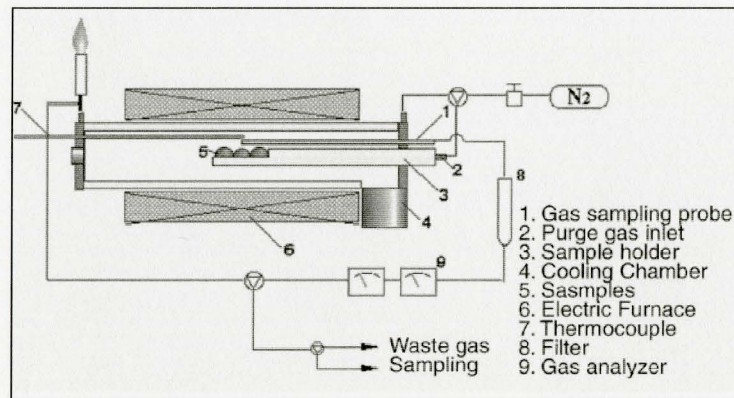


Figure 1- 11- schematic view of the apparatus [2]

The coal ore composite pellets used in the preliminary experiments were made from a magnetite ore A (80.3 mass %) and coal A (18.5 mass %) with bentonite (1.2 mass %) as the binder.

The chemical content of the raw materials used can be seen in Table 1- 1. The weight of the pellets being used by Matsumura et al was within the range of 6.5-7.0 g, and the range of density was 2.3-2.4 g/cm³. Reduction was carried out at different temperatures (1250C, 1300C and 1350 C) in a controlled atmosphere of 100 % N₂ and gas flow was adjusted to 2.0 NI/min.

Table 1- 1- the chemical compositions of raw materials (wt %) [2]

Ore	Total Fe	FeO	CaO	SiO ₂	Al ₂ O ₃	MgO
A	69.72	38.50	0.21	2.15	0.17	0.27
B	69.51	30.22	0.41	1.42	0.46	0.36

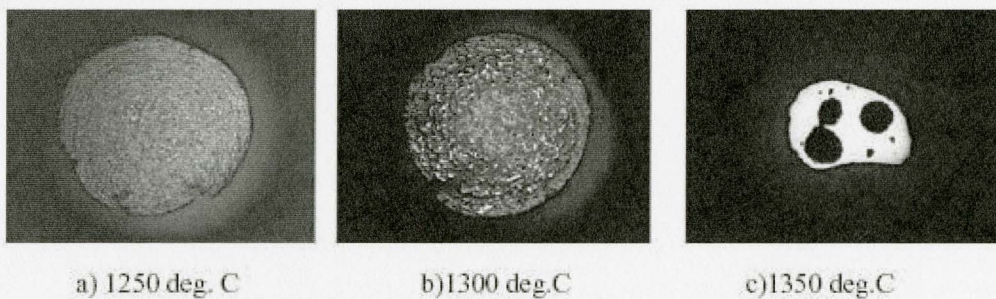
Coal	Moisture	Ash	VM	C	H	N	S
A	1.26	4.53	17.12	83.53	4.22	1.08	0.84
B	0.70	9.66	17.61	82.20	4.24	0.78	0.23

First three pellets were put on the sample tray. The tray and the pellets were inserted into the furnace at the time when the furnace temperature rose and reached the required level. That was the time when the O₂ content in the furnace dropped to zero. During the pellets reduction, the atmospheric temperature and the CO and CO₂ contents in the waste gas were continuously monitored.

After the required holding time pellets were quenched to room temperature under N₂ atmosphere. Samples were taken for microscopic observation of the structure and chemical analysis.

1.4.2. Result of reduction and melting test

A cross-sectional view of the pellets reduced at different temperatures is shown in Figure 1-12. Pellets which were reduced at 1250C had reduced uniformly. In contrast, a dense metallic iron shell was formed on the pellet surface for the pellets which were reduced at 1300C. Inside those pellets some melted and condensed phase could be observed. Pellets reduced at 1350C had melted perfectly in 5 or 6 minutes and a lump of metallic iron had separated from some black glassy slag.

**Figure 1-12-Cross sectional view of the reduced pellets [2]**

The liquid slag was formed from the gangue and ash minerals in the iron ore and coal.

By Those preliminary tests, Kobayashi et al had the idea that, it might be possible to separate the melted metallic iron from the melted slag, by carrying out the reduction at the temperature of 1350C or above in a very short time and obtain a metallic iron which contains no slag.

To study the pellet behavior during the melting and separation stages, second series of samples were taken at various times where the furnace temperature was controlled at 1450C.

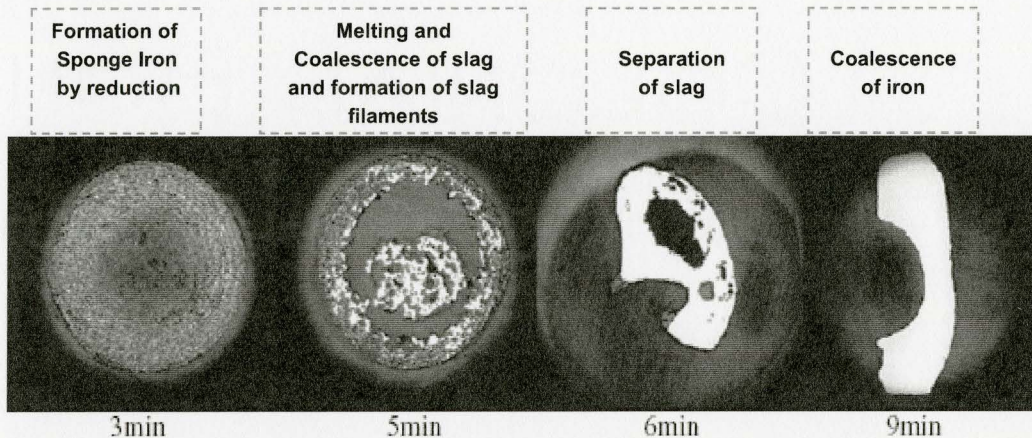


Figure 1- 13-Overall and cross- sectional view of time sampled pellets [2]

In Figure 1- 13 views of the time sampled pellets, both overall and cross-sectional, are shown. Sample pellet being taken after 3 minutes, had a typical sponge iron shape, in the 5 minute sample, the dense metallic shell was formed on the surface and inside included liquid slag and a big void space. In the 6 minute sample pellet, metal and slag both were melted and separated. The separation was almost completed for the samples being taken after 9 minutes.

The following reactions were considered by Kobayashi et al to take place:

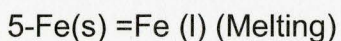
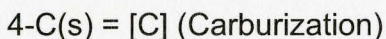
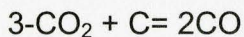
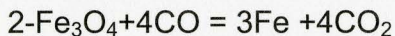
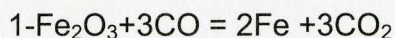


Figure 1- 14 shows how CO and CO₂ vary in the waste gas when the furnace temperature was kept at 1450C. When the pellets were inserted into the furnace, volatization took place which lasted for about 1 minute, and then no shape

change was observed for about 4 minutes. At that point, the CO and CO₂ contents in the waste gas increased. At 2 to 3 minutes after insertion, the CO and CO₂ contents had rapidly decreased. According to Matsumura et al,[19], in 5 or 6 minutes after insertion, the pellets had already softened and been transformed, and with the passage of a little more time, the pellets had melted completely.

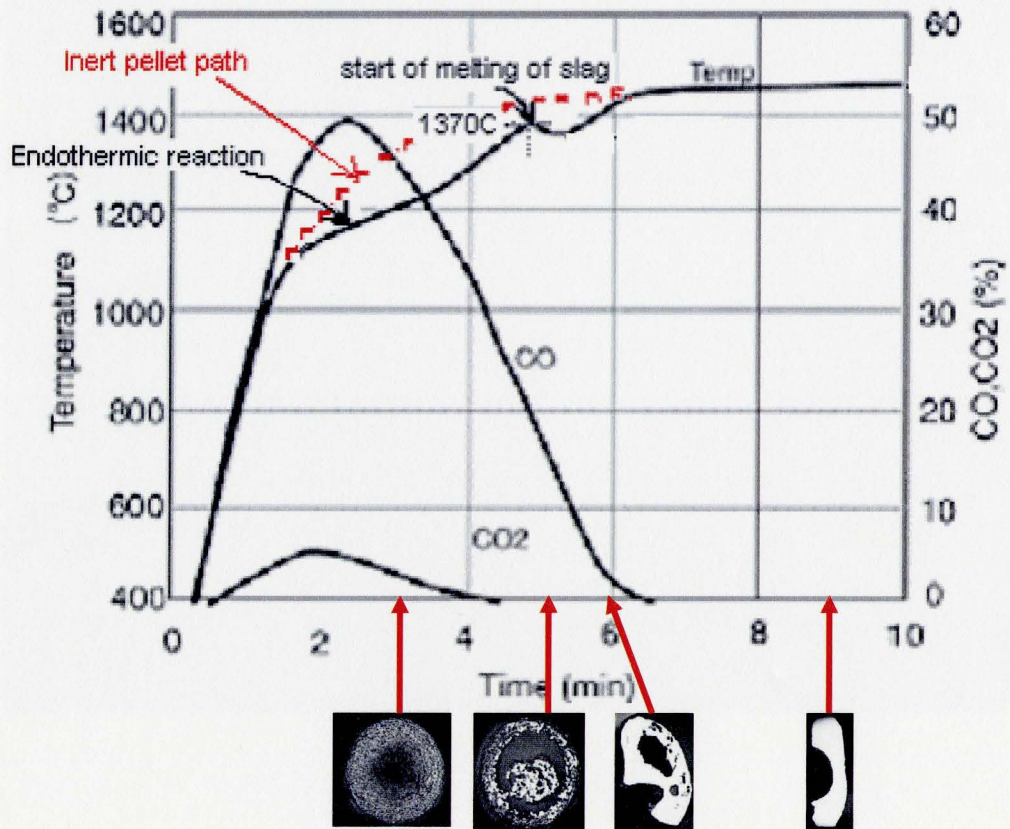


Figure 1- 14-Variation of pellet temperature and CO, CO₂ [19]

Figure 1- 14 shows that the temperature of the pellet center after being inserted into the furnace continued to rise until it reached about 1100°C, then the increase slowed down. The CO content was also rising during this stage. As the heating temperature continued to increase to about 1230°C, the heating rate increased again. During this period, the CO content in the gas had decreased rapidly.

In Figure 1- 14 it can be seen that at about 1370°C, the pellet temperature decreased once and then rose again. According to Matsumura et al, by that time, the pellets had been melted. After this point, pellet center temperature was

heated up again and rose to the furnace temperature. The relationship between the reduction degree and the pellet temperature can be seen in Figure 1- 15.

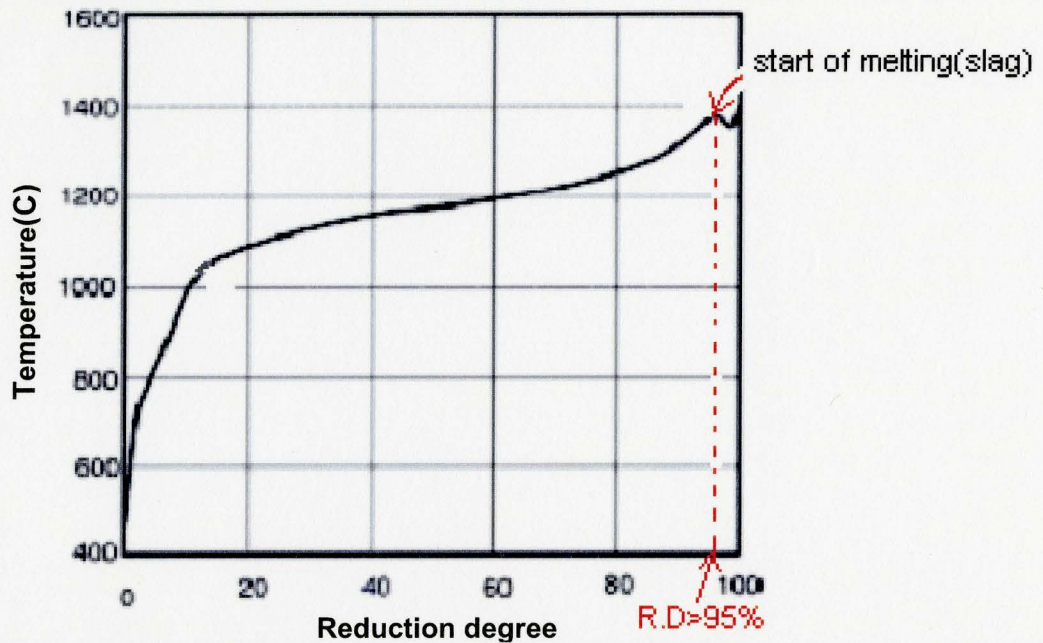


Figure 1- 15-Reduction degree and pellet temperature [2]

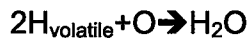
The reduction degree was achieved from the oxygen balance of CO and CO₂ contents in the furnace gas. As can be seen in Figure 1- 15, temperature rose rapidly to 1100C in the early stages of reduction. When about 95% of reduction was completed, the temperature fell once and rose again, the meaning of the temperature drop would be the occurring of some endothermic reactions that according to the above observations is likely to represent the slag melting.[2],[19].

1.4.3. Modeling of the melting behavior

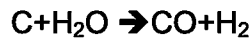
After the preliminary tests for discovering the phenomena occurring in the Itmk3 process, Meissner et al, [20], developed a numerical model for the process of reduction and meltdown of coal ore composite pellets. Their model covered the temperature, composition and phase changes in a single pellet during reduction by CO and H₂, solution-loss reaction (CO₂ + C = 2CO), carburization and melting of iron. [20]

The reactions assumed to occur were as follows:

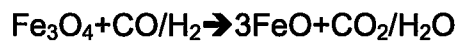
Devolatilisation reactions:



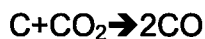
Generation of CO by steam:



Reduction reactions:



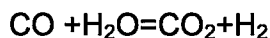
Boudouard reaction:



Carburization of iron by CO:



Water gas reaction:



In the above mentioned model, heat was considered to be transferred to the pellet surface from the outer stream and also radiation from the atmosphere. Inside the pellet, heat transfer was considered to take place by conduction and convection. They took into account heats of all reactions and phase changes. The pellet was assumed to be a sphere with a certain diameter containing ore, coal and binder which later transformed by phase changes and chemical reactions. [20]

By the results of the computations with the model, Meissner et al could consider a sequence of regimes occurring in the pellet during heating as follows:

- 1-Devolatilisation and gas evolution from coal.
- 2-Reduction and boudouard reaction in solid pellets.
- 3-Carburization of solid iron.
- 4- Melting of iron.

According to Meissner, [20] Boudouard reaction is the rate controlling reaction.

Figure 1- 16 shows a typical result from the computations of the Meissner's model.

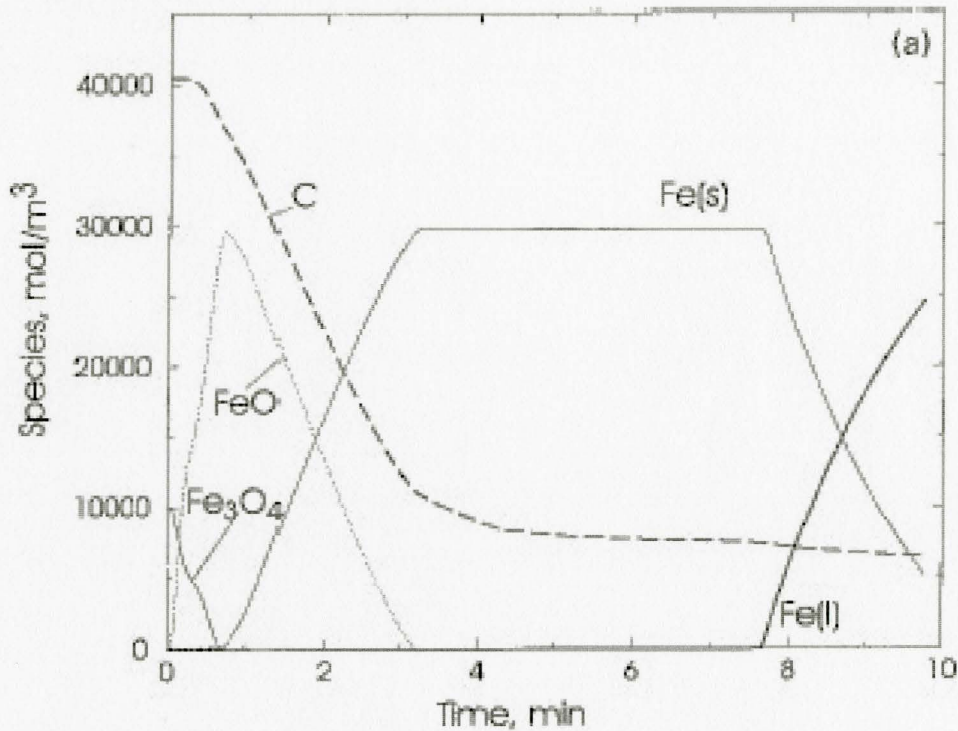


Figure 1- 16-species and phases as a function of time in the pellet [20]

Figure 1- 16 shows how species vary in a region near the surface of the pellet. The magnetite ore was reduced very rapidly to FeO. After 1 minute FeO begins to be reduced to solid iron and after about 3 minutes, all FeO is reduced to iron. According to Meissner, after reduction was completed, the iron phase remains solid for some time, during this time carbon diffuses into the solid iron, thereby lowering its melting point. After about 8 minutes, melting starts and liquid iron appears [20]. It should be noted that Meissner's model did not include slag formation and the indirect role of slag in carburization.

1.5. Melting steps

By reviewing the studies of researchers who tried to investigate the reduction and melting behavior of the coal ore composites, the following steps can be considered for the pellet from the beginning of reduction to the complete separation of liquid iron and liquid slag:

- a -Devolatization and gas evolution
- b -Reduction and Boudouard reaction
- c- Formation of soft phases from coal ash, gangue minerals and residual FeO
- d- Densification of iron shell on the surface
- e- Formation of a dense shell of iron on the surface, lump of liquid slag and an empty region inside the pellet
- f- Carburization of iron
- g- Melting of iron
- h- Separation of iron and slag melts
- i- Aggregation of iron melt and formation of relatively pure iron nuggets after cooling.

As mentioned before, up to now, many studies have been done on the reduction behavior of coal ore composites, but the issues of melting and phase separation are relatively new and many investigations should still take place for the complete understanding of the phenomena occurring during melting stages of coal ore composites. Hence, in this study the focus is mainly on the steps from the beginning of melting to the phase separation of liquid metal and slag.

1.5.1. Formation of initial dispersed liquid slag from ash and gangue minerals

According to Kobayashi et al the onset of melting is the point where a low melting point slag containing FeO forms, the CaO-SiO₂-Al₂O₃ slag softens and melts. The melting point of the metallic iron is lowered because of the carburization from the carbon and CO gas that are remained after the reduction of the iron oxide. Figure 1-17 shows a schematic of microscopic structure of composite pellet at this stage [21].

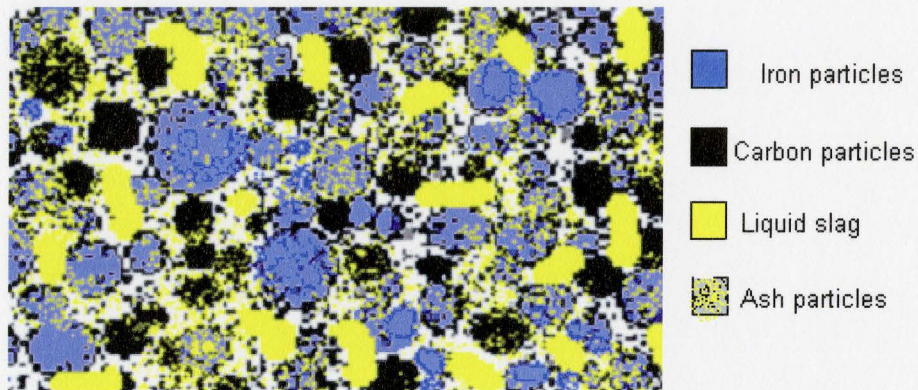


Figure 1-17- Pellet microstructure schematic – initial formation of liquid slag from gangue and ash and remaining unreduced particles of FeO[this study]

In the presence of liquid slag between the mixed particles of iron and carbon the following stages are likely to take place:

1.5.2. Liquid penetration

After the melting of particles with the lower melting point and formation of liquid slag phase, the liquid slag formed can penetrate into the spaces between the carbon and iron particles. According to German for a system of particulate mix containing liquid between particles, [21], penetration of the liquid flow occurs through the pores and particle structure and can be caused by capillary forces. Penetration causes fragmentation of the solid particles. The liquid initially is not at an equilibrium composition; thus, surface energy is not at equilibrium. The spreading liquid can penetrate the solid-solid interfaces. Penetration happens in the early stage of liquid formation. The actual rate of penetration can depend on the liquid reactivity, viscosity, and contact angle. A schematic diagram of the penetration and fragmentation process is shown in Figure 1- 18,[21].

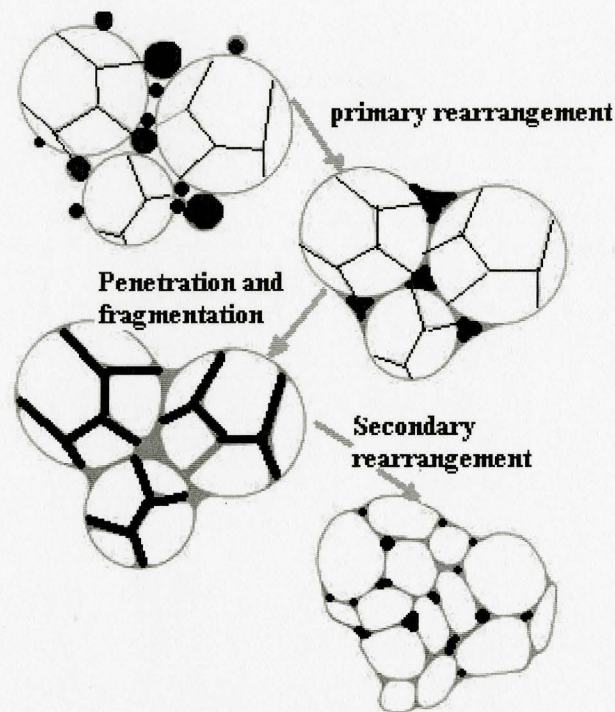


Figure 1- 18-A schematic diagram of penetration and fragmentation of particles [21]

1.5.3. Change in inter-particle distances

German [22] has shown that, strong compressive forces exist between contact points of particles wetted by liquid. In the case of formation of a liquid between particles the contact angles, particle size, and amount of liquid affect the contact forces. During the initial stage of liquid formation, there is an appreciable attractive force for small contact angles. If contact angles are large, repulsive forces can exist and swelling can occur. The amount of swelling is proportional to the amount of liquid. For all liquid contents low contact angles cause shrinkage, while high contact angles cause swelling at low liquid contents.

For irregular particles the situation is different from that for spherical particles. When volume fraction of liquid is low and neighboring contacts do not merge, the misalignment of the center of gravity due to an irregular shape gives a torque which may lead to rapid particle rearrangement, making contact between flat surfaces. The force on an irregular particle changes with the volume fraction of liquid. This can make a difference in rearrangement behavior between spherical and irregular particles. In spheres, as the volume fraction of liquid increases, the force decreases. An inverse relation may exist for irregular particles; that is to say as volume fraction of liquid increases, the rearrangement force may increase. In practice, both systems show better rearrangement at

intermediate quantities of liquid. Usually lower contact angles and smaller particle size are better for rearrangement independent of particle shape [22].

1.5.4. Rearrangement

Liquid slag can create an attractive force between particles of reduced iron and carbon. As a consequence, in a three dimensional network of solid particles and liquid, a hydrostatic pressure would exist on the pores. In the case of low inter-particle friction, the particles will repack to a higher coordination. Density increases in the presence of small and smooth particles (low friction). Rearrangement often takes place in two stages. Primary rearrangement takes place between the individual particles while secondary rearrangement takes place between clusters of primary particles. Figure 1- 19 shows how clustering takes place. With an excess liquid (in this study slag), it spreads and creates a cluster of wetted particles with closer packing. The clusters continue to repack as they increase in mass, and accordingly rearrangement becomes slower [23].

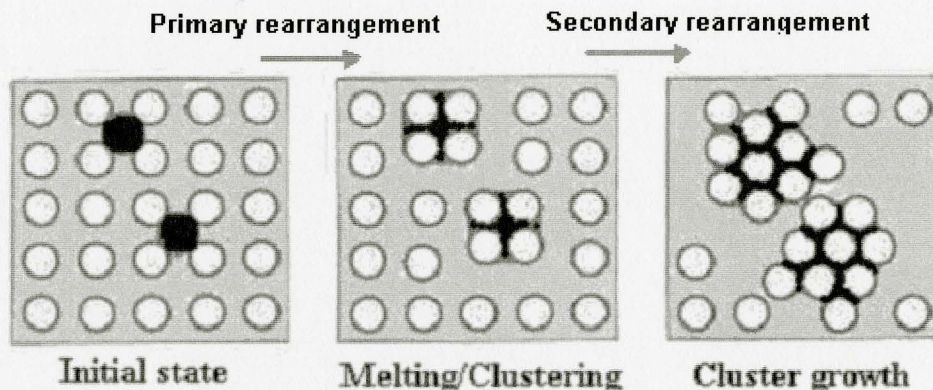


Figure 1- 19-Rearrangement of particles in the presence of liquid [21]

Secondary rearrangement may also involve particle fragmentation and subsequent repacking of fragments and the kinetics of their rearrangement depends on the fragment size. Packing of these clusters releases liquid to the regions between them. As a result, while the cluster size continually increases the extent of the microstructure undergoing rearrangement increases with time.

The volume fraction of liquid is important to the rearrangement stage. At a high volume fraction of liquid (in this study slag), complete densification is possible by, rearrangement and pore filling on formation.

Particle shape can also influence rearrangement. Irregular particles have a greater friction force and will undergo less rearrangement. The contact angle can also have influence on rearrangement. Better wetting of the solid by the liquid would result in more rearrangement. At large contact angles, no rearrangement can be possible. Homogeneous composite mixtures would result in better

densification. Besides differences in the degree of densification, there are also micro structural differences. [21], [23]

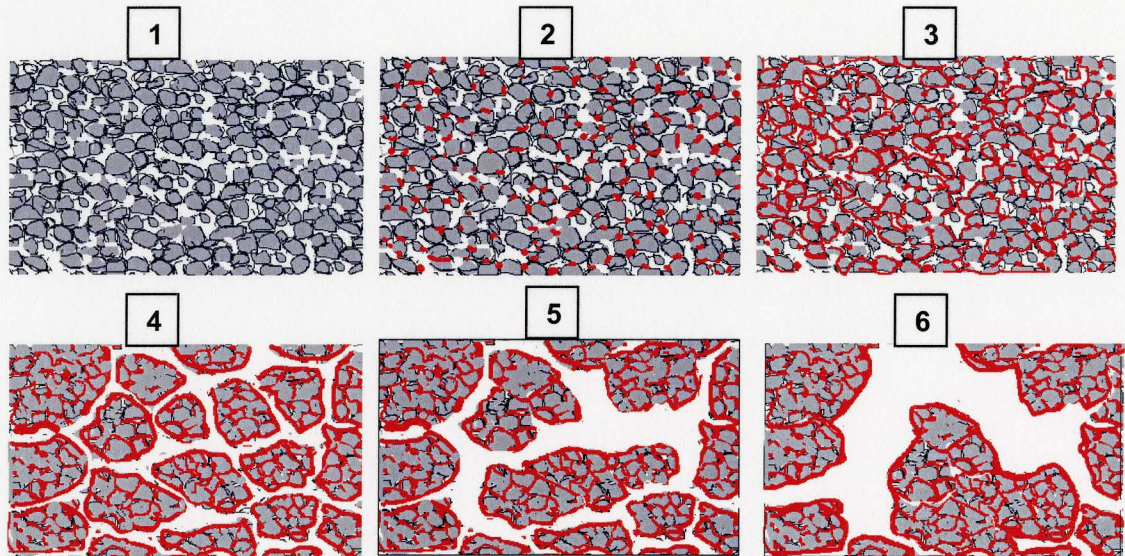


Figure 1- 20-Schematics showing the rearrangement and fragmentation in a simple model of one type particles and one type liquid [this study]

1.5.5. Pore size change

Pore size changes during the formation and penetration of liquid slag in the composite pellet. In general it was shown by Park et al, [24], for a mixture of spherical solid particles containing liquid that pores can be filled by liquid flow after a critical time. According to Park, in a fully densified specimen (in general solid particles containing liquid), the particles are kept in a contact flattened shape by the liquid menisci at the specimen surface.

The pore filling can be considered with a system containing a spherical pore of a constant size. When the pore is stable in the initial stage, a liquid meniscus with radius r_m , can be maintained between particles. For bigger particles, the liquid pressure would be less. At a critical particle size, r_m becomes equal to the radius of the pore and the meniscus forms a spherical pore surrounded by liquid. If the volume fraction of liquid increases, the pore size decreases. Further increase in volume fraction of liquid would result in pore filling and elimination.

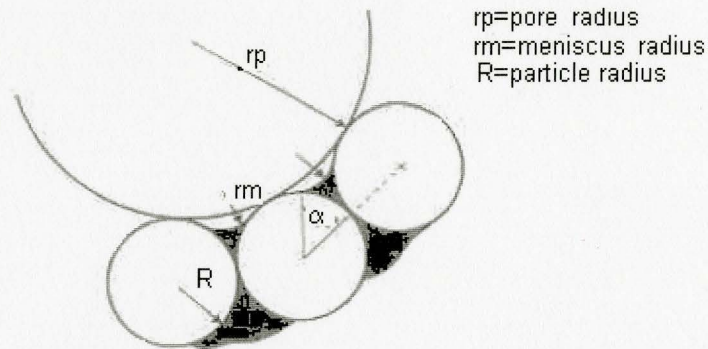


Figure 1- 21-Geometry of the particle and liquid menisci around a spherical pore [24]

1.5.6. Contact increase

Associated with rearrangement, reaction, swelling, and shrinkage in the initial stage of liquid slag formation in the mix charge, is the formation of new contacts. Contacts between the solid particles result in an increased contiguity and connectivity. Without these contacts, the compact has no rigidity. As the liquid slag spreads, capillary forces create new contacts between solid iron and carbon particles which bond together to increase the compact rigidity.

It should be noted that although liquid phase between particles can increase contacts and helps particles coalescence, but in the presence of very high amount of liquid, particles may be separated and contacts reduced [21].

1.5.7. Formation of slag percolations (coalescence of dispersed liquid slag)

Coalescence is a natural phenomenon that may occur when two or more droplets come in contact. The driving force is the lower surface energy of a larger droplet compared to the total surface energy of two or more droplets. When two bodies of liquid merge, their interfaces must also rupture and rearrange into one.

Coalescence can be assumed to occur in two steps; drainage of the liquid droplets separating solid particles until they form a film with a critical thickness, followed by formation of a bigger liquid droplet.

Figure 1- 22, shows a schematic of the coalescence of droplets sitting on a partly wetted surface.

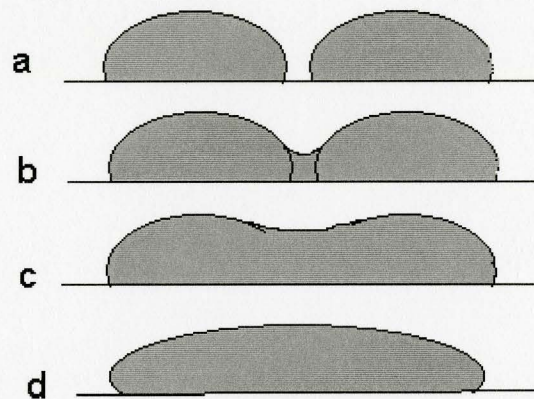


Figure 1- 22-Schematic of the coalescence of liquid droplets [this study]

Image “a”, shows two separate liquid droplets, these two droplets tend to touch and form a liquid bridge in image “b”. In image “c”, it can be seen that droplets have merged together to become a united droplet. Liquid is changing its shape to find a shape with the lowest surface energy. Which is a typical sessile drop shape here as the liquid is considered to wet the surface of the below substance. (For non wetting condition it will be spherical).

Apart from the effect of surface active contaminants, mass transfer process may have a large effect on the ease of coalescence. Motion of an interface may occur in the presence of mass transfer and this may be attributed to local variations in surface tension associated with concentration gradients. This generation of motion in the interface by surface tension gradients is known as the Marangoni effect.

The concentration gradients resulting from mass transfer leads to surface tension gradients. Surface tension gradients depending on their direction may draw liquid into solid surfaces and delay coalescence, or expel liquid from the solid surface, thus assisting coalescence. Mass transfer may help coalescence when the solute is transferred from the dispersed to the continuous phase, and to oppose coalescence when it is transferred from the continuous to dispersed phase [21].

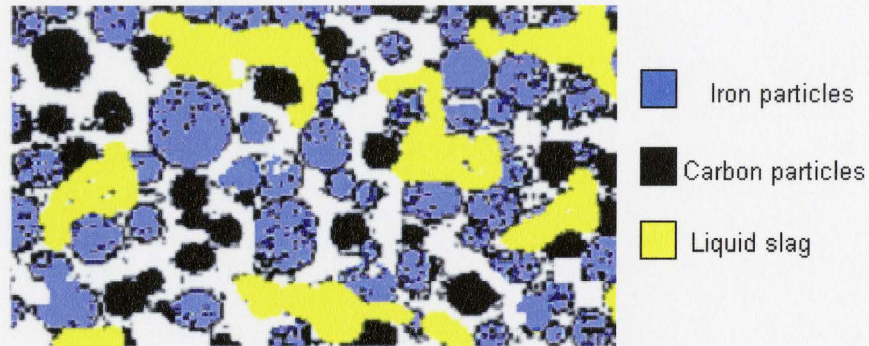


Figure 1- 23-A schematic of the pellet microstructure with slag percolations [this study]

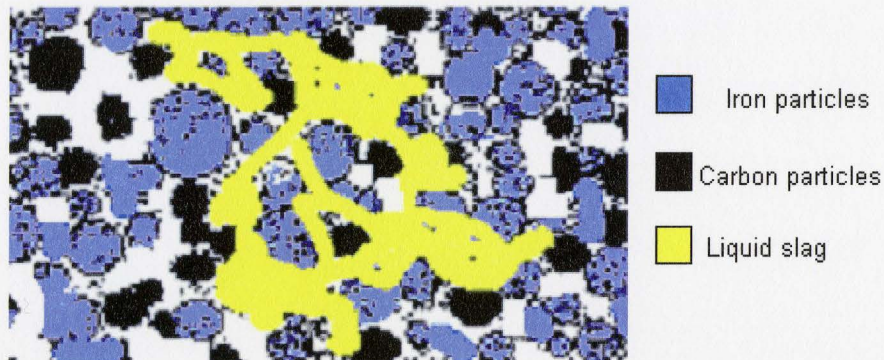


Figure 1- 24-A schematic of the pellet microstructure with a network of slag [this study]

As seen in Figure 1- 23 and Figure 1- 24, dispersed slag droplets in the pellet tend to join together and coalesce. The driving force is decreasing the total surface energy. It can be seen in Figure 1- 24 that a continuous slag network is formed in which a closed path can be considered to connect all regions of it.

1.6. Carburization and local melting of iron

Carburization of the iron during and after the reduction of the coal composites is one of the most important steps in the process of producing iron nuggets from a coal ore composite. As can be seen in Figure 1- 25, in the operational area of ITmk3 in Fe-C diagram carburization of iron, decrease its melting point and causes faster melting at a lower temperature.

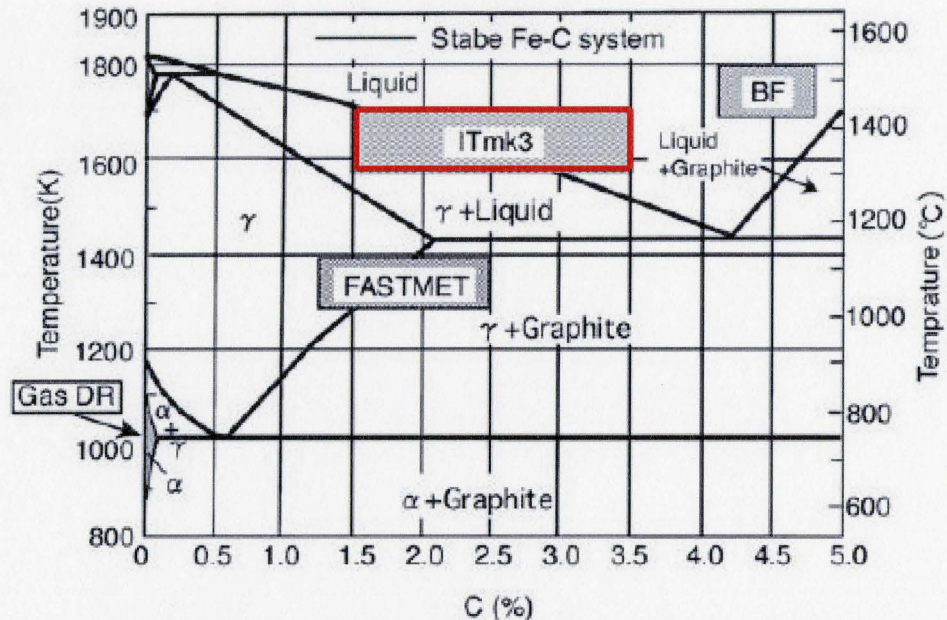


Figure 1- 25- Fe-C phase diagram, Itmk3 operational area is shown [2]

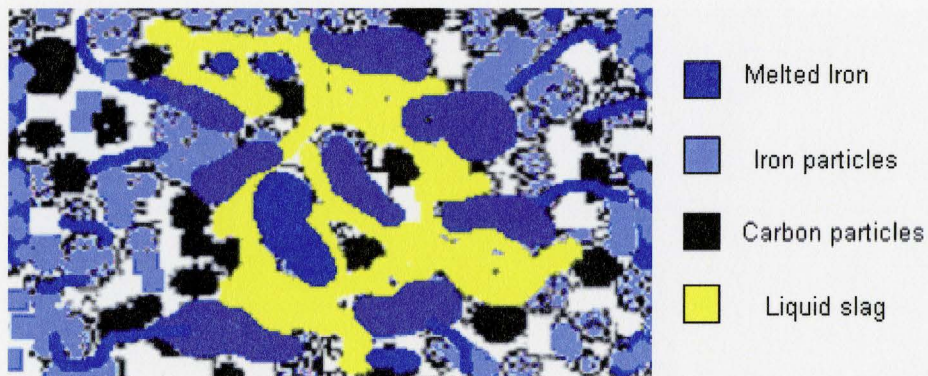


Figure 1- 26-A schematic of the microscopic pellet structure after melting of iron [this study]

There may be different mechanisms for carburization of the iron during and after reduction, these include; carburization by CO gas during the reduction, carburization by direct contact of carbon with solid iron and carburization by carburized iron.

According to Murakami et al, [25], after reduction of iron ore by CO gas, (generated from Boudouard reaction), carburization of reduced iron by CO gas proceeds until 1423K. At higher temperatures, carburization continues by absorbance of carbon to reduced iron by direct contact with solid carbon. Usually

carbon is added to an extent higher than necessary for making CO for reduction. According to Murakami et al, after reduction, carbon matrix can remain in the composite mix and prevent coalescence of liquid droplets at lower temperatures.

Figure 1- 27 shows the relation between the operating temperature and carbon content in reduced iron. The open circles are carbon in reduced iron; the closed triangles are total remained carbon in the pellet.

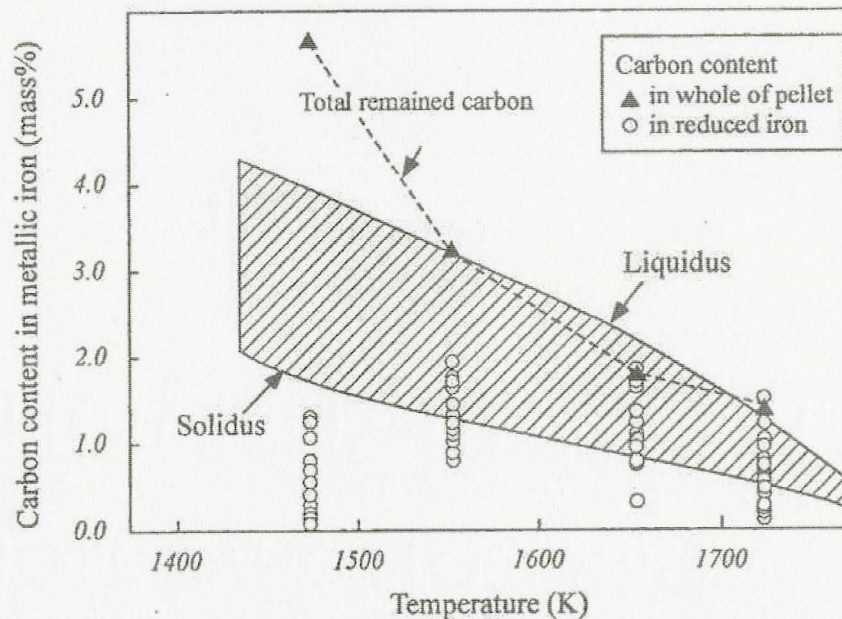


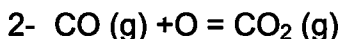
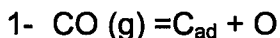
Figure 1- 27-Variation of carbon content in metallic iron and whole of the pellet [26]

Carbon content was calculated from the difference between the total carbon and carbon weight percent in iron. In Figure 1- 27 it can be seen that at 1473K, as carbon content in reduced iron was less than on solidus line, iron did not melt and big portion of carbon (5.5mass %) remained in the whole mix.

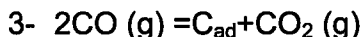
It is also shown that at 1553K, carbon content of the iron is 1.3 mass% while in the whole pellet it is 3.2mass%. This shows that a lot of carbon remains in the mix without carburizing the iron. According to Murakami et al, reduced iron is carburized in two ways, one from CO gas and the other from direct contact with solid carbon.

1.6.1. Carburizing by CO gas

According to Murakami, the following reactions express the carburization reaction on iron surface. The subscript "ad" means adsorbed on iron surface.



The sum of two reactions gives the inverse of solution-loss reaction:



Murakami have suggested that the rate of carburization is controlled by reaction 2 and diffusion of carbon in solid iron and iron carburization and melting begins in a temperature range of 1486K-1673K [26].

Sasaki et al [27] and Asano [28] also determined the rate of iron carburization and concluded that rate of carburization with CO has is much smaller than the rate of carburization with solid carbon.

1.6.2. Iron melting by solid carbon

It has been reported by Murakami et al, [26] that mass transfer in liquid phase and heat transfer to the reaction interface control the rate of iron melting. They were able to observe the melting of iron in contact with graphite with in situ observation method.

It was reported that melting began immediately from the carbon and iron plates interface as soon as graphite contacted with the iron plate. The rate of liquid iron growth using graphite was compared with the rate using CO gas for carburization.

The rate of carburization and melting was larger with graphite as the rate of carbon supply at the interface is higher using graphite. The required time for the initial melt formation when using graphite was 1s, while CO gas the required time was 1260s. It was concluded that carburization is greatly more effective with graphite rather that CO gas.

Figure 1- 28 shows the calculated liquid phase thickness of iron by graphite and 100% CO gas as a function of carburization time after the beginning of iron melting at 1523 K.

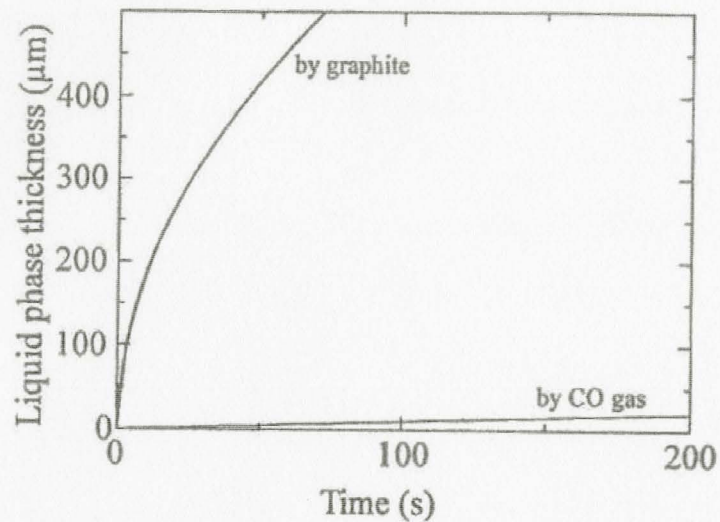


Figure 1- 28-Calculated liquid phase thickness of iron by graphite (Murakami et al) and 100% CO gas (Sasaki et al) as a function of carburization time [25]

The third mechanism mentioned above was first discussed and evidenced by Ohno [29], who investigated the carburization mechanism under the presence of liquid slag. In their work, they used a graphite rod as the carbon source and electrolytic iron rod as reduced iron. Pre-melted Slag (formed from coal ash and a small amount of FeO) was put between the rods.

Ohno's experiments included heating experiments of the sample assembly during which slag melted and microscopic "in situ" observation during the heating experiments of this micro model. Ohno made his observation of carburization behavior by a confocal laser-scanning microscope combined with an infrared image-heating furnace to clarify the effect of slag on iron carburization. From his observations he presumed that the liquid slag would act as an important medium for the carbon transfer from coal to iron.

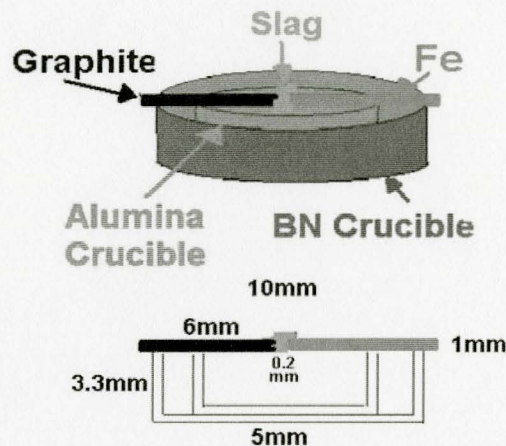


Figure 1- 29-Schematic sketch of sample set up [29]

Based on observations, Ohno et al considered the carburization mechanism during the smelting reduction as follows:

When slag containing iron oxide melted down and contacted carbon, iron oxide in the slag was reduced and the formation of iron particle as well as carburization happened simultaneously at the slag-carbon interface and carbon saturated iron droplets formed. Carburized iron droplets were transferred from slag-carbon to slag-iron interfaces due to the slag convection flow caused by the difference of the interfacial tension between the carbon-slag and iron-slag interfaces. They found that carburization of iron could proceed with a repeat of the above-mentioned mechanism [29].

According to Ohno et al observations, the above-mentioned behavior was more remarkable at higher initial FeO concentration of the slag sample. It indicated that frequencies of iron particle and CO bubble formation is strongly affected by the FeO content in slag.



Figure 1- 30-Image of sample observed using laser microscope [30]

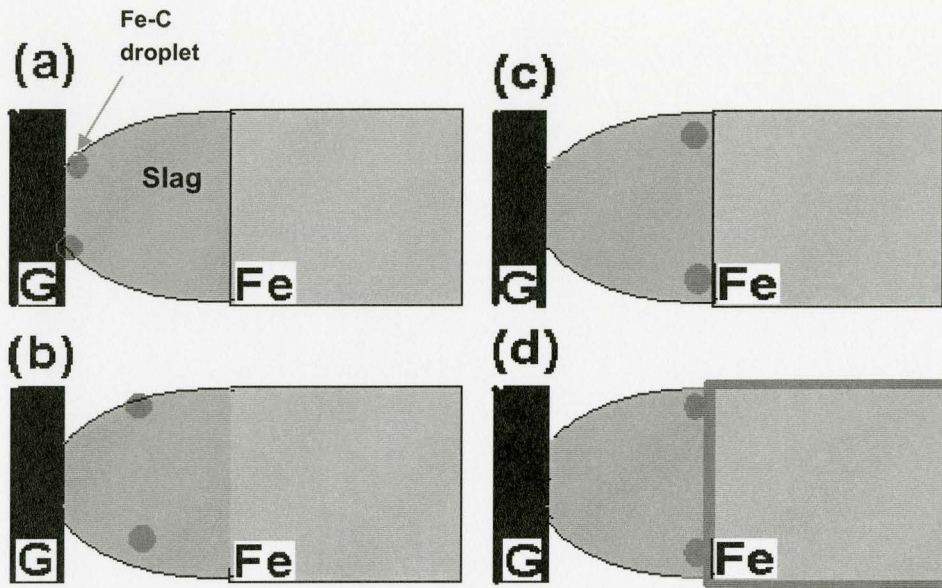


Figure 1- 31-Schematic sketch of carburization mechanism during the smelting reduction [30]

1.6.3. Carbon Content Analysis in Iron Rod

After the experiment they polished the iron rod and analyzed the carbon concentration profile in the iron. Carbon content in the iron rod near the slag-iron interface was found to be much higher than that in the iron bulk in all samples. Ohno et al again concluded that molten iron particles which contained certain amount of carbon were carried from carbon-slag interface to the iron-slag interface and immediately spread out on the entire surface of iron sample due to its wetting nature. They suggested that such mechanism can be a reason of higher carbon content at the surface of iron rod. This was evidence that carbon did obviously transfer from carbon rod to iron through slag phase in the form of molten Fe-C droplets which resulted in the carburization of the iron rod [30].

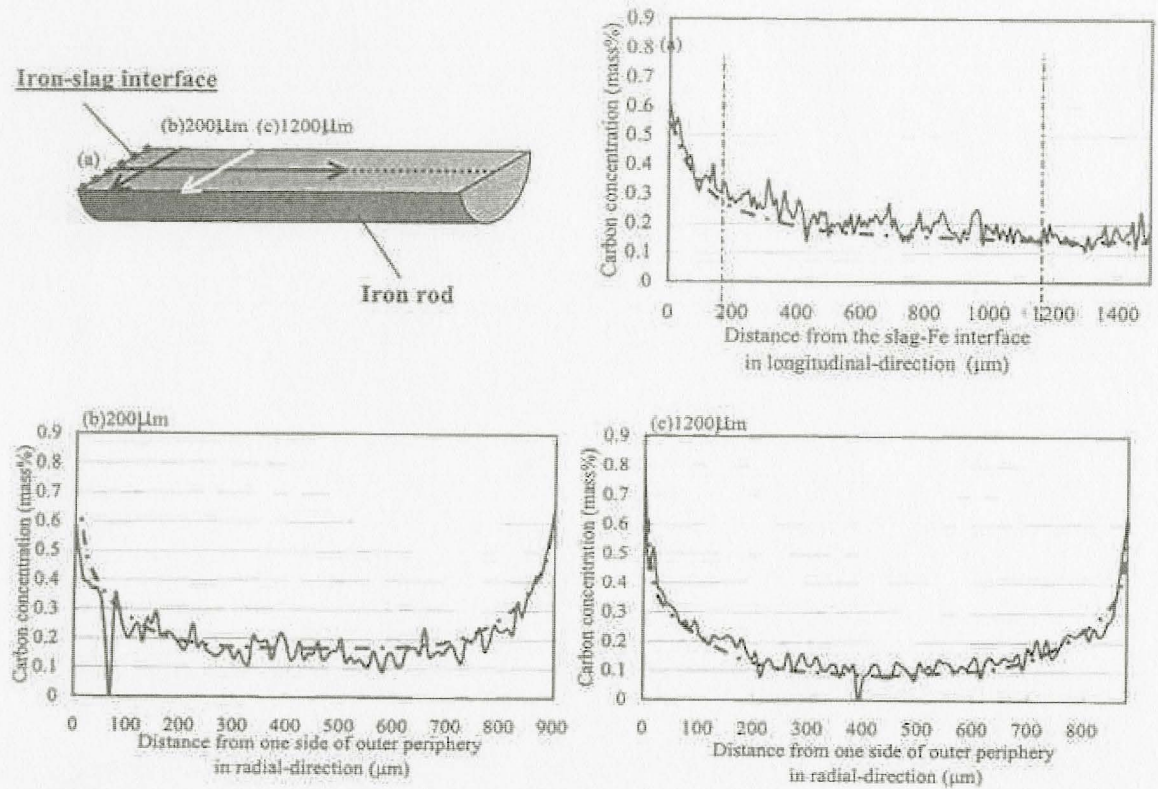


Figure 1- 32-Line analysis of carbon concentration distribution in iron rod determined by EPMA [30]

1.7. Densification of iron

In general for particulate materials during heating different transport processes can lead to densification. Densification may result from the uniform center to center motion of the neighboring particles as illustrated in Figure 1- 33 . The flattening of the interface between particles occurs by transport of material from the contact with simultaneous shrinkage. Another mechanism may be the dissolution of small grains. In this case, large particles grow at the expense of neighboring small particles. The neck growth is another possible mechanism which could result in grain shape changes and center-to-center approach of the particles. This form of contact flattening does not involve particle coarsening [31].

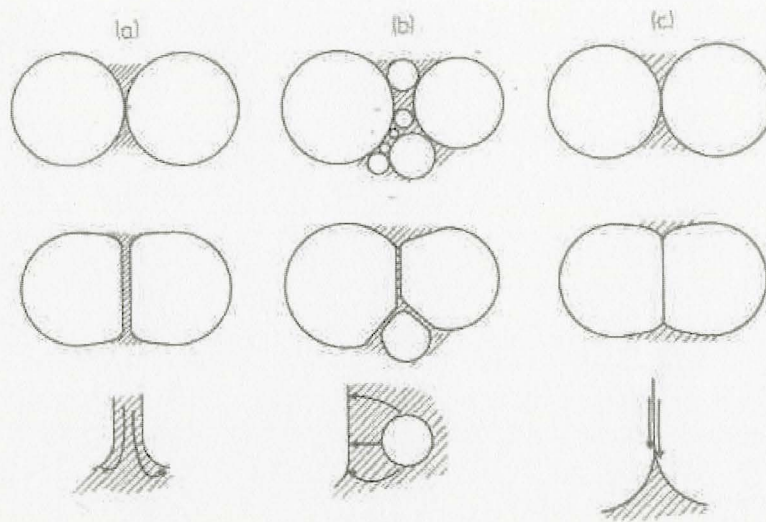


Figure 1- 33-The three mechanisms of shape accommodation and neck growth during the intermediate stage (a) contact flattening, (b) dissolution of fine grains, and (c) solid-state diffusion [21]

Major differences in the possible mechanisms explained above are in the source of material and conditions in which densification occurs. All three contribute to better packing and a higher density. Grain growth occurs as a result of dissolution of the fine grains, but not of contact flattening. All mechanisms mentioned would lead to densification. They differ in the transport path, material source, particle size. The rate of material transport from the contact point for the case of contact flattening, determines the densification rate. By the growth of contact area, the stress along the interface is decreased and densification slows down. After liquid flow, particles are put into contact by the liquid (slag). Coalescence is a possible intermediate stage for densification and coarsening mechanism. A sketch of coalescence is given in Figure 1- 34.

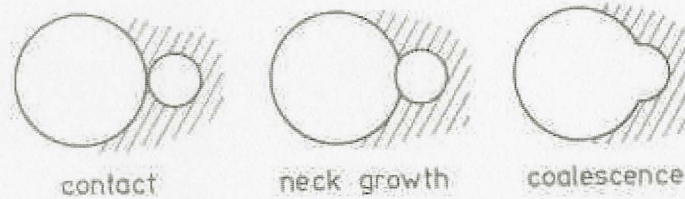


Figure 1- 34-A schematic diagram of the steps leading to grain growth by coalescence [21]

Contacting particles of different size fuse into a single grain by a continuous process of directional grain growth and grain reshaping. The grain size increases by coalescence and the number of grains continuously decreases. When the melt appears contacts form quickly. Contact may probably form a low angle grain boundary. A low disorientation angle between the contacting grains results in a high chance of coalescence. Other possible causes of coalescence can be chemical, strain, or temperature gradients. Contact formation may also lead to coalescence. New contacts between grains may have been caused by gravity, thermal motion, and settling. Before liquid slag formation many contacts exist, especially when volume fractions of solid is high. After a short time, boundaries form between particles and continuity increase. For low volume fractions of solid, there will be rapid movement of particles in the liquid. During motion, grain contacts can form which may coalesce. When the time for coalescence is short, the particles are likely to be separated. Alternatively, when the coalescence time is long, a skeletal microstructure occurs [31].

This later case is most typical to liquid phase sintering where the volume fraction of solid exceeds 70%. Figure 1- 35 contrasts two extreme examples of the microstructure for a 50 volume percent solid system [21].

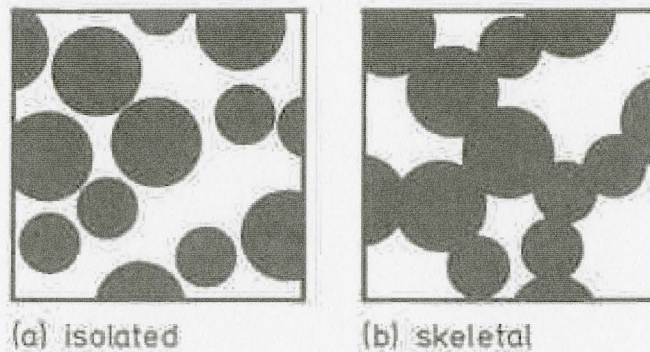


Figure 1- 35- The contrast between an isolated and skeletal microstructure for 50% vol. liquid [21]

1.8. Melting of iron and phase separation

As described in Section 1.6, the melting point of iron is reduced by carburization. According to Kobayashi and Matsumura, [2], shortly after the formation of a dense iron shell on the pellet surface (while the center of pellet contains liquid slag and a big empty region), iron shell melts away completely and the melted iron separates from the melted slag. The reason for clean separation of iron and slag in the ITmk3 process is not yet clearly known (is discussed later in chapter 4). Generally in metallurgical systems containing liquid metal and slag, separation of iron and slag is seen from two aspects; one is settling of the metal through the slag and its getting incorporated to the metal phase, and the other is interfacial phenomena in liquid iron and slag systems.

1.8.1. Settling of Iron Droplets through Slag

The motion of liquid metal droplets in molten slags was studied by Iwamasa et al [32] using low temperature physical modeling and X-ray observation at high temperatures. Their results show that settling times of metal droplets in stagnant slags can be accurately predicted utilizing Stokes equation modified for the appropriate experimental conditions. To estimate the terminal settling velocities, they used the stoke's equation as follows:

$$V_{Stoke's} = \frac{gd^2(\rho_m - \rho_s)}{18\eta_s}$$

Where V_{stokes} is the terminal velocity of droplet, g is the acceleration due to gravity, d is the droplet diameter, ρ_s is slag density, ρ_m , is metal density and η_s is viscosity of slag.

1.8.2. Surface Tension of Liquid Iron

For the measurements of interfacial tensions and contact angles of liquids at high temperatures and in a variety of atmospheres, the sessile drop profile method can be combined with the X-ray radiography to develop a precise method. Digital image processing can also be used to capture, enhance and determine the coordinates of the X-ray shadow image of the droplet.

The surface tension of liquid iron is about 1.8N/m at 1823K. Typical nonmetals, particularly the elements of VIA group in the periodic table, are highly surface active and their addition to liquid iron cause a large decrease in surface tension. Surface tension of liquid iron decreases with increasing oxygen concentration in the iron in the temperature range between 1873 -2023K. The

effect of surface active elements on the surface tension of liquid iron can be numerically expressed by the following equation:

$$\sigma_{Fe-i} = \sigma_{Fe} - RT\Gamma_i^0 \ln(1 + K_i a_i)$$

Where K_i is equilibrium constant for adsorption reaction, a_i is activity of i -element in liquid phase and Γ_i^0 is surface excess quantity of i -element at the full coverage. [33], [34], [35]

1.8.3. Surface Tension of Slag

Surface tension of slags had not been so extensively investigated and the experimental results are often scattered. Values of surface tensions of pure liquid iron oxides and slags are significantly lower than those of metals.

According to Nakashima [36], the following relation is often used to calculate the surface tension of slag.

$$\sigma_{slag} = \sum_i \sigma_i \cdot N_i$$

Where σ_i is the surface tension factor of slag component i and N_i is molar fraction of i -component.

1.8.4. Interfacial Tension between Iron and Slag

Equilibrium interfacial energies between liquid slags and liquid iron follow the trend found in the surface tensions of liquid metals; however, interfacial energies in slag-steel systems are significantly lower than the corresponding liquid-metal-gas interfacial energies due to secondary bonding between the slag and the metal. Interfacial energies are also a strong function of oxygen and sulfur contents.

One model to determine the interfacial tension between metal and slag is Girifalco and Good's [37] model where the values of surface tension of the initial phases are used to calculate the interfacial energy of the combined phases.

Interfacial tension between liquid metal and slag can be calculated from knowledge of the surface tensions of the pure liquid metal and the slag. According to Girifalco and Good's equation:

$$\gamma_{m-s} = \gamma_m + \gamma_s - 2\phi(\gamma_m \cdot \gamma_s)^{1/2}$$

Where γ_{m-s} is the interfacial tension between the metal and the slag, γ_m and γ_s are surface tensions of the metal and the slag respectively, and ϕ , which is

the interaction coefficient, is a measure of the interaction between the liquid metal and the liquid slag.

The interaction coefficient from the Girifalco and Good equation is defined as work of adhesion (W_{ad}) between two phases divided by the square root of work of cohesion of each phase W_{co} , as follows:

$$\Phi = \frac{W_{ad}}{(W_{co}^m \cdot W_{co}^s)^{1/2}} = \frac{\gamma_m + \gamma_s - \gamma_{m-s}}{2\sqrt{\gamma_m \cdot \gamma_s}}$$

The interaction coefficient varies from 1, which indicates strong attraction between the two liquid phases, to 0, which indicates weak attraction between the two liquid phases.

The ability of metals to form low energy interfaces could also be related to the oxygen affinity of the metals [38]. The value of Φ was calculated as a function of slag composition by regression analysis as follows:

$$\Phi = 0.00284(\%CaO) + 0.00451(\%Al_2O_3) + 0.00721(\%SiO_2)$$

1.9. Review Summary

The review has identified that:

- 1- The ITmk3 process has significant advantage in short reaction time and producing a slag free iron for the EAF from coal and iron ore.
- 2- The overall reaction system has been modeled,[20] considering metal phase only and not slag.
- 3- The system prior to and during melting is multiphase. Phases are intermixed and contain porosity:
 - Minerals from gangue and ash,(S).
 - Residual FeO_x , (S).
 - Metallic iron (S).
 - Carburized metallic iron (S, L).
 - Slag (L).
 - Coal char (S).
 - Gas (CO , CO_2).
- 4- FeO_x plays a role in slag melting and in reduction and carburization of iron.
- 5- Melting and coalescence have been studied in single phase particulate system.ITmk3 system known is multiphase. (~6phases).
- 6- Surface and interfacial tensions measured from single and two phase studies provide important data for this study.

1.10. Focusing questions

Many focusing questions were developed from the review; it was decided to select the following questions from the study as follows:

- 1. *Can we demonstrate the ITmk3 process on coal and ore samples sourced locally?***
- 2. *What are the pathways and sequence for melting and coalescence of slag and metal?***
- 3. *What is the mechanism for the observed iron shell formation?***
- 4. *What is the effect of the following variables on melting behavior?***
 - a- *Time***
 - b- *Temperature***
 - c- *Coal type***
 - d- *Amount of slag***
 - e- *CaO/SiO₂ in Slag***

Chapter 2

2. Initial Experiments – Effects of Furnace Temperature, Time, Coal Type and Coal/Ore ratio

The first series of experiments were performed to investigate the general effect of furnace temperature, residence time in the furnace, coal type and coal/ore ratio on the behavior of composite mixes of iron ore and coal at high temperatures.

Furnace temperatures were 1300C, 1325C, and 1350C. Heating time before quenching were 5, 10 and 15 minutes. One ore type was used; the composition of which can be seen in Table 2- 1. Three types of coals were used in the experiments performed. The composition of coals is shown in Table 2- 2.

2.1. Assumptions

- The ore used was a magnetite ore and did not contain hematite
- The overall reduction reaction is considered to take place as below:
$$\text{Fe}_3\text{O}_4 + 4\text{C} \rightarrow 3\text{Fe} + 4\text{CO}$$
- Reduction by C and H from volatile matter is ignored as the composition of the volatile matter in coal is not available.
- No oxides in ore gangue and coal ash are reduced by carbon.
- Carbon in coal was only considered for reduction and not carburization.

2.2. Material Preparation

Composites were prepared in 6 groups, with the same type of iron ore and 3 types of coal. From each coal 2 composites were made, one composite with stoichiometric coal (coal needed for 100% reduction) and one with sub-stoichiometric coal (coal needed for 80% reduction), based on the fixed carbon in each coal type as seen in table Table 2- 2, the coal/ore ratio percent for all the samples prepared can be seen in table 7-1 in the appendix (chapter 7).

Table 2- 1-Ore chemical composition as analyzed in Actalabs No.m10703

Fe ₃ O ₄ %	SiO ₂ %	Al ₂ O ₃ %	MnO%	MgO%	CaO%	Na ₂ O%	K ₂ O%	TiO ₂ %	P ₂ O ₅ %	LOI%	Others%
97.24	0.82	0.10	0.10	0.22	0.42	0.01	0.01	0.02	0.01	0.33	0.72

Three types of coals were analyzed in Dofasco Labs; the compositions of the coals used are as below:

Table 2- 2-Coal composition

Weight %	Coal A	Coal B	Coal C
Volatile Matter	19.33	23.82	35.03
ASH	6.76	9.03	7.81
Fixed carbon	73.91	67.15	57.15
S	0.81	0.52	0.89

Table 2- 3 shows the ash composition of each coal:

Table 2- 3-Ash composition in weight percent

Wt%	Coal A	Coal B	Coal C
SiO ₂ %	50.27	58.48	53.29
Al ₂ O ₃ %	29.54	29.45	28.71
Fe ₂ O ₃ %	8.93	3.92	7.67
MgO%	1.11	0.51	1.09
CaO%	2.07	1.79	1.63
K ₂ O%	2.09	0.92	2.44
Na ₂ O%	0.62	<0.001	0.62
TiO ₂ %	1.35	1.9	1.38
MnO ₂ %	0.05	0.03	0.04
P ₂ O ₅ %	0.42	1.06	0.22
BaO%	0.14	0.26	0.22
SrO%	0.13	0.14	0.18

2.3. Screening

All types of coal were screened to pass a 300 micron sieve and iron ore was screened to pass a 100 micron sieve.

2.4. Mixing

Composite batches were made by mixing the screened ore and coals with the ratios specified in the table7-1 in the appendix.

2.4.1. Mixing Method

In order to mix the composites uniformly, the "cone and & quarter" technique was used.

First each composite was spread on a glazed paper and rolled towards the center by moving a corner of the glazed paper towards the center, the same technique was repeated for several times to ensure the proper mixing of the powders.

2.4.2. Final Samples

From each one of 6 composites made, 9 samples of (1 ± 0.01 g) weight were prepared, each in a small alumina crucible with given dimensions of 18mm height and 8.2 mm diameter.

2.5. Heating

Before heating the samples, furnace was preheated to the desired temperature as shown in table 7-1 in the appendix. After the furnace reached the desired temperature, samples assembled on a refractory tray were put rapidly inside the furnace. To retain a reducing atmosphere, a close fitting graphite cap was put on each alumina crucible. Samples stayed inside the furnace for the required period of time according to the heating table. Figure 2- 1 shows a schematic and figure shows a photo of the furnace used:

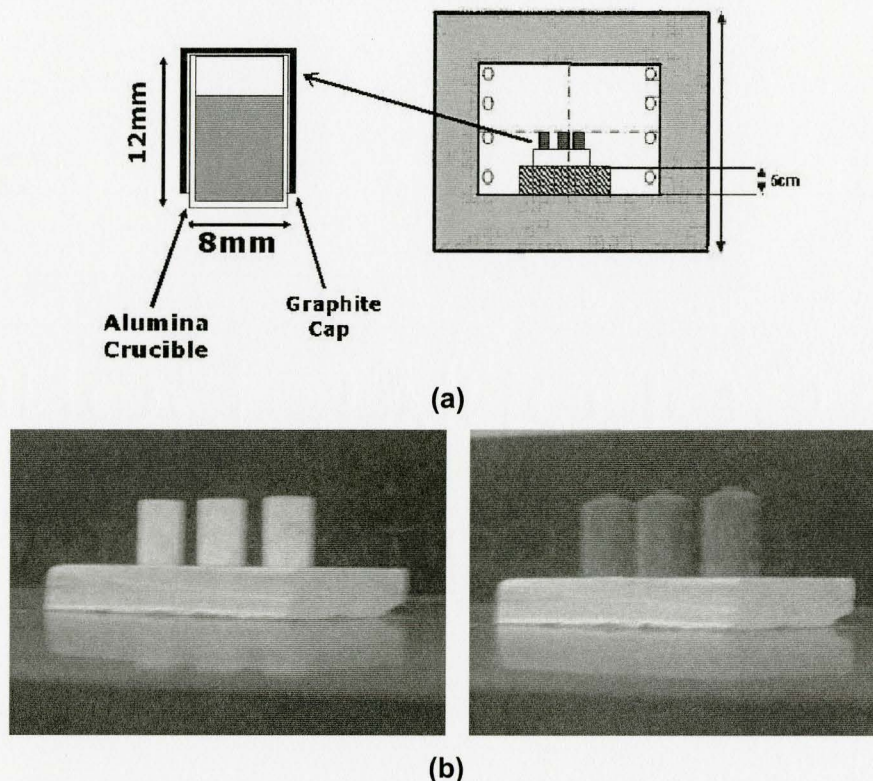


Figure 2- 1- (a)Schematic of the box furnace , (b)left shows the alumina crucibles on zirconia tray ,(b)right shows graphite caps on the alumina crucibles with semi-porous zirconia tray

2.6. Cooling

After heating, samples trays were rapidly taken out of the furnace and were put in a desiccators and desiccators lid was put on. Desiccators was connected to argon gas cylinder, after putting the samples inside the desiccators an argon stream was applied to samples to prevent re-oxidation of the samples.

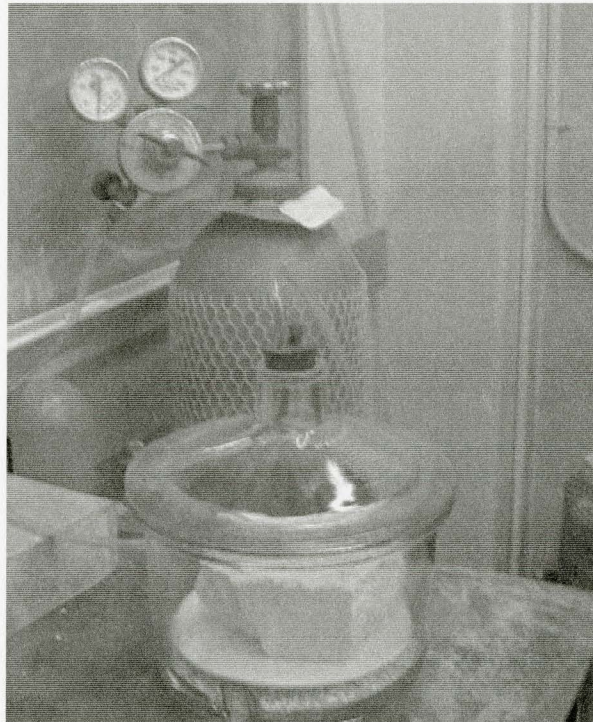


Figure 2- 2-Cooling the samples

2.7. Characterization

2.7.1. Primary Characterization-(Weighing- Optical Scanning)

After cooling, samples were weighed (Denver 0191396 balance). Table 7-1 in the Appendix shows the sample weights after heating. As the mix during heating and slag formation sticks to crucible walls, there is an error in final weight measured.

Samples were scanned by a scanner (hp3970). A scaled paper was used to show the dimensions of the final samples. Figure 2- 3 to Figure 2- 5 also figures 7-1 to 7-3, show the scanned images of the samples as below:

Figure 2- 3, substoichiometric coal at 1300C

Figure 7-1, (appendix),substoichiometric coal at 1325C

Figure 7-2, (appendix), substoichiometric coal at 1350C

Figure 2- 4, stoichiometric coal at 1300C

Figure 7-3, (appendix), stoichiometric coal at 1325C

Figure 2- 5, stoichiometric coal at 1350C

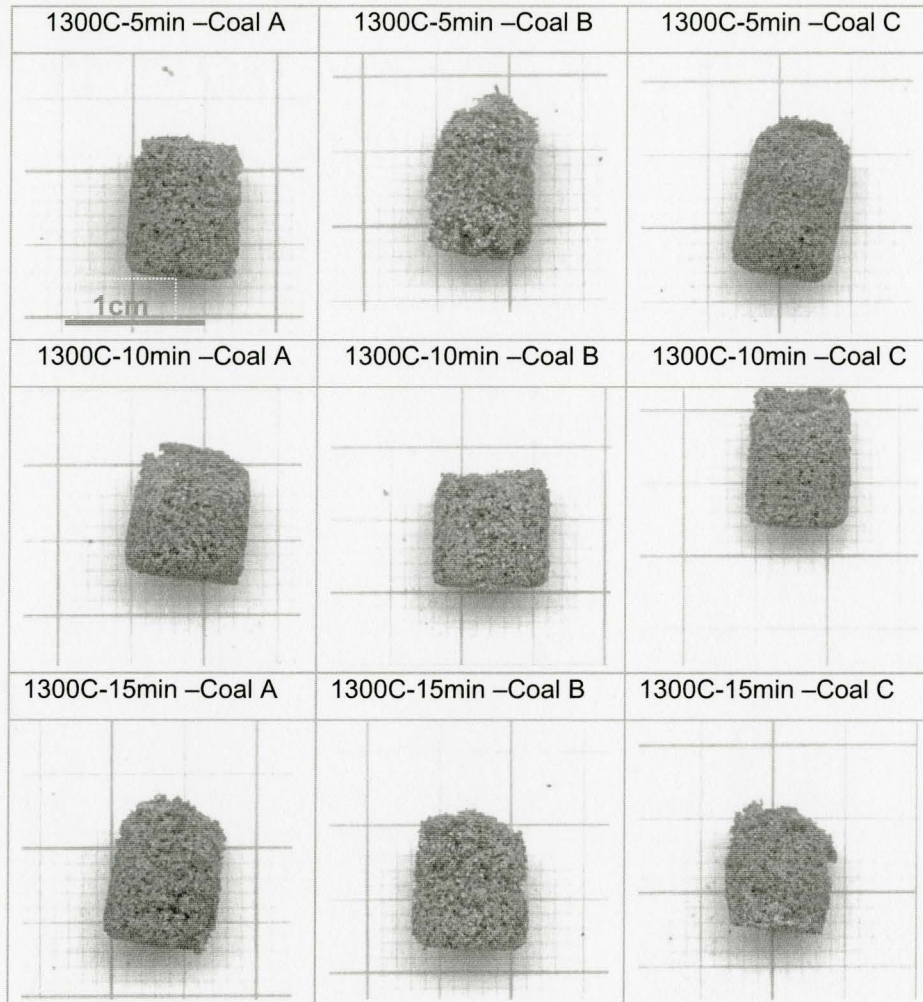


Figure 2- 3- Scanned images, samples with sub-stoichiometric coal at 1300C

The results show that melting and coalescence and separation of slag requires stoichiometric coal for a minimum time of 10 minutes at 1300C and 5 minutes at 1350C. There were some second order differences between the three coals which require further investigation at the microstructure level.

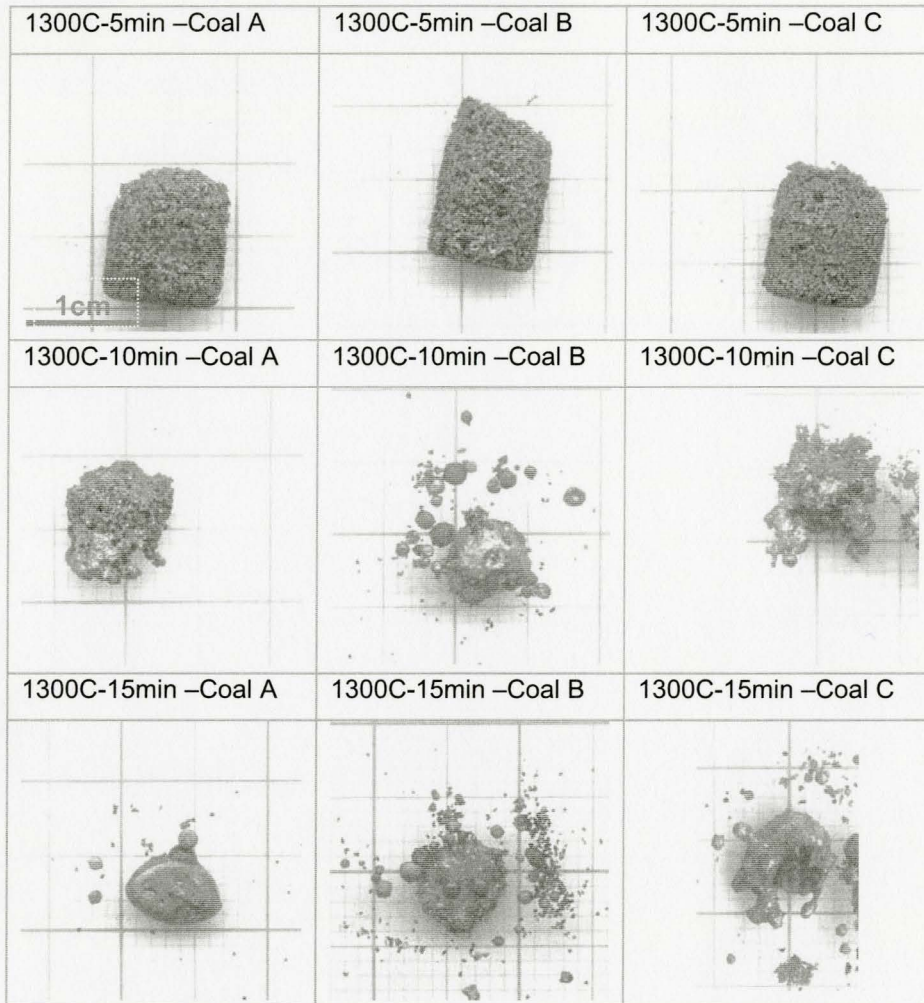


Figure 2- 4- Scanned images, samples with stoichiometric coal at 1300C

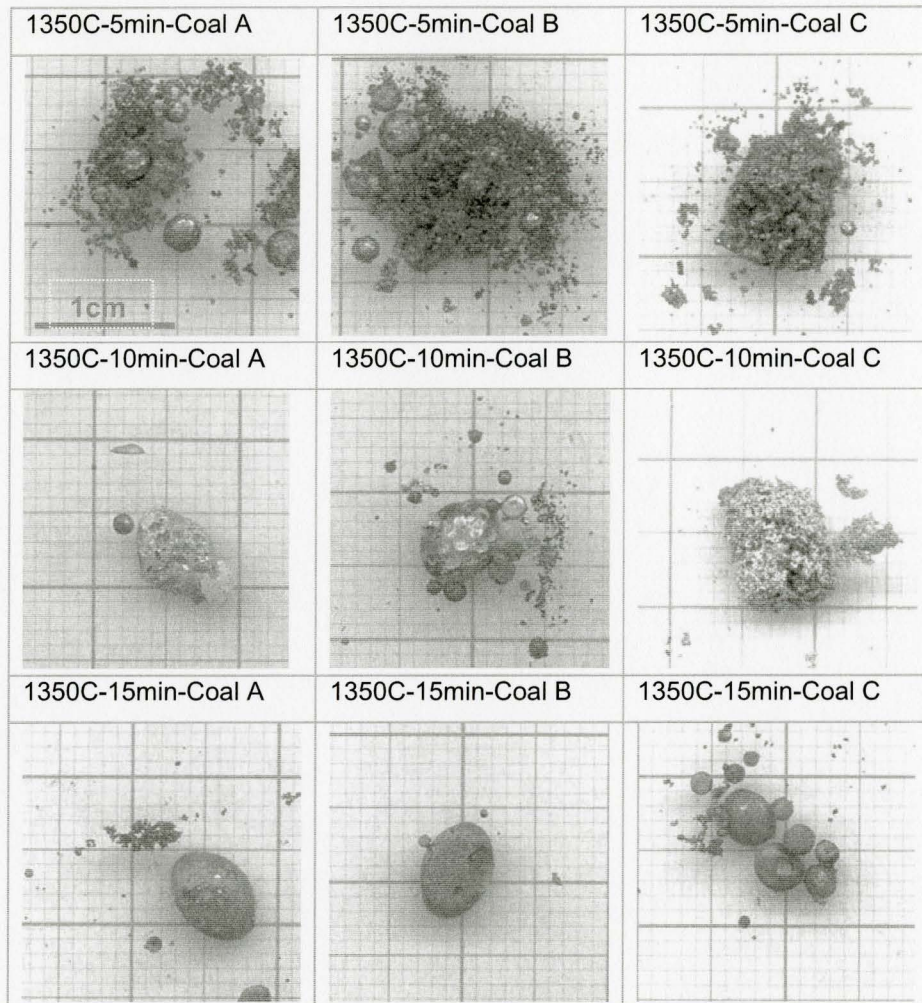


Figure 2- 5- Scanned images, samples with stoichiometric coal at 1350C

2.7.2. Mounting and Cutting

Samples were cold mounted with Epofix resin and hardener and remained under vacuum to get free of air bubbles.

Samples were then cut by the precision cutter Struers Accutom2. Struers 356CA blade was used with 0.5mm thickness. After cutting samples were polished in several stages from coarse to fine.

2.7.3. Observation of Microstructure

After polishing samples were subjected to microscopic observations. Stereo Microscope type WILD M3C was used to take low magnification images. The 40X lens was used.

For each set of conditions, three pictures were taken by Nikon D1 digital camera at random locations to give some idea of the variations in the sample.

Figure 2- 6 to Figure 2- 8, show the cross sectional images of samples in following sequence:

- 1300C, 5min, Figure 2- 6
- 1300C, 10min, Figure 2- 7
- 1300C, 15min, Figure 2- 8

The rest of microstructures (samples heated at 1325C and 1350C) are presented in the appendix in figures 7-4 to 7-9.

Each figure contains series of three microstructures in the following sequence:

- Sub stoichiometric coal A
- Stoichiometric coal A
- Sub stoichiometric coal B
- Stoichiometric coal B
- Sub stoichiometric coal C
- Stoichiometric coal C

When looking at the following microstructures it should be reminded that the ore particles were originally $d_{50}=30\mu\text{m}$ and the coal $d_{50}\sim 60\mu\text{m}$.

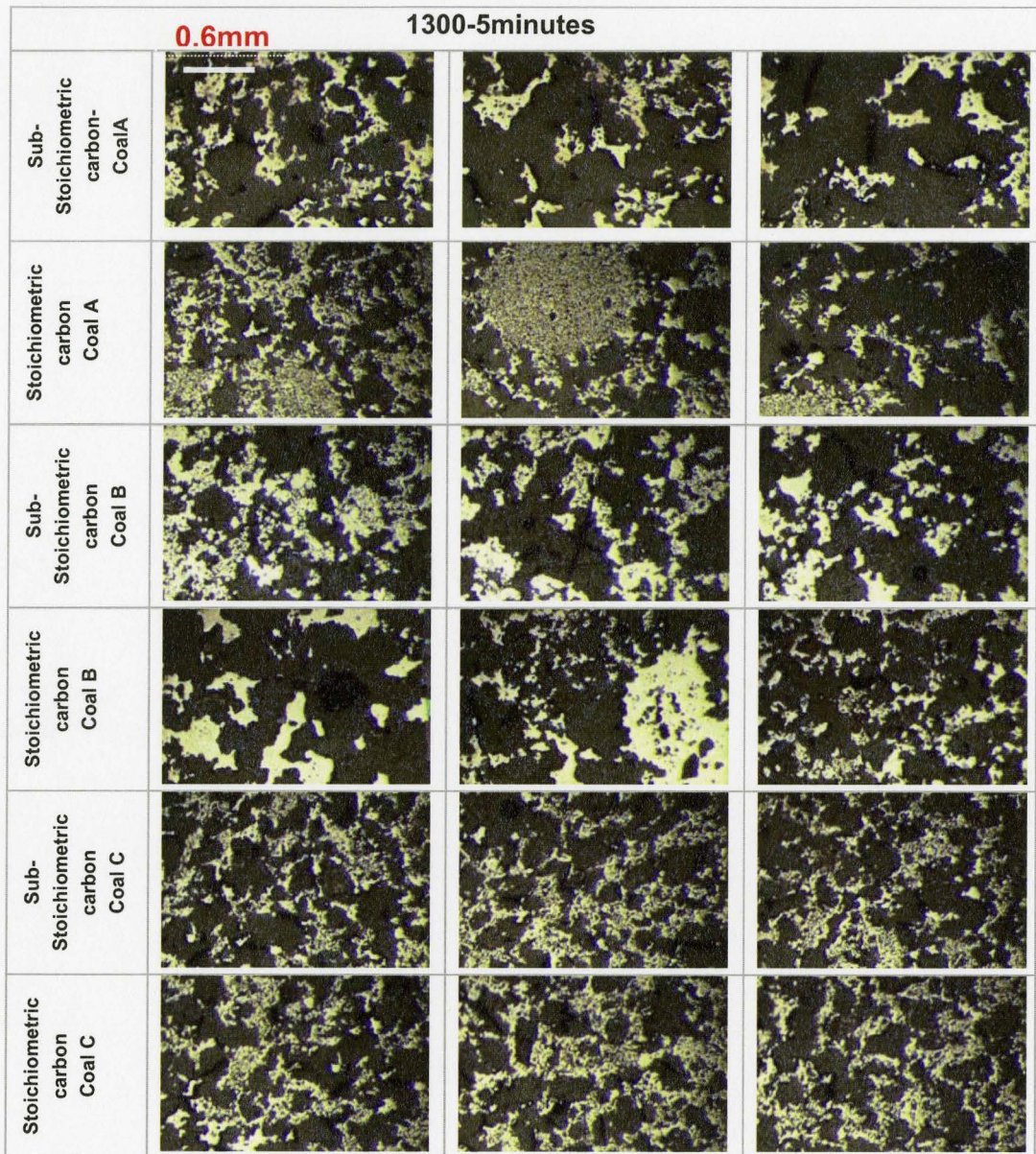


Figure 2- 6- Samples reacted at 1300C for 5min

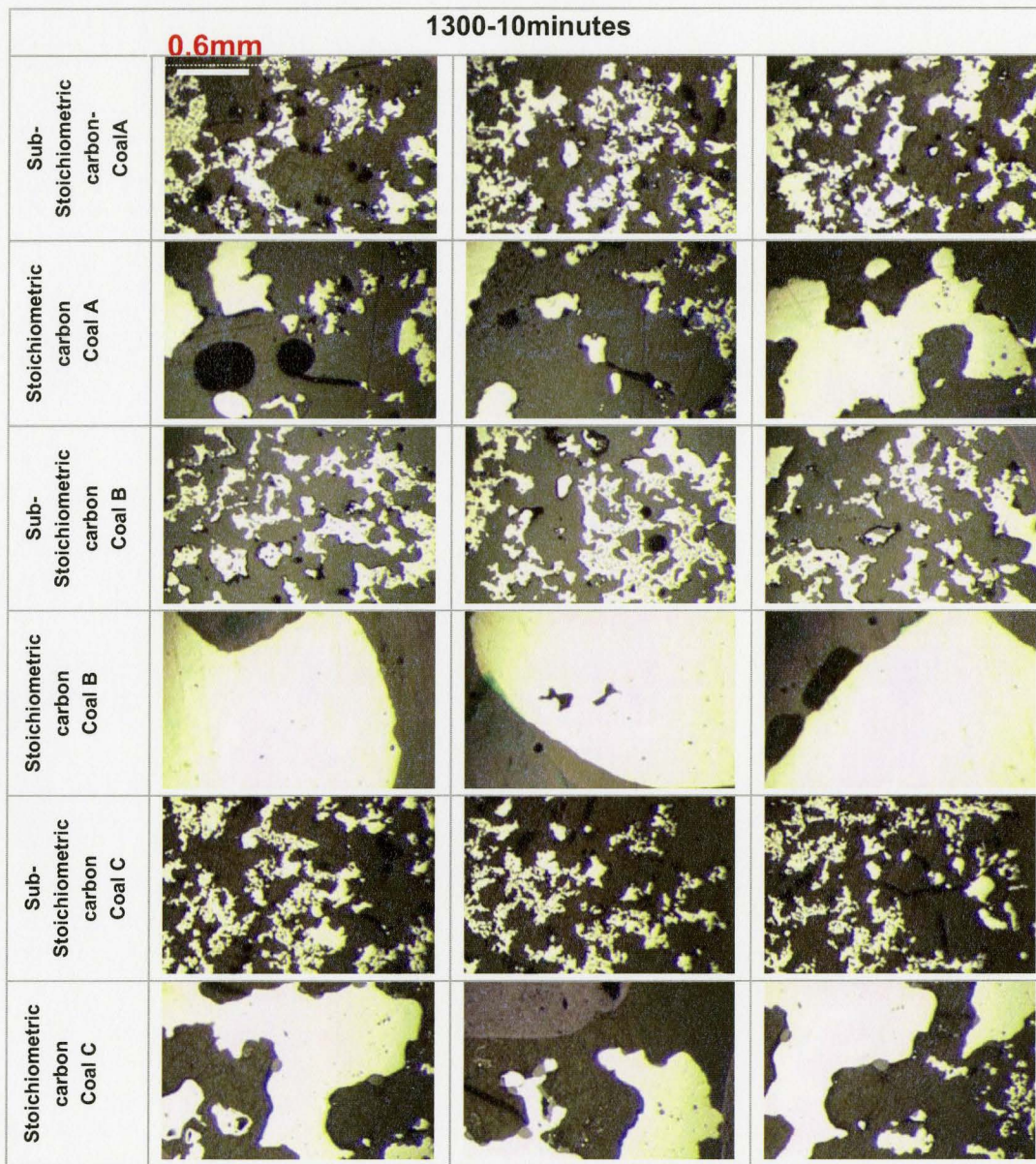


Figure 2- 7- Samples reacted at 1300C for 10min

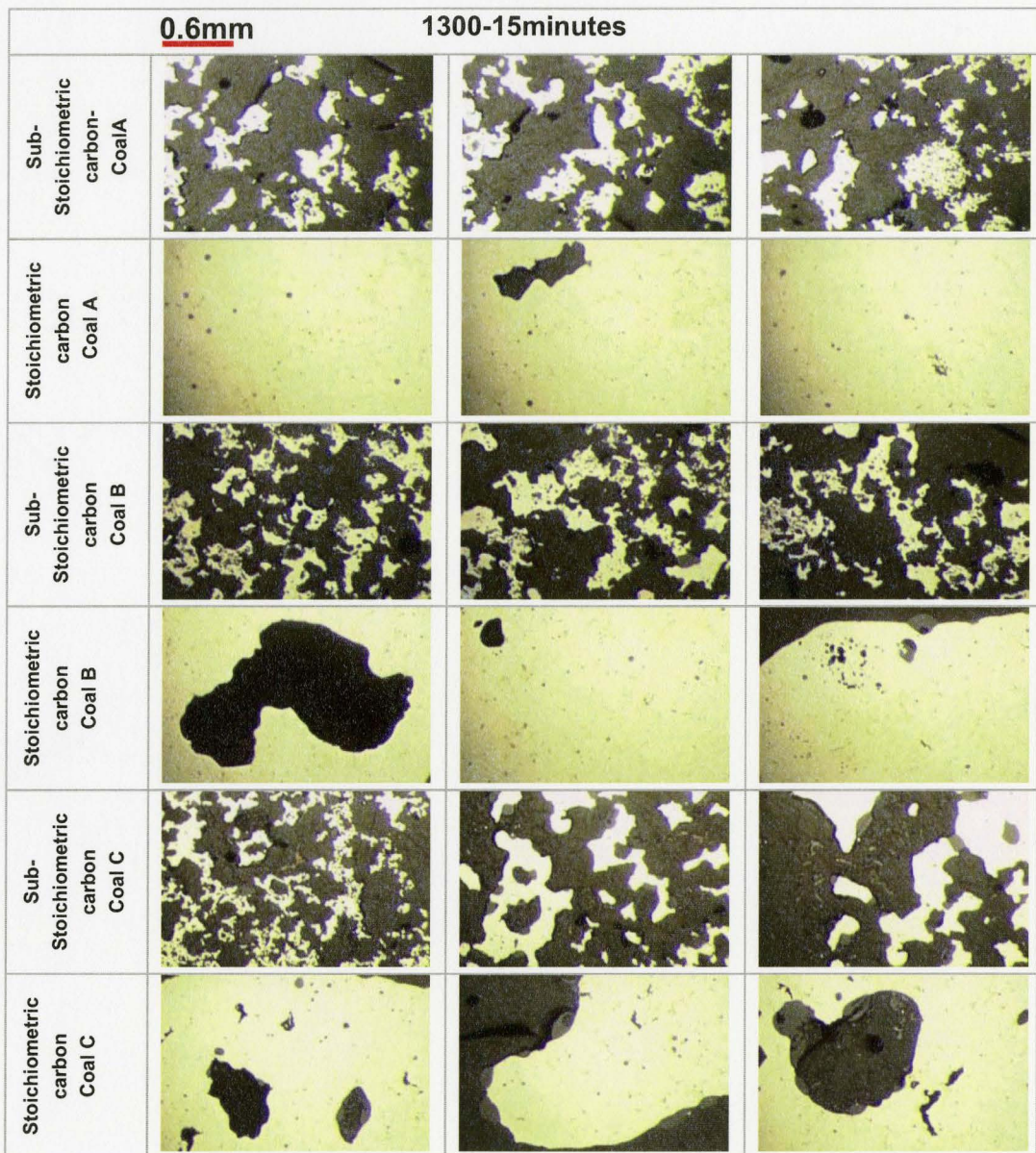


Figure 2- 8- Samples reacted at 1300C for 15min

As seen in Figure 2- 3 also figures 7-1 and 7-2 in the appendix, the overall images of the samples with sub-stoichiometric coal at 1300C,1325C,1350C and all time intervals tested show similar sponge iron structure, the microstructures of these samples (example at 1300C, sub-stoichiometric samples Figure 2- 6 to Figure 2- 8) shows solid state sintered iron structure. It can be seen that solid particles have coalesced and formed networks. In samples reacted for longer times, (Figure 2- 8, coalC, sub-stoichiometric, 15 minutes), coarsening of iron and exudation of slag droplets (right image) from the iron grains can be seen.

According to Figure 2- 4, 5 minute samples at 1300C, show a sponge iron structure with no melting. However images of 10 minute samples reveal partial melting in samples with coal A and C, and full melting of iron and phase separation of slag from iron for samples with coal B. The same trend exists between 10 minutes samples at 1325C and 1350C. There are some differences between samples of different temperatures. For example sample with coal C reacted for 10 minutes shows more melting at 1325C than 1350C, (figure 7-3 in the appendix and Figure 2- 5). These are due to inconsistencies caused by the sources of error in the procedure as is explained in section 2.9. It was tried to minimize this sources of error while performing the main series of experiments later by developing experimental skills.

Samples being reacted for 15 minutes show full melting at 1325C and 1350C, (figures 7-6 and 7-9 in the appendix). At the same period of 15 minutes at 1300C, samples with coal A and B, show full melting and slag separation but sample with coal C shows uneven shape which means sample was densifying but not yet fully melted.

Images of the microstructures of the stoichiometric samples at 1300C for 5 minutes in Figure 2- 6, show that all samples have porous sintered structures. Images of sample with coal B shows coarser iron grains. According to Figure 2- 7, increasing the reaction time to 10 minutes lead to slight coarsening of sub-stoichiometric samples. However, samples with stoichiometric coal show high degree of coalescence and slag separation.

In Figure 2- 7, it can be seen that in sample with coal A and stoichiometric carbon, coarse grains of iron has formed, with coal B, iron has fully densified and slag separated as droplets on the surface and with coal C grains are coarser and separated droplets of slag can be seen. The same type of samples after 15 minutes have greatly densified and big porosities can be seen in the iron cross section. Figures 7-4 to 7-9 in the appendix show images of samples reacted at 1325C and 1350C. For sub-stoichiometric samples no major difference is seen between 1325C, 1350C and 1300C samples in the microstructure except the slight coarsening of the porous sinter. But for the stoichiometric samples it can be seen that 5 minutes samples at 1325C show high degree of coalescence and phase separation and samples reacted for 10 minutes show full densification.

2.8. Conclusions from Initial Experiments

- In samples with sub-stoichiometric coal
 - o Sponge iron structure remained in all temperatures and times tested.
 - o At longer times, the grains in the microstructure slightly coarsened to $\sim 300\mu\text{m}$.

- In samples with stoichiometric coal
 - o Samples with different coal types, show different degrees of melting and phase separation at a certain temperature and time (Figure 2- 4, 1300C, 10 and 15 minutes).
 - o Even at temperatures as low as 1300C, full densification of the iron and separation of iron and slag was seen in 15 minutes (example Figure 2- 7 ,stoichiometric coal B).
 - o The presence of uneven surfaces in dense iron (stoichiometric samples in Figure 2- 8), shows that iron was densified but was probably not fully liquid as many surfaces were not perfectly rounded and seen to be irregular. This suggests that more densification in these samples might not be the result of more carburization and liquid iron formation, but the effect of more slag present resulting from higher ash content.
 - o At this stage of the study there is still uncertainty as to which of the two variables carbon or slag has more influence on the melting behavior. Coal types with different carbon, volatile matter and ash, may not be the best choice of variable. It might be more useful to study the effects of carbon and slag by separate experiments in which one (carbon or slag) varies and the other is kept constant.

- It was decided that it would be more suitable to use pellets of coal-ore composites instead of using alumina crucibles to eliminate the problems associated with material sticking to crucible wall, reaction of slag with alumina, and difference in heat transfer rates due to difference in crucible thickness.

2.9. Sources of Error

- The stoichiometric coal was calculated using fixed carbon only. It was assumed that volatile matter did not contribute in reduction.
- After putting samples in the furnace, temperature fell rapidly as the furnace door was opened and took 1-2 minutes to reach the adjusted temperature. In order to reach the desired temperature more quickly after putting the samples into the furnace, the initial temperature was adjusted to 50 degrees higher, so that the temperature compensation time to desired temperature after opening the furnace door could be shortened.

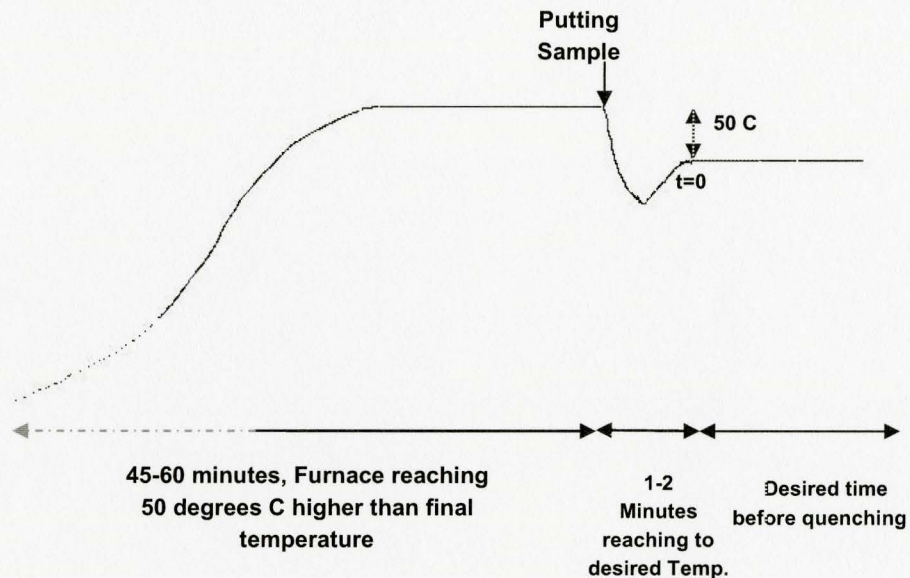


Figure 2-9-Schematic showing the times required for the furnace to reach the desired temperature

- Due to variation in procedure and the limitations of the furnace design, there may be 1-2 minutes error in samples heating time. At the time immediately after closing the furnace door temperature of the furnace fluctuates to $\pm 10^\circ \text{C}$.
- Samples might be slightly oxidized when they are taken out of the furnace.

- The refractory crucibles and trays delay the heat transfer to sample.
- The dimensions of the crucibles, including diameter, height and thickness were not uniform, for this reason heat transfer rates may vary.
- During heating, some material from the mix adhered to the crucible wall which caused errors in the final weights measured.
- The dimensions of the crucibles, including diameter, height and thickness were not uniform, for this reason heat transfer rates may vary.
- During cutting and polishing the samples, some pieces of sample especially slag separates from the sample and was washed away .This could influence the judgment on the amount of liquid slag.

Chapter 3

3. Main Series of Experiments: Changing Slag Composition and Content

3.1. Experiments

The objective of the main series of experiments was to investigate the influence of gangue, ash composition and ash content on the melting behavior of coal ore composites.

In these series of experiments, SiO_2 , Al_2O_3 and CaO were the components of oxide additions, as SiO_2 and Al_2O_3 are the major components of iron ore gangues and coal ashes and CaO is usually used as flux. The CaO/SiO_2 ratio which controls the melting point was chosen to be the main variable. Al_2O_3 was kept at 15Wt% of the SiO_2 - CaO - Al_2O_3 slag system. The other variable changed was the weight percent of total slag present in the composite. The experiments were done at a single temperature 1310C and 3 time intervals 6,8,10 minutes.

All other variables such as temperature, ore type, coal type, carbon ratio, particle size, sample size, sample shape, bulk density were kept constant and investigating their influence was out of the scope of this work.

3.1.1. SiO₂-CaO- Al₂O₃ System

According to Matsumura [19], the onset of melting in heating experiments of coal ore composites is when a low melting point slag of SiO₂, CaO, and Al₂O₃ forms. In this study it was decided to keep Al₂O₃ constant and change SiO₂ and CaO contents to produce slags with different melting points.

In the ternary phase diagram of SiO₂-CaO-Al₂O₃, Figure 3- 1, it can be seen that along the 15%Al₂O₃ line, it is possible to produce slags with different melting points including regions of low melting points. For more accurate prediction of melting points, FACT software was used and it was predicted that when Al₂O₃ is kept constant at 15Wt%, and CaO weight percent is changed to 10, 30 and 50, the melting point of slags are 1525C, 1275C and 1500C respectively. It was decided to make samples with the constant coal/ore ratio and alumina content (15wt%), but different CaO contents of 10, 30 and 50 weight percents, which gives CaO/SiO₂ ratios of 0.13,0.54 and 1.42 .

It would later be seen that the presence of FeOx will tend to lower the melting point of slag.

Table 3- 1- Change in melting points of the CaO-SiO₂-15%Al₂O₃ slag with compositions

	CaO wt%	SiO ₂ wt%	Al ₂ O ₃ wt%	Melting point (C)
1	10	75	15	1525
2	30	55	15	1275
3	50	35	15	1500

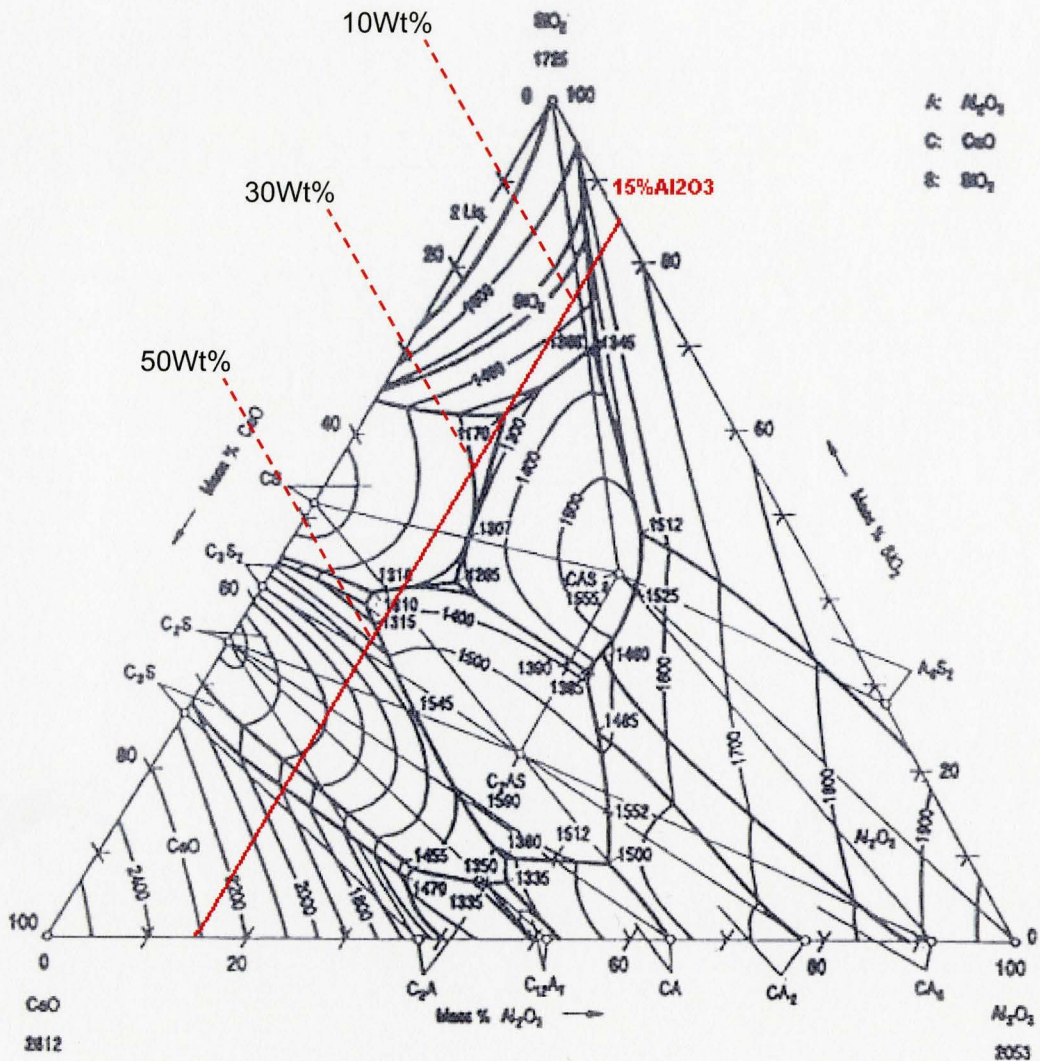


Figure 3- 1-Ternary phase diagram of SiO₂-CaO-Al₂O₃ system[39]

3.1.2. Material Preparation

In these series of experiments the reference composite (with no addition of slag forming oxides) was made based on the stoichiometric coal (coal needed for 100% reduction) from iron ore and coal A.

Table 3- 2-Composition of ore used in the second series of experiments

Fe ₃ O ₄ %	SiO ₂ %	Al ₂ O ₃ %	MnO%	MgO%	CaO%	Na ₂ O%	K ₂ O%	TiO ₂ %	P ₂ O ₅ %	LOI%	Others%
97.24	0.82	0.10	0.10	0.22	0.42	0.01	0.01	0.02	0.01	0.33	0.72

Particle size distribution of coal and ore used was measured by particle size analyzer. A small powder sample (arbitrary quantity) in a container full of ethanol was put in the HORIBA CAPA700 particle analyzer machine. The result is shown in the diagram below:

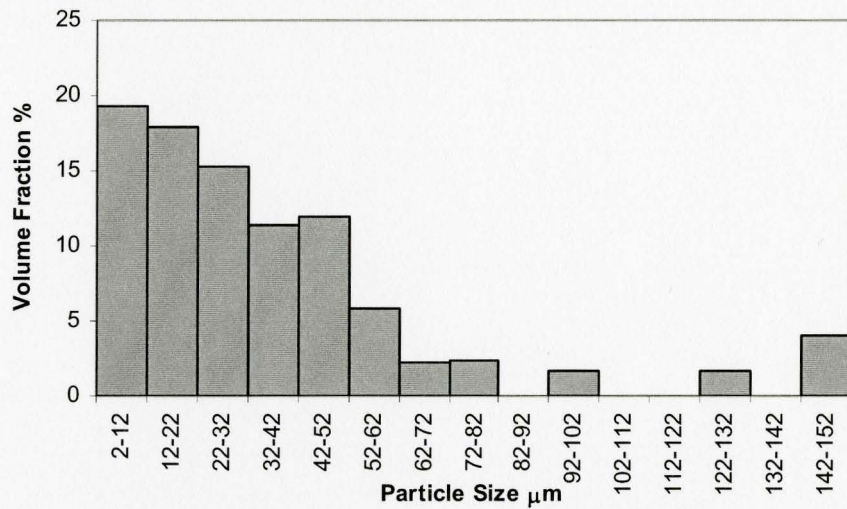


Figure 3- 2-Particle Size distribution of iron ore

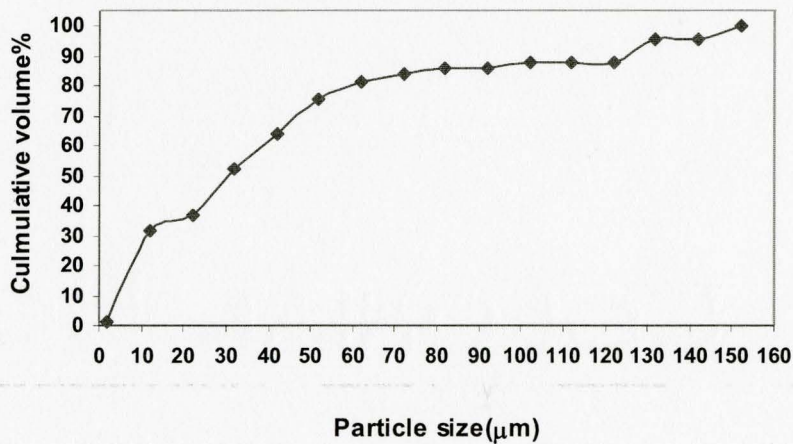


Figure 3- 3-Cumulative probability diagram of iron ore particle size

According to Figure 3- 3, for ore particles, $d_{10}=5\mu\text{m}$, $d_{50}=30\mu\text{m}$ and $d_{90}=125\mu\text{m}$.

Table 3- 3-Composition of Coal A used

VM%	Ash%	FC%	S%
19.33	6.768	73.91	0.81

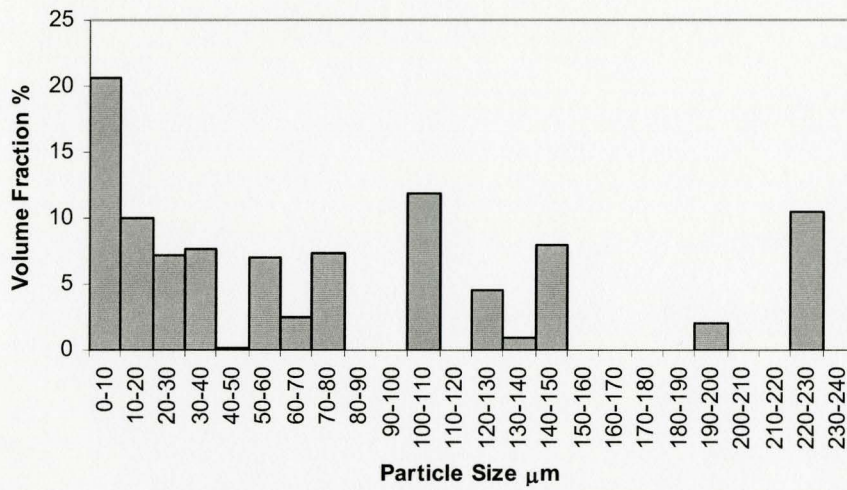


Figure 3- 4- Particle size distribution of coal

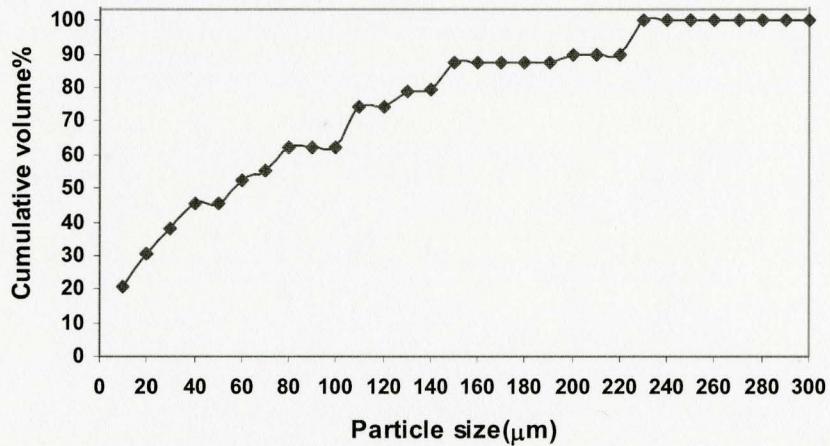


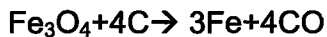
Figure 3- 5- Cumulative probability diagram of coal particle size

According to Figure 3- 5, for coal particles, $d_{20}=10\mu\text{m}$, $d_{50}=57\mu\text{m}$ and $d_{90}=200\mu\text{m}$.

Table 3- 4-Composition of Ash in coal used in the second series of experiments

SiO ₂ %	Al ₂ O ₃ %	Fe ₂ O ₃ %	MgO%	CaO%	K ₂ O%	Na ₂ O%	TiO ₂ %	MnO ₂ %	P ₂ O ₅ %	BaO%	SrO%
50.27	29.54	8.93	1.11	2.07	2.09	0.62	1.35	0.05	0.05	0.14	0.13

Based on the overall reduction reaction:



And the composition of the coal and ore from which the composite was made, for each 100grams of ore the calculated coal needed for reduction would be 27.22 g.

The contribution of both carbon and hydrogen in volatile matter was not considered in the calculations of coal needed as the composition of volatile matter was not given.

The composition of non-ferrous oxides in the composite is provided in table below:

Table 3- 5- Composition of composite gangue and ash

SiO ₂ %	Al ₂ O ₃ %	CaO%	MgO%	MnO%	Na ₂ O%	K ₂ O%	TiO ₂ %	P ₂ O ₅ %	Total gangue+Ash %
1.37	0.50	0.36	0.19	0.08	0.01	0.03	0.03	0.01	3.7

The objective in material preparation was to add additional oxides to the stoichiometric composite (composite with coal for 100% reduction) to make samples with slags (formed from gangue, ash and additional oxides) of different CaO/SiO₂ ratios. Alumina was kept constant at 15Wt% in CaO-SiO₂-Al₂O₃ system. CaO was changed to 10, 30 and 50 Wt% which gives CaO/SiO₂ ratios of 0.13, 0.54, and 1.42. For each CaO/SiO₂ composition the total slag content (considering the ash and gangue already present) was also changed to 5Wt%, 10Wt% and 15Wt%.

Table 3- 6- Samples

	CaO/ SiO ₂ =0.13	CaO/ SiO ₂ =0.54	CaO/ SiO ₂ =1.42
Total gangue and ash 5 Wt %	Sample 1	Sample2	Sample3
Total gangue and ash 10 Wt %	Sample 4	Sample 5	Sample 6
Total gangue and ash 15 Wt %	Sample 7	Sample 8	Sample 9

Table 3- 7-The weight percent of additional CaO, SiO₂ and Al₂O₃ in 100grams of each composite batch

	Batch1	Batch 2	Batch3
CaO	0.05	0.88	1.72
SiO ₂	1.75	0.91	0.08
Al ₂ O ₃	0.11	0.11	0.11
Raw(ore+coal)-mix	100	100	100
	Batch4	Batch 5	Batch6
CaO	0.62	2.58	4.55
SiO ₂	6.00	4.03	2.06
Al ₂ O ₃	0.96	0.96	0.96
Raw(ore+coal)-mix	100	100	100
	Batch7	Batch 8	Batch9
CaO	1.25	4.48	7.72
SiO ₂	10.74	7.51	4.28
Al ₂ O ₃	1.91	1.91	1.91
Raw(ore+coal)-mix	100	100	100

3.1.3. Mixing

After adding the oxides to the stoichiometric mix of iron ore and coal according to table Table 3- 7, powders were well mixed by pestle and mortar followed by "Cone and Quarter" technique to make powder mixes as uniform as possible.

3.1.4. Pellet Making

In these series of experiments one gram pellets were made and put on zirconia tray instead of loose powder in crucible to avoid slag reacting with the alumina crucible wall. Pellets of 1g weight and about 0.8 mm diameter were made from each of the 9 batches. Each pellet was made by hand after spraying a small amount of water on the powder. Green pellets were kept at 100C for 24 hours to be dried.

3.1.5. Heating

Pellets were placed on a porous zirconia tray (grade ZAL45) and each pellet was covered with a graphite cap. The trays were placed into furnace already hot. Control temperature was 1310C. The heating times were 6, 8 and 10 minutes.

3.1.6. Cooling

After heating, pellets were transferred to desiccators and kept under argon gas flow to minimize re-oxidation of the samples.

Chapter 4

4. Results and Discussion

The results from characterizations are presented in this chapter. The characterizations include Optical Microscopy, Energy Dispersed X-ray analysis (EDX), Leco carbon and sulfur analysis on metal and simultaneous Differential Thermal Analysis and Thermo Gravimetric Analysis. In this section also the experimental results showing the influence of slag composition and weight percent on the melting behavior of coal ore composites are discussed. The results show significant role of slag in the carburization, densification and separation of iron from slag.

According to experimental results, each CaO/SiO₂ ratio used caused a different melting behavior. It is also revealed that the type of slag significantly influence the degree of reduction and separation of iron and slag.

As shown in the previous chapter, pellets with 3 different CaO/SiO₂ weight ratios (0.13, 0.54, and 1.42) each in 3 slag weight percents were heated at 1310C for 6, 8 and 10 minutes.

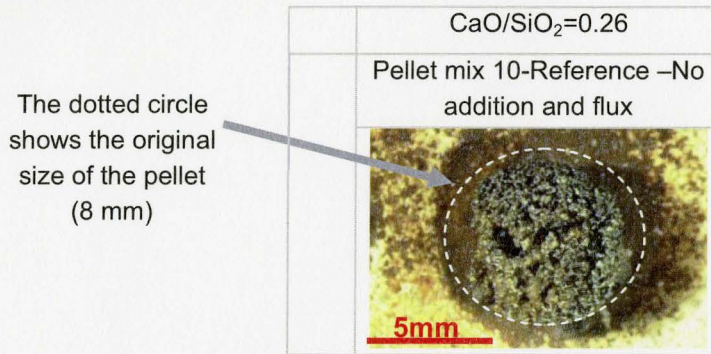
Quenched pellets after 6 and 8 minutes showed quite similar degrees of densification and melting, but most pellets showed high densification and melting after 10 minute. That is why comparison is made between the pellets only after 8 and 10 minutes.

4.1. Low Magnification Microscopy

In this section results from optical microscopy are presented. A stereo microscope was used to take pictures of the whole pellet at a magnification of 6.5X. The results are shown in Figure 4- 1 to Figure 4- 3. The stereo microscope used was WILD M3C.

After mounting, cutting and polishing, images of the whole cross-sections were taken at a 10X magnification. Cross-sectional images are shown in Figure 4- 4 and Figure 4- 5.

Temperature: 1310C,
 Substrate: Zirconia
 Lens Magnification: 6.5X




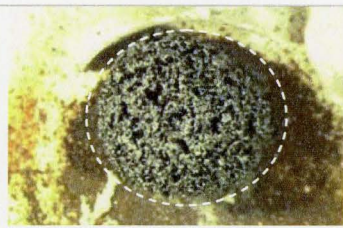
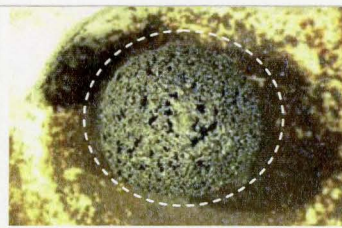
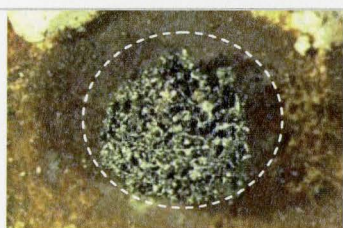




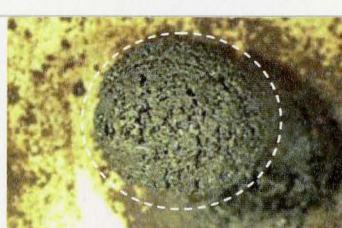
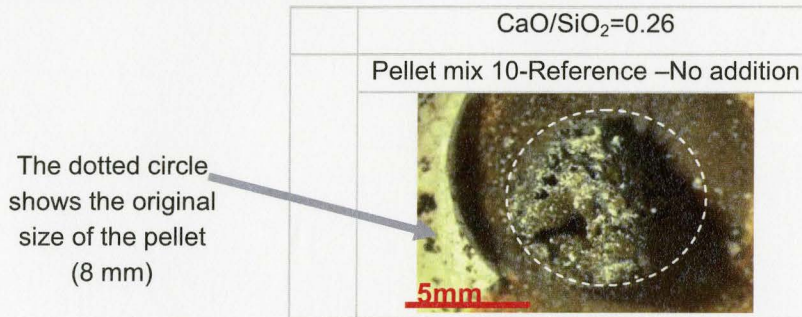
	CaO/SiO ₂ =0.13	CaO/SiO ₂ =0.54	CaO/SiO ₂ =1.42
	Pellet mix1	Pellet mix2	Pellet mix3
Total gangue+ash 5Wt%			
	Pellet mix 4	Pellet mix 5	Pellet mix 6
Total gangue+ash 10Wt %			
	Pellet mix 7	Pellet mix 8	Pellet mix 9
Total gangue+ash 15Wt %			

Figure 4- 1-Images of pellets heated for 6 minutes

Furnace temperature: 1310C,

Substrate: Zirconia

Lens Magnification: 6.5X



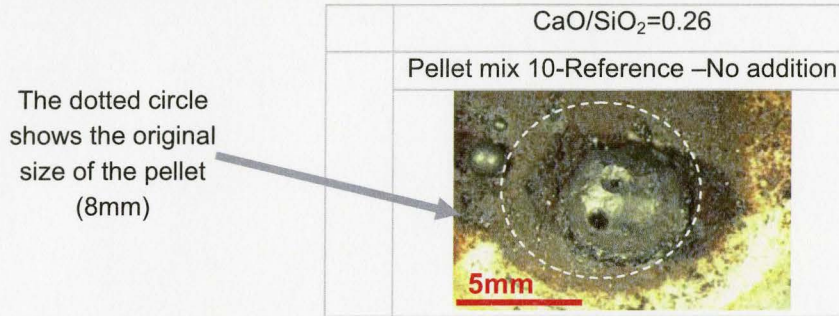
	CaO/SiO ₂ =0.13	CaO/SiO ₂ =0.54	CaO/SiO ₂ =1.42
Total gangue+ash 5Wt %	Pellet mix1 	Pellet mix2 	Pellet mix3
	Pellet mix 4 	Pellet mix 5 	Pellet mix 6
	Pellet mix 7 	Pellet mix 8 	Pellet mix 9
Total slag 10 Wt %			
Total gangue+ash 15Wt %			

Figure 4- 2- Images of pellets heated for 8 minutes

Furnace temperature: 1310C,

Substrate: Zirconia

Lens Magnification: 6.5X



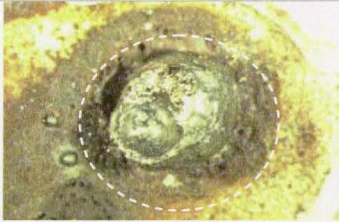
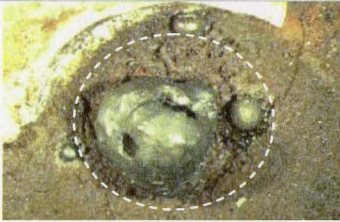
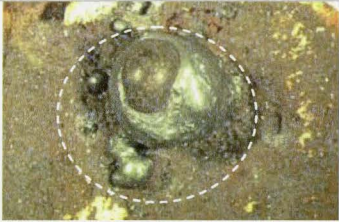



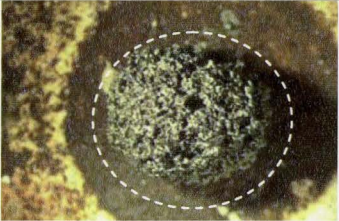
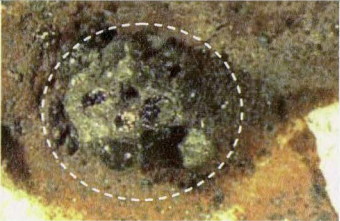
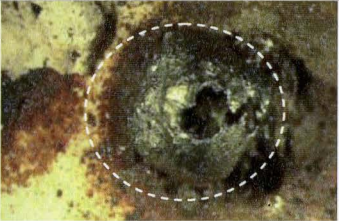
	$\text{CaO/SiO}_2=0.13$	$\text{CaO/SiO}_2=0.54$	$\text{CaO/SiO}_2=1.42$
Total gangue+ash 5Wt%	Pellet mix1	Pellet mix2	Pellet mix3
			
Total gangue+ash 10Wt%	Pellet mix 4	Pellet mix 5	Pellet mix 6
			
Total gangue+ash 15Wt%	Pellet mix 7	Pellet mix 8	Pellet mix 9
			

Figure 4- 3- Images of pellets heated for 10 minutes

Furnace temperature: 1310C,

Substrate: Zirconia

Lens Magnification: 10X

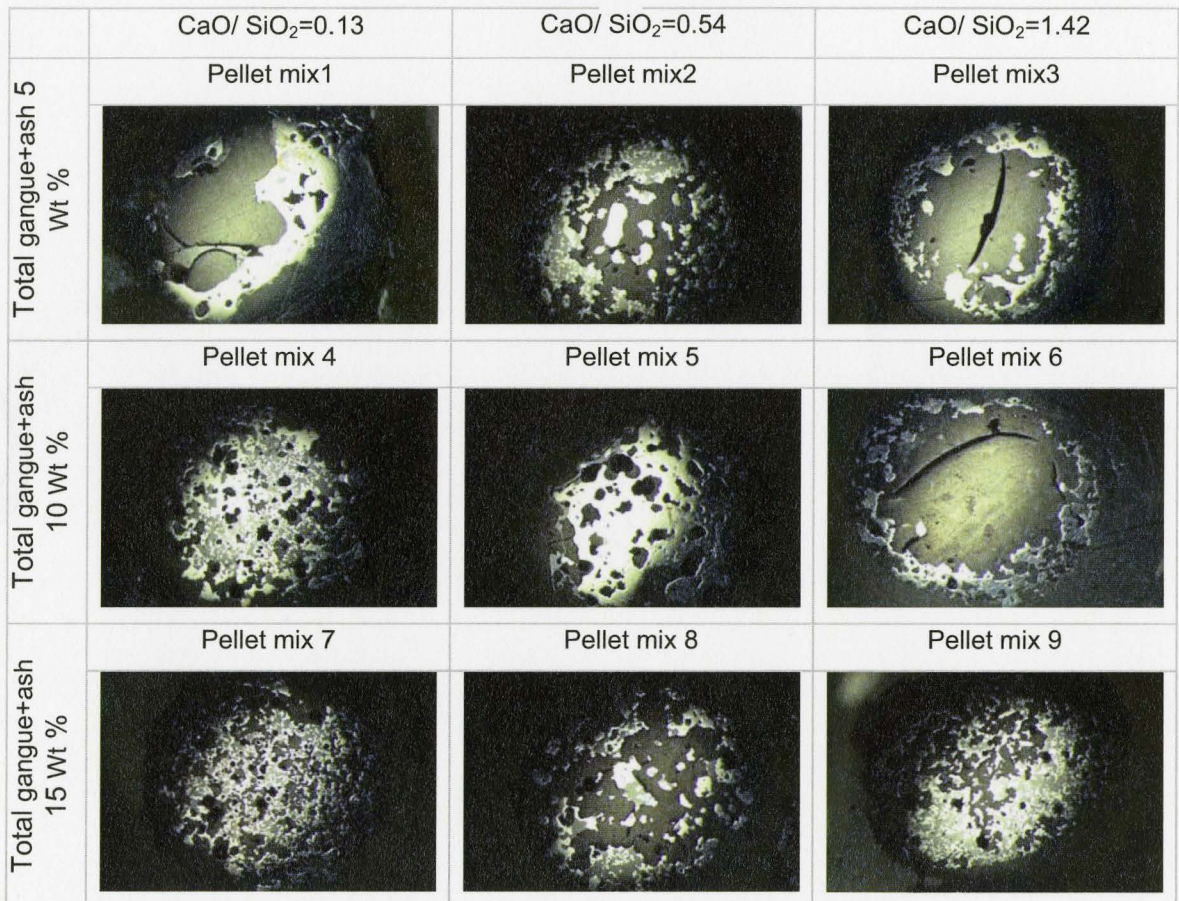
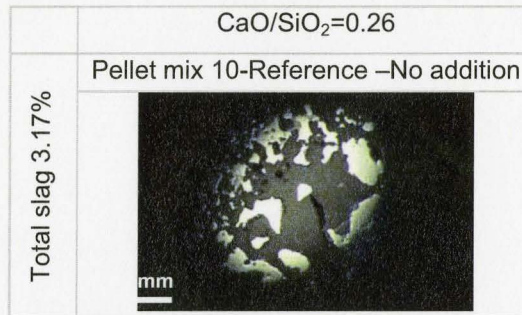


Figure 4- 4- Cross sectional images of pellets heated for 8 minutes

Furnace temperature: 1310C,

Substrate: Zirconia

Lens Magnification: 10X

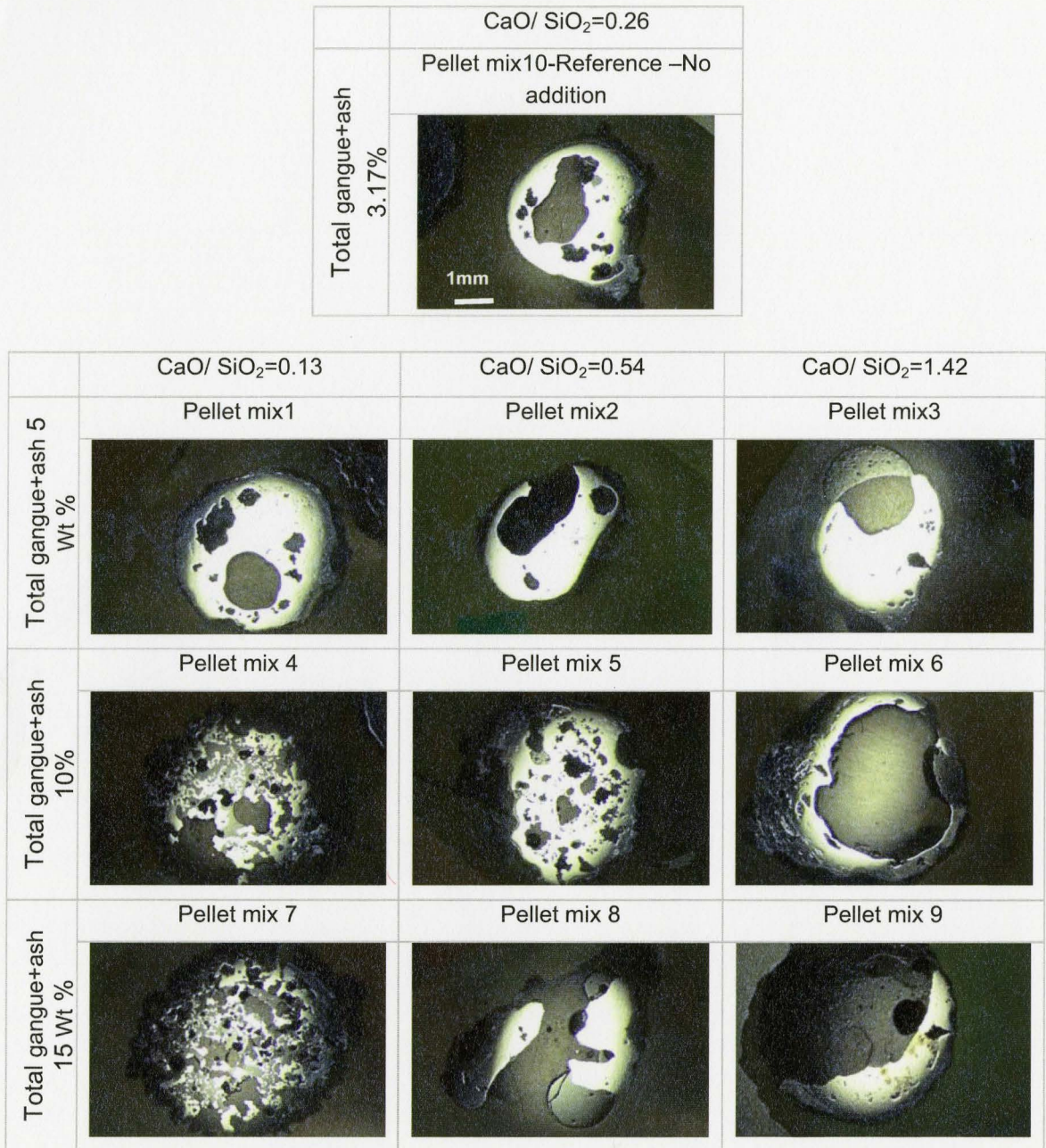


Figure 4- 5- Cross sectional images of pellets heated for 10 minutes

4.1.1. Higher Magnification Optical Microscopy on Polished Cross Sections and Energy Dispersed X-Ray Analysis (EDX)

In this section the pellet images at low magnification is combined with higher magnification images to show details. Microscope used was Leitz Metalloplan.

In the following images “**M**” stands for metallic iron phase, “**S**” stands for slag, and “**R**” represents mounting resin. To avoid confusion in some images the letter “**P**” is used which represents porosity.

The polished cross sections of the pellets were analyzed by Scanning Electron Microscope (SEM) after sputtering with gold for conductivity for Energy dispersive X-ray analysis (EDX).

EDX analysis was performed on several points on slag phase for each pellet. The elements selected were Si, Ca, Al, Mg, Mn, Fe, and oxygen. Other elements were ignored in the analysis since their quantities in slags were quite small.

Based on the stoichiometric oxygen in the related oxides, the composition of oxides in slag for the points being analyzed is tabulated. The results of the EDX analysis are also shown in this section.

Pellet 1: CaO/SiO₂=0.13, 5Wt% gangue and ash, 1310C

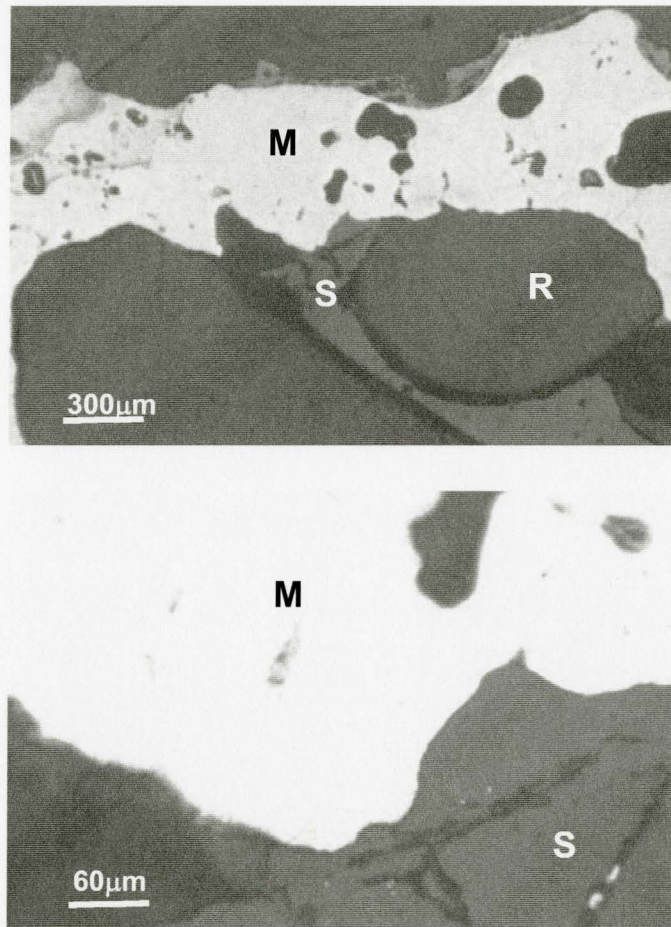


Figure 4- 6- Pellet 1, CaO/SiO₂=0.13, 5Wt% gangue and ash, 1310C, 8min

Figure 4- 6 shows the structure formed from initial particles of iron ore where about 85% of particles were smaller than 70 micron. It is evident that the prereduced iron formed from many particles of ore formed a continuous metal phase and densified to give the structure shown. A simple calculation for the metal phase shown in Figure 4- 6 indicates that probably ~3000 ore particles have contributed to form the continuous metal phase shown.

The process by which a continuous densified metal phase formed include, (a) diffusion to form bonds between particles, (b) repacking due to surface tension driven effects of a molten slag phase and (c) partial melting to form a mushy phase.

It should be noted that melting can be the result of temperature rise and/or carburization. Slag is known to play an important role in carburization.

Figure 4- 7, shows that at 10 minutes,

- The metal is free of slag.
- The slag wets the surface of the metal.

For a view of the changes in the cross section of the whole pellet refer to Figure 4- 4 and Figure 4- 5. It is also apparent that during densification liquid slag is exuded out of the iron structure to leave slag free iron which is a very important mechanism.

In this pellet, quenched from 1310C after 8 minutes, compared to other two pellets with the same quantity of slag and higher CaO/SiO₂ ratios, more densification was observed but also iron loss by slag was high (Figure 4- 2 and Figure 4- 4).

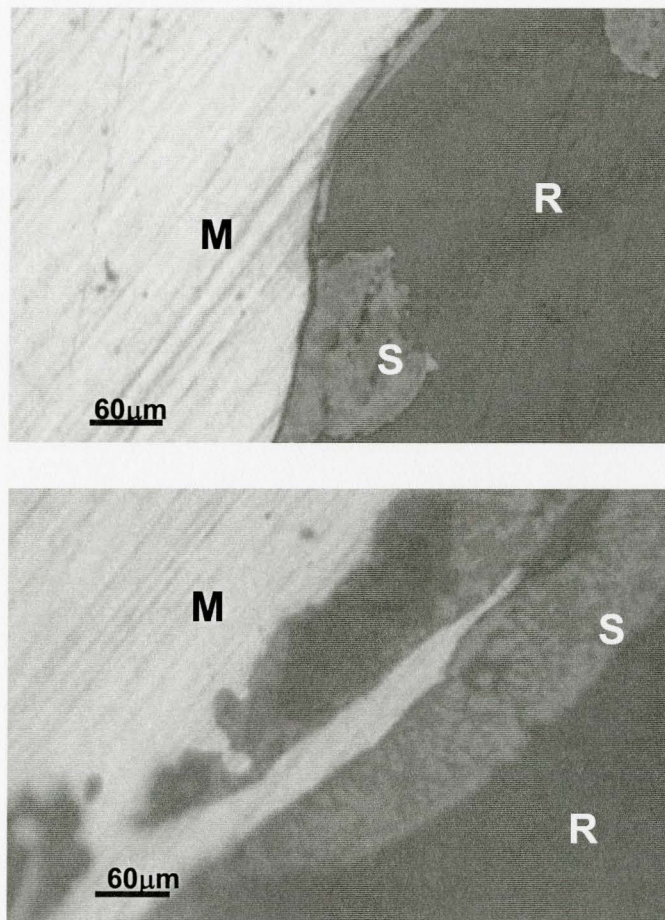


Figure 4- 7- Pellet 1, CaO/SiO₂=0.13, 5Wt% gangue and ash, 1310C, 10min

EDX analysis of slag (Table 4- 1) showed the formation of a silicate slag in 8 minute pellet. It also shows the increased amount of FeO in these slags in 10 minutes pellet. This indicates that there has been a barrier to FeO reduction and also by passage of time more FeO has dissolved in slag. The barrier could have been formation of non-reducible iron-silicate slag phases such as fayalite.

Table 4- 1-EDX-results, pellet 1, CaO/SiO₂=0.13, 5Wt% gangue and ash, heated at 1310C

	8 minutes					10 minutes				
	Point1	Point2	Point3	Point4	Point5	Point1	Point2	Point3	Point4	Point5
MgO	1.74	4.09	4.9	4.47	5.09	3.8	1.85	1.32	2.3	2.59
Al ₂ O ₃	2.5	10.51	11.04	10.26	9.87	52.6	7.88	9.35	15.37	15.65
SiO ₂	14.8	65.4	67.69	55.36	52.4	3.4	30.86	31	39.13	39.67
CaO	2.15	6.86	7.2	6.09	5.9	0.9	3.89	4.64	5.33	5.95
MnO	4.47	1.63	1.66	1.51	1.1	0.62	0.45	1.25	1.21	1.17
FeO	74.35	11.51	7.5	22.31	25.63	38.67	55.07	52.43	36.65	34.97
CaO/SiO ₂	0.15	0.10	0.11	0.11	0.11	0.26	0.13	0.15	0.14	0.15

Pellet 2: $\text{CaO}/\text{SiO}_2=0.55$, 5Wt% gangue and ash, 1310C

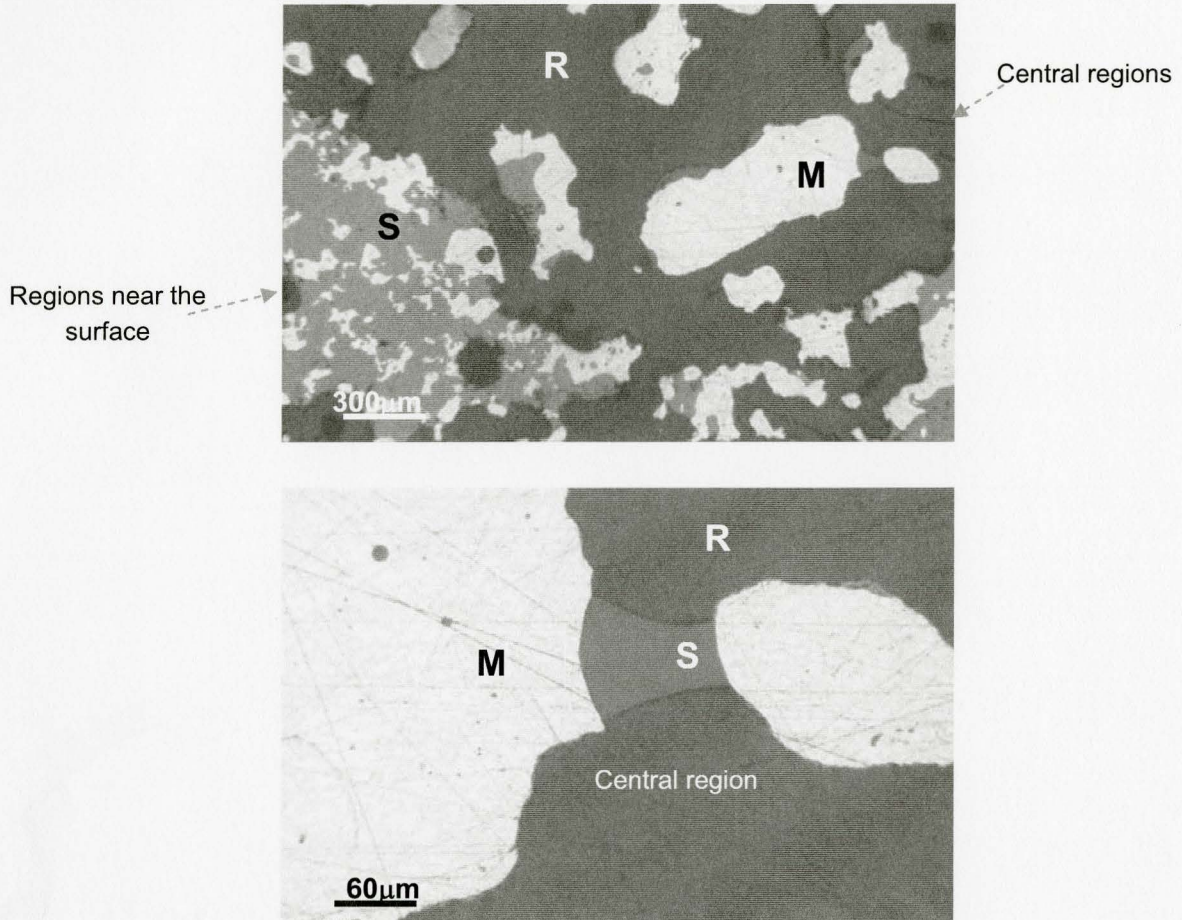


Figure 4- 8-Pellet 2, $\text{CaO}/\text{SiO}_2=0.55$, 5Wt% gangue and ash, 1310C, 8min

Images of 8 minute pellet in Figure 4- 8, show that the morphology near the surface is different from the morphology in central regions.

The microstructure near the surface shows minor coarsening of iron and higher ratio of slag to iron. It can also be seen that the solid sintered iron structure has been fully wetted by slag.

In central regions a few isolated coarse grains of iron can be seen, these iron grains are shown to be separated from slag (only partially wetted by slag) and located in the middle of a void area. The slag seen in the central regions is darker than the slag in the locations near the surface showing that the compositions of these two slags are different.

The EDX (Table 4- 2) of 8 minute pellet was done on slag in the center with darker color (point 1 and 2, 8 min) and slag near the surface with lighter color, (point 3, 4, 5 of 8 min) showed that the slag in the central regions which was separated from iron had much lower amount of FeO than the slag near the surface.

The fact that iron sintered structure near the surface (must have formed in early stages of reduction in solid state) was filled with FeO rich slag, and also the fact that interior regions (except the center) was empty, brings the conclusion that FeO rich slag must have been moved from interior regions and penetrated to the sintered iron pores near the surface. The driving force could have been capillary force of iron porous structure. This shows that after certain progress of reduction in solid state, slag formed in the interior regions with still unreduced FeO.

However presence of remaining iron and slag in the center shows that when FeO rich slag formed in the interior regions and was absorbed to the iron sinter near the surface, a portion of composite remained in the core. The fact that darker slag in the core had very little amount of FeO shows that remaining iron oxide in the core had been reduced very rapidly compared to FeO in the part of slag which was penetrated to the sinter structure near the surface. It is possible that slag in the sintered structure near the surface blocked the escape of CO gas and therefore the central regions could have been reduced rapidly.

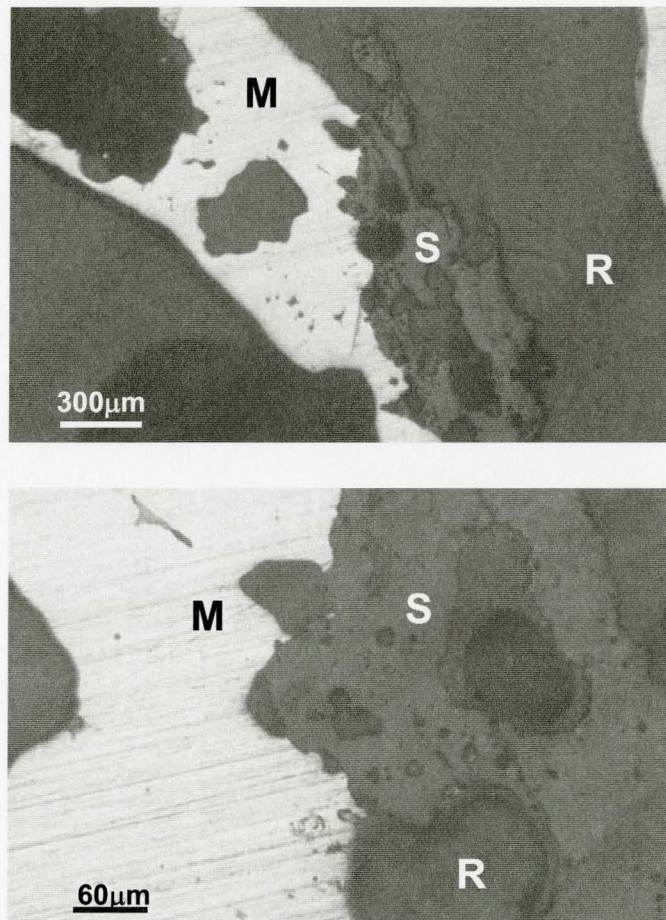


Figure 4- 9- Pellet 2, $\text{CaO/SiO}_2=0.55$, 5Wt% gangue and ash, 1310C, 10min

The cross sectional image of 10 minute pellet (Figure 4- 9, pellet 2) shows a dense metallic iron shell containing a few large cavities and a big void space inside. Slag was only seen on the surface. (Also see pellet 2 in Figure 4- 5).

Table 4- 2- EDX-results –pellet 2, CaO/SiO₂=0.55, 5Wt% gangue and ash, heated at 1310C

	8 minutes					10 minutes				
	Point1	Point2	Point3	Point4	Point5	Point1	Point2	Point3	Point4	Point5
MgO	4.32	3.25	0.54	0.64	1.64	4.41	4.64	4.47	5.09	5.34
Al ₂ O ₃	10.28	12.62	1	3.33	3.12	13.62	13.23	13.11	12.92	13.21
SiO ₂	46.98	43.83	1.92	11.59	10.53	49.13	49.73	49.56	49.87	49.93
CaO	19.06	16.72	1.07	4.21	2.98	29.36	29.36	30.07	29.69	28.97
MnO	1.26	1.17	0.14	0.36	0.18	1.37	1.26	1.26	1.39	1.57
FeO	18.1	22.4	95.33	79.87	81.55	2.1	1.78	1.53	1.07	0.98
CaO/SiO ₂	0.41	0.38	0.56	0.36	0.28	0.60	0.59	0.61	0.60	0.58

The EDX analysis of this final slag, Table 4- 2, also showed the composition to be relatively uniform in all points analyzed (FeO in most regions identified to be less than 2%). This analysis showed the slag to be rich in silica with about 13% Al₂O₃ and 30 %CaO.

Comparison of EDX results in 8 and 10 minute samples in Table 4- 2, shows that FeO reduction took place very rapidly and effectively. By reduction of FeO, iron structure was coarsened and densified. The presence of cavities in the iron and slag on the surface shows that after certain degree of metallization the slag drainage had occurred.

Exudation of slag to the surface could have been occurred by coarsening of iron structure which can be helped by gas pressure.

The behavior can be summarized in the following steps.

- Formation of a sponge iron structure during reduction
- Formation of the first liquid slag from gangue oxides and unreduced FeO and penetration of this slag to the iron sinter shell
- Reduction of FeO in slag
- Densification of the iron shell and exudation of slag to the surface and formation of large cavities in the iron.

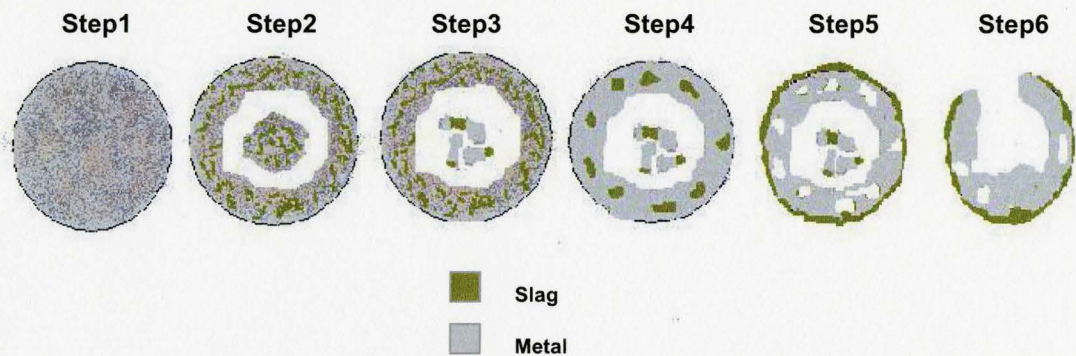


Figure 4- 10-Schematic showing the steps occurring in pellet 2

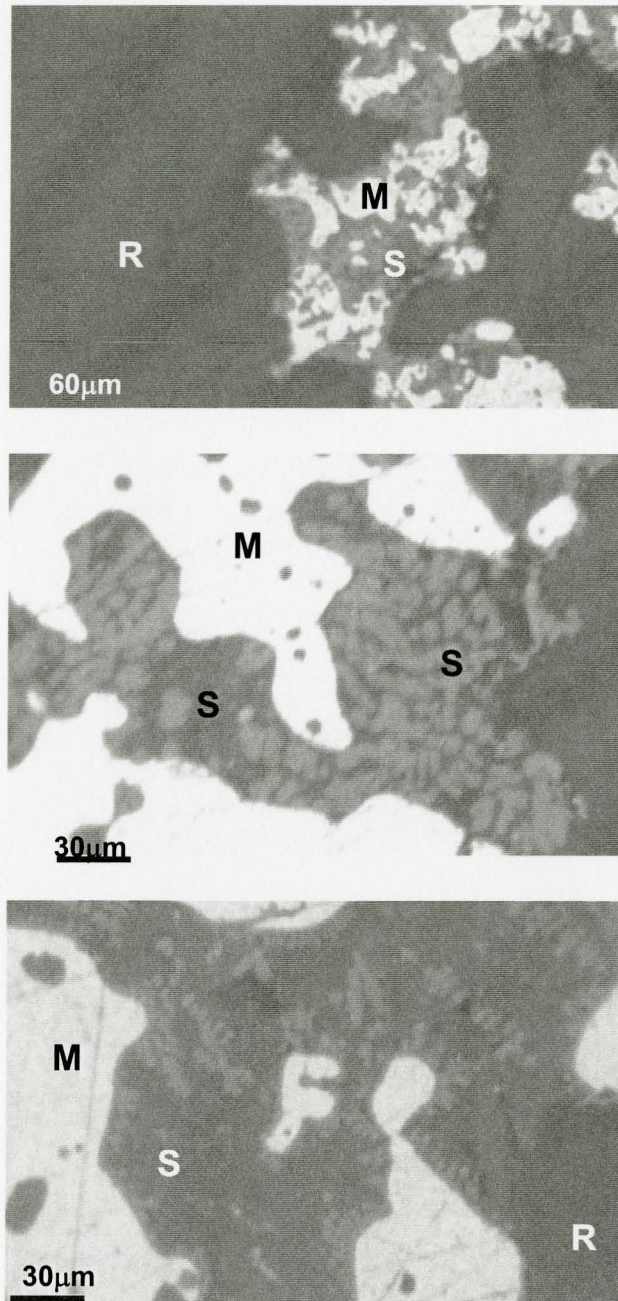
Pellet 3: $\text{CaO}/\text{SiO}_2=1.42$, 5Wt% gangue and ash, 1310C

Figure 4- 11- Pellet 3, $\text{CaO}/\text{SiO}_2=1.42$, 5Wt% gangue and ash, 1310C, 8min

Images of the 8 minute in Figure 4- 4 of pellet 3 shows that the pellet has maintained its spherical shape and a dense shell formed on the surface. Figure 4- 4 confirms that inside the pellet is completely empty.

Microstructure of the shell, Figure 4- 11, shows iron grains that are wetted by slag. At this stage slag contains two phases, EDX analysis results in Table 4- 3 shows the dendrites which have formed during cooling from the matrix phase to be FeO.

Table 4- 3- EDX-results - pellet 3, CaO/SiO₂=1.42, 5Wt% gangue and ash, heated at 1310C

	8 minutes					10 minutes				
	Point1	Point2	Point3	Point4	Point5	Point1	Point2	Point3	Point4	Point5
MgO	3.31	3.96	3.71	4.6	5	0.64	7.4	1.14	7.55	2.03
Al ₂ O ₃	1.56	9.14	11.11	0.64	0.69	41.54	12.49	54.7	13.7	4.04
SiO ₂	0.04	31.27	21.59	0.03	0.02	19.19	34.87	15.76	34.39	33.1
CaO	0.77	33.4	21.28	1.17	0.81	38.19	43.49	27.57	43.26	57.62
MnO	0.7	0.31	1.29	0.93	1.02	0.02	0.79	0.47	0.42	0.99
FeO	93.61	21.91	41.02	92.63	92.46	0.42	0.96	0.36	0.68	2.22
CaO/SiO ₂	19.25	1.07	0.99	39.00	40.50	1.99	1.25	1.74	1.26	1.74

The initial FeO rich slag must have been generated from still unreduced FeO particles and gangue and ash in the core of the pellet. This melt was penetrated into the regions near the surface by capillary force. When the slag formed in the core fills the iron sintered shell, the pores begin to disappear. The liquid FeO in slag is reduced to iron and leads to densification of the iron sinter and formation of a dense iron shell.

FeO in slag can be reduced by carbon particles. The other possibility is reduction of FeO in slag by carburized iron.

The final slag (with darker color compared to initial slag) unlike the primary slag has a very high interfacial tension. It separates from the iron shell and forms the minimum interfacial area with the iron shell which is shown in Figure 4- 12.

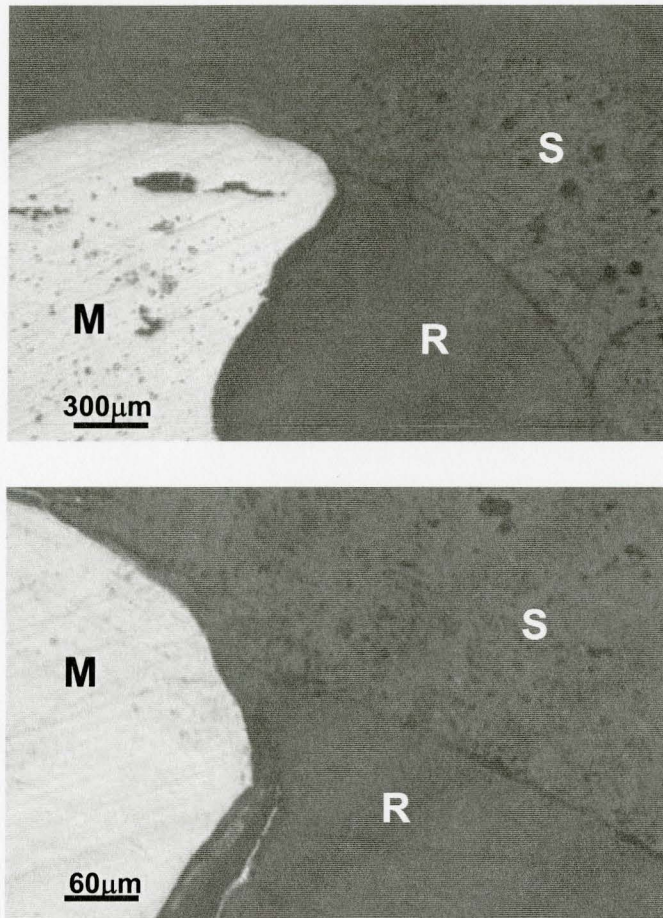


Figure 4- 12- Pellet 3, $\text{CaO}/\text{SiO}_2=1.42$, 5Wt% gangue and ash, 1310C, 10min

Images of 10 minute pellet, figure 4-12, (also pellet 3 in Figure 4- 5) show densification of the shell and separation of slag from it. Slag has formed the minimum interfacial area with iron.

The following diagram, Figure 4- 13, for the slag systems of CaO , FeO , SiO_2 and Al_2O_3 , can be useful in understanding the sudden change in the iron and slag interfacial tensions. According to this diagram, [39], the decrease in FeO quantity of slag can lead to a sudden increase in the interfacial tension and separation of slag from iron.

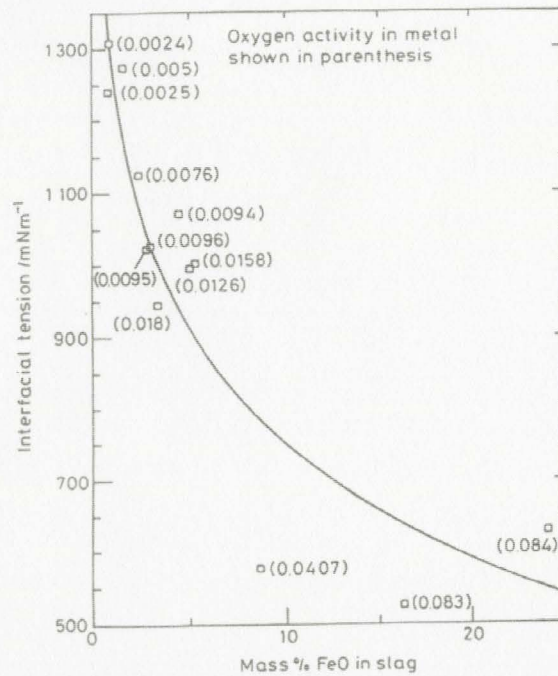


Figure 4- 13-General effect of variation in FeO content of various Al_2O_3 -CaO- SiO_2 slags on the interfacial tension with Iron [39]

Very high degree of FeO reduction in slag could be caused by high fluidity of slag (lower viscosity) and therefore efficient mass transfer in slag.

The following diagrams, Figure 4- 14, show the effect of FeO in lowering the viscosity of slag in CaO- SiO_2 -FeO-15% Al_2O_3 system. It is generally known that FeO reduces the viscosity by breaking the silica chains in slag. [39]

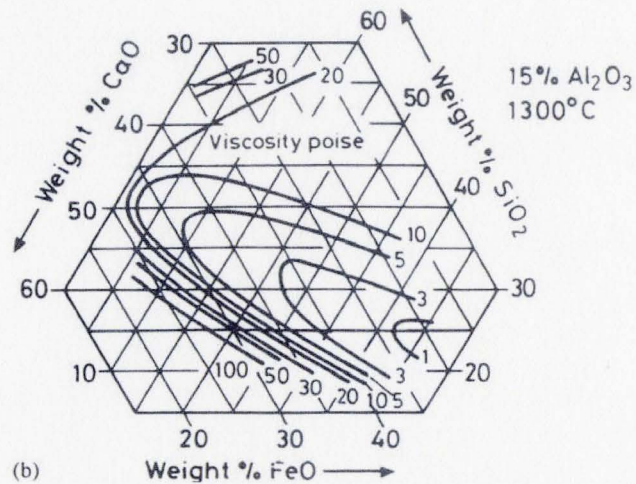


Figure 4- 14-Viscosities of $\text{CaO-SiO}_2\text{-Al}_2\text{O}_3\text{-FeO}$ slag systems [39]

The events occurring in this pellet can be summarized as following steps.

- Formation of a hollow sintered iron shell.
- Formation of a wustite rich melt in the core of the pellet.
- Penetration of the slag into the reduced iron shell by the capillary force.
- Reduction of FeO in slag and densification of iron shell.
- Separation of slag from iron.

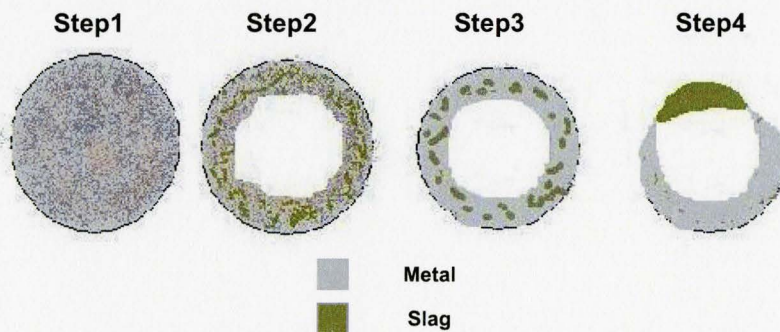


Figure 4- 15-Schematic showing the steps occurring in pellet 3

Pellet 4: $\text{CaO}/\text{SiO}_2=0.13$, 10Wt% gangue and ash, 1310C

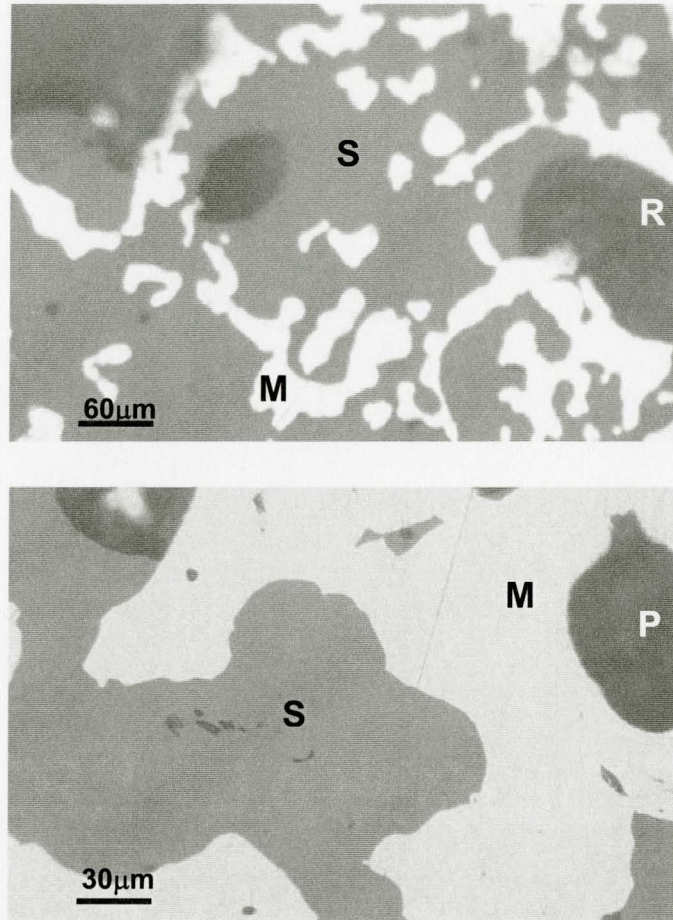


Figure 4- 16- Pellet 4, $\text{CaO}/\text{SiO}_2=0.13$, 10Wt% gangue and ash, 1310C, 8min

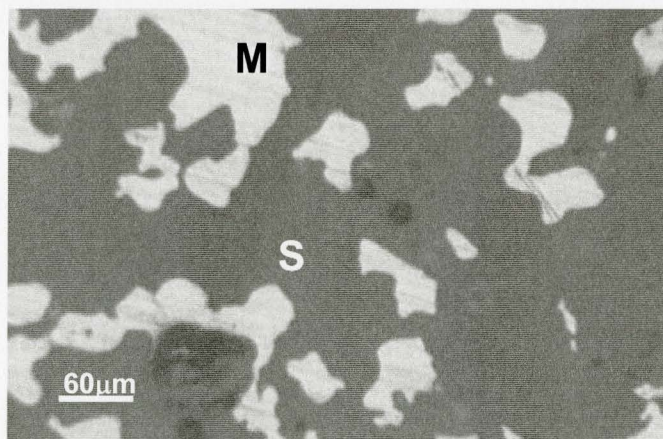
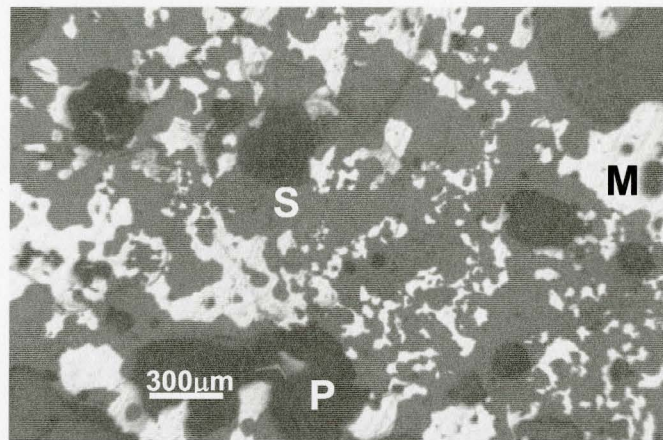
Cross-sectional image of 8 minute pellet (pellet 4 in Figure 4- 4 , also Figure 4- 16) shows the sponge iron structure and the slag that is distributed over the cross-section and highly wetted the iron sintered structure.

EDX analysis of slag at this stage (Table 4- 4) shows that silicate slag formed also contained FeO (~25-40%).

EDX analysis of 10 minute pellets (Table 4- 4) shows lower FeO content in final slag. This reveals that although FeO has been partially reduced but the reduction was not completed.

Table 4- 4- EDX-results - pellet 4, CaO/SiO₂=0.13, 10Wt% gangue and ash, heated at 1310C

	8 minutes					10 minutes				
	Point1	Point2	Point3	Point4	Point5	Point1	Point2	Point3	Point4	Point5
MgO	2	1.92	1.58	0.84	2	1.19	1.46	1.89	1.29	1.58
Al ₂ O ₃	9.56	10.07	7.69	8.08	7.96	12.72	11.27	14.13	10.72	12.48
SiO ₂	52.02	57.25	53.05	37.94	44.23	64.43	70.91	74.15	55.4	69.74
CaO	5.33	5.38	5.18	4.58	4.48	8.21	5.93	7.06	8.1	9.44
MnO	0.63	0.5	0.69	0.16	0.8	0.48	0.29	0.43	0.84	0.6
FeO	30.45	24.39	31.81	48.41	40.53	11.55	8.82	2	22.99	4.51
CaO/SiO ₂	0.10	0.09	0.10	0.12	0.10	0.13	0.08	0.10	0.15	0.14

**Figure 4- 17- Pellet 4, CaO/SiO₂=0.13, 10Wt% gangue and ash, 1310C, 10min**

In pellet 4 although iron grains in 10 minute pellet were slightly coarser than 8 minute pellet (see pellet 4 in Figure 4- 4 and Figure 4- 5), separation of slag from iron was not observed. Sponge iron structure which wetted by silicates slag kept its structure for all the 10 minute period of time.

The behavior seen in this type of pellet was also seen for pellet 7, (15Wt% gangue and ash) with the same CaO/SiO₂ ratio. It can be imagined that in this pellet the silica rich slag droplets were too viscous and highly wetted the particles that the coalescence of individual droplets was so difficult and slow. For this reason porous structure remained and reduction in solid state could progress to the center of the pellet and sponge iron structure was seen. However the residual FeO after 10 minutes is relatively high which shows that there was a barrier to efficient reduction. It is generally well known that the activity of FeO in silicate slags is low. Formation of non-reducible iron-silicate slag droplets, most probably fayalite can be the reason behind less reduction taking place in this pellet.

In this pellet also iron and slag could not be separated. This agrees with the fact that high silica content of slag would lead to a low interfacial tension between metal and slag (Figure 4- 18).

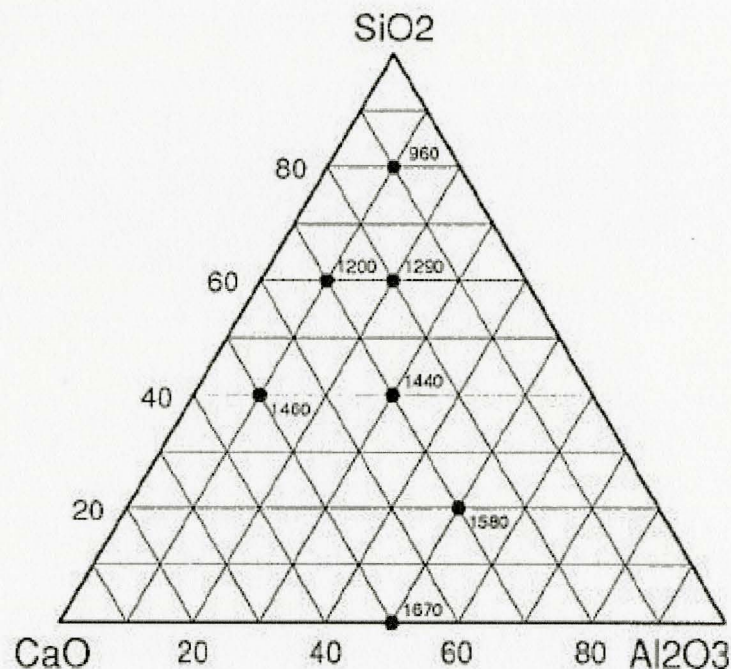


Figure 4- 18- Interfacial tension between liquid iron and liquid CaO-Al₂O₃-SiO₂ slags (mN/m) at 1550C, [33]

The following steps can be considered to have occurred for reduction-melting behavior of pellet 4 in 10 minutes.

- 1-Formation of a sintered iron structure due to reduction.
- 2-Formation of silica rich slag.
- 3-Partial reduction of FeO and coarsening of iron grains.

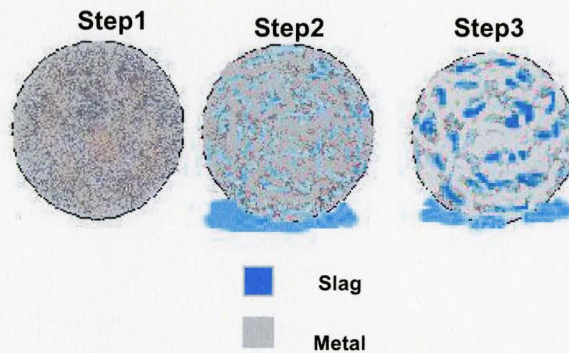


Figure 4- 19- Schematic showing the steps occurring in pellet 4

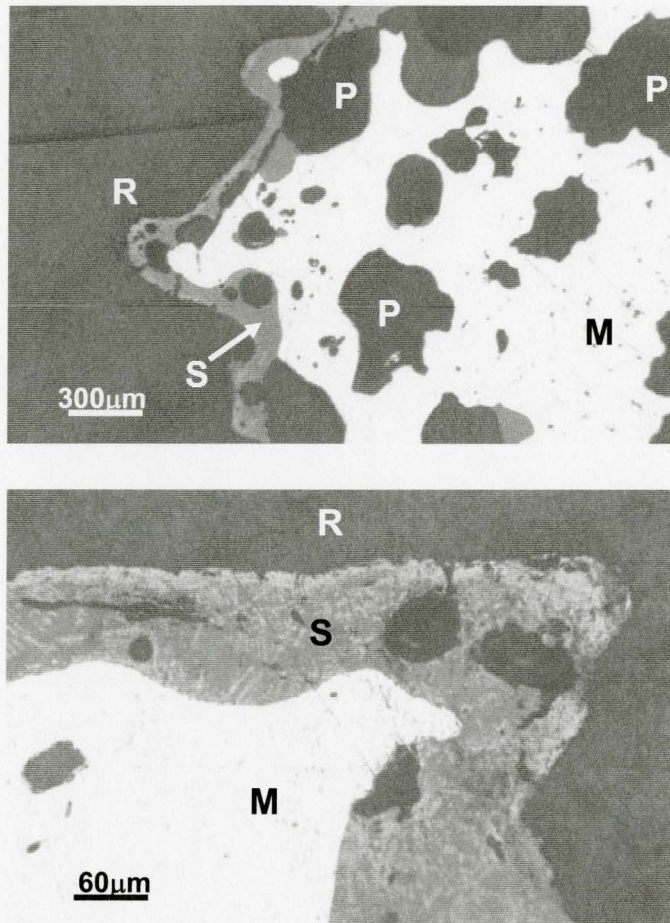
Pellet 5: $\text{CaO}/\text{SiO}_2=0.55$, 10Wt% gangue and ash, 1310C

Figure 4- 20-Pellet 5, $\text{CaO}/\text{SiO}_2=0.55$, 10Wt% gangue and ash, 1310C, 8min

Cross-sectional image of 8 minute pellet shows that slag has formed a layer on the surface and left big cavities inside (Figure 4- 20).

Table 4- 5- EDX-results - pellet 5, CaO/SiO₂=0.55, 10Wt% gangue and ash, heated at 1310C

	<i>8 minutes</i>					<i>10 minutes</i>				
	Point1	Point2	Point3	Point4	Point5	Point1	Point2	Point3	Point4	Point5
MgO	0.18	0.16	0.63	0.95	1.13	1.53	1.92	4.37	2.17	2.11
Al ₂ O ₃	8.3	8.34	9.43	8.53	6.38	13.12	13.49	13.33	13.72	13.71
SiO ₂	40.76	40.95	34	40.09	27.16	52.5	52.13	50.2	51.2	51.44
CaO	14.39	13.97	13	13.7	10.45	29.88	28.81	28.73	29.64	28.7
MnO	0.46	0.03	0.08	0.26	0.54	0.61	0.78	1.48	0.6	0.95
FeO	35.9	36.88	42.87	35.88	54.34	2.37	2.88	1.87	2.66	3.09
CaO/SiO ₂	0.35	0.34	0.38	0.34	0.38	0.57	0.55	0.57	0.57	0.56

The EDX analysis on 8 minute pellets, (Table 4- 5) show significant amount of FeO in this slag layer. Cross-sectional image of 10 minutes pellets does not show any significant change in pellet shape, except the slight densification of surface iron which is caused by reduction of FeO in slag layer.

The FeO amount in the final slag is about 2-3%, this shows that in this pellet intermediate iron silicate compounds has not been formed significantly.

The presence of large empty cavities inside the pellet and a slag layer on the surface shows that the drainage of slag has occurred. Exudation of slag from the central regions to the surface can be due to coarsening of the iron structure or existence of cracks in the shell or lowered interfacial energy of slag with gas (more investigation is needed in this case).

Gas bubbles observed in the metal/slag interface suggest that exudation of slag might have been intensified by the release of CO gas during the reduction of FeO in slag.

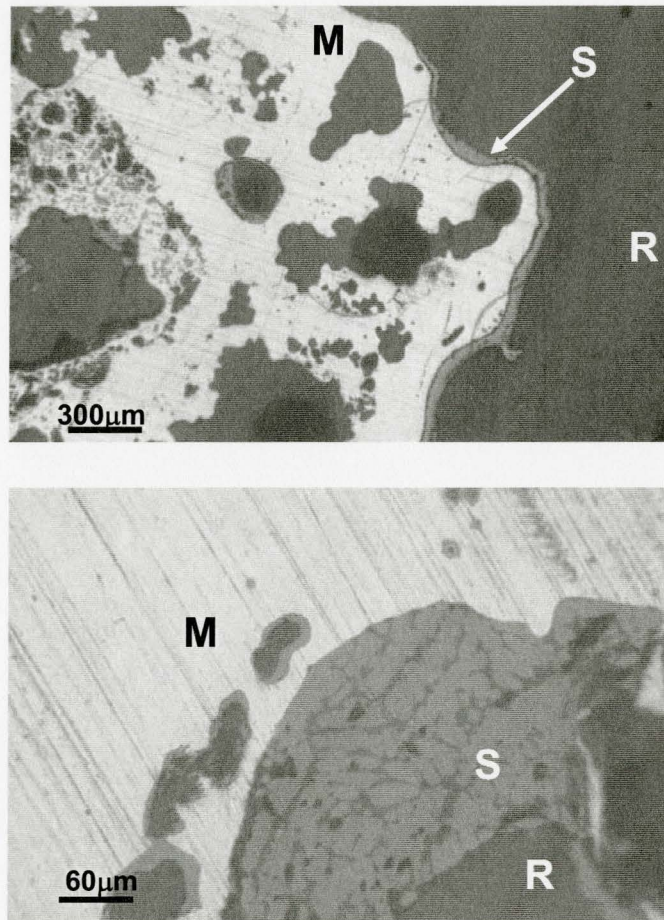


Figure 4- 21- Pellet 5, $\text{CaO/SiO}_2=0.55$, 10Wt% gangue and ash, 1310C, 10min

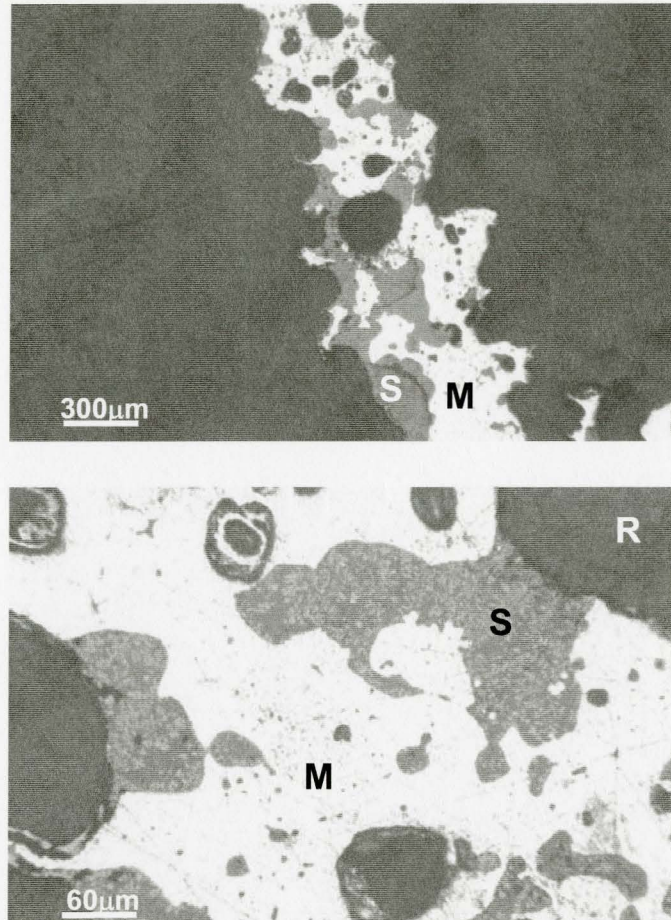
Pellet 6: $\text{CaO}/\text{SiO}_2=1.42$, 10Wt% gangue and ash, 1310C

Figure 4- 22-Pellet 6, $\text{CaO}/\text{SiO}_2=1.42$, 10Wt% gangue and ash, 1310C, 8min

Pellets 6 (10Wt% gangue and ash) having the same CaO/SiO_2 ratio as pellet 3 (5Wt% gangue and ash), also shows a behavior similar to pellet 3. The cross-sectional image of the 8 minute pellet shows the formation of shell on the surface of the pellet and a big void space inside. Similar to pellet 3, FeO rich slag forms in the core of the pellet and is penetrated to the porous iron shell by strong capillary forces which densify the reduced iron shell. FeO in the slag is smelted and iron in the shell is coarsened.

Figure 4- 22 reveals that the shell has been formed from iron grains highly wetted by a two phase slag. EDX analysis results (Table 4- 6) indicates that the matrix phase is rich in CaO and the second phase (lighter regions seen in slag), being FeO precipitated.

Table 4- 6- EDX-results - pellet 6, CaO/SiO₂=1.42, 10Wt% gangue and ash, heated at 1310C

	<i>8 minutes</i>					<i>10 minutes</i>				
	Point1	Point2	Point3	Point4	Point5	Point1	Point2	Point3	Point4	Point5
MgO	1.42	1.55	3.01	1.99	2.99	4.59	4.18	0.5	2.56	0.31
Al ₂ O ₃	0.84	10.92	8.37	0.64	11.78	14.94	14.19	54.1	7.58	8.17
SiO ₂	1.9	23.43	21.56	0.4	31.22	34.49	35.43	13.76	34.19	39.4
CaO	5.55	46.6	50.67	2.12	29.58	43.58	44.6	29.17	53.99	49.29
MnO	0.73	0.34	0.33	1.44	0.65	0.47	0.38	0.62	0.59	0.77
FeO	89.55	17.17	16.06	93.42	23.78	1.93	1.21	0.66	1.09	2
CaO/SiO ₂	2.92	1.99	2.35	5.30	0.95	1.26	1.26	2.12	1.58	1.25

EDX analysis (Table 4- 6) on 10 minutes pellets show very low amount of FeO ($\sim \leq 2\%$), pointing that significant reduction of FeO in slag has occurred. The reduction of FeO in slag causes densification of iron shell. When FeO amount is decreased to very low quantities, the interfacial tension would be highly increased; hence slag is separated from iron and forms a very small interfacial area.

Very high degree of FeO reduction in slag can be caused by high fluidity of basic slag and therefore efficient mass transfer of FeO and subsequent reduction.

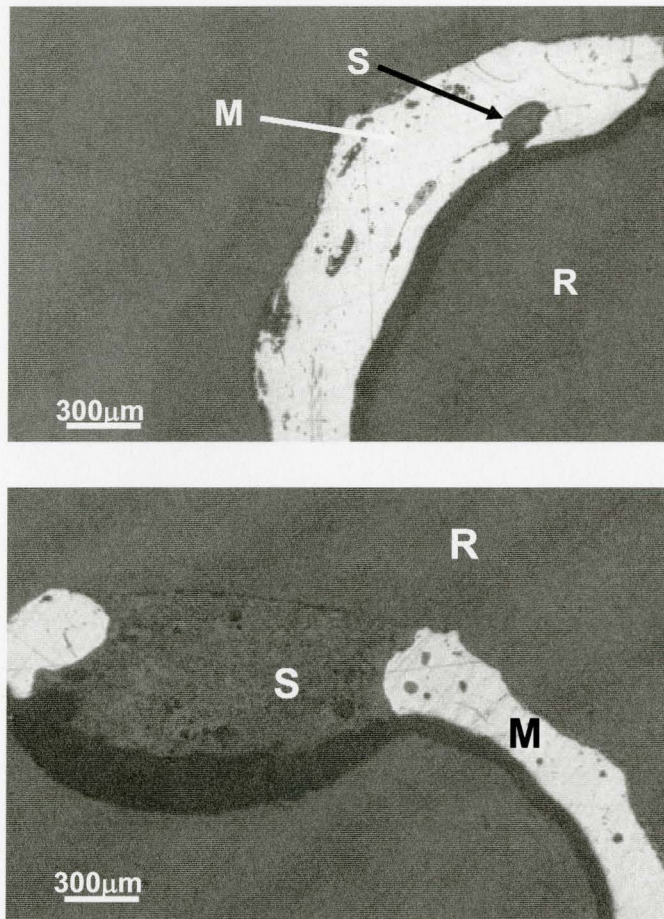


Figure 4- 23- Pellet 6, $\text{CaO/SiO}_2=1.42$, 10Wt% gangue and ash, 1310C, 10min

The steps occurring are quite similar to pellet 3.

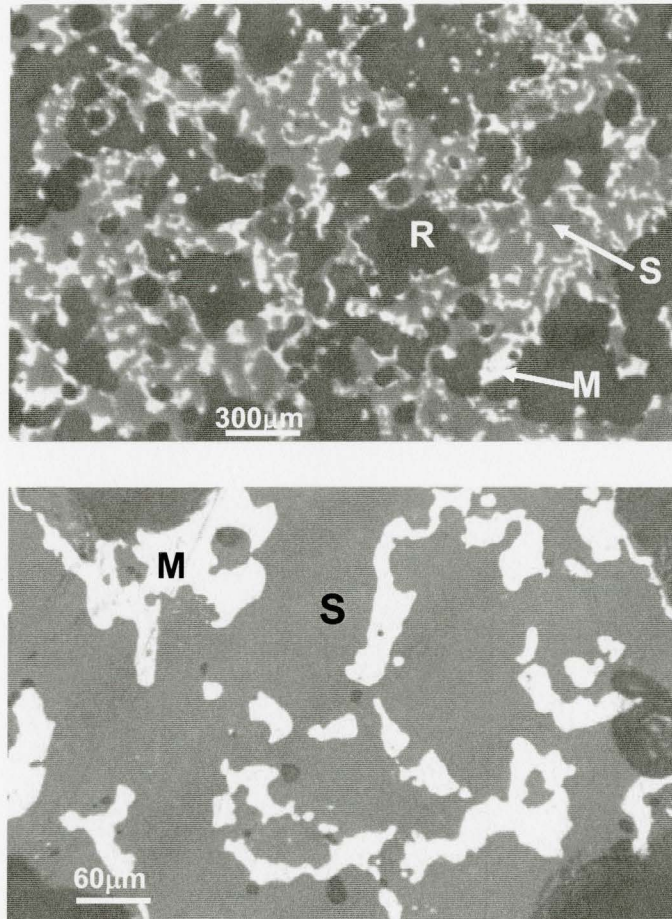
Pellet 7: $\text{CaO}/\text{SiO}_2=0.13$, 15Wt% gangue and ash, 1310C

Figure 4- 24-Pellet 7, $\text{CaO}/\text{SiO}_2=0.13$, 15Wt% gangue and ash, 1310C, 8min

Pellet 7 (15Wt% slag, $\text{CaO}/\text{SiO}_2=0.13$), showed an overall sponge iron shape. A sintered iron structure wetted with slag was seen in the cross-sectional image, Figure 4- 24 . The behavior in this pellet was generally very similar to pellet 4 with the same CaO/SiO_2 ratio.

Table 4- 7- EDX-results - pellet 7, CaO/SiO₂=0.13, 15Wt% gangue and ash, heated at 1310C

	8 minutes					10 minutes				
	Point1	Point2	Point3	Point4	Point5	Point1	Point2	Point3	Point4	Point5
MgO	1.74	3.15	1.94	1.12	1.07	1.27	0.54	0.81	1.17	1.79
Al ₂ O ₃	8.83	9.93	9.31	12.04	11.94	12.27	8.52	11.28	12.77	12.49
SiO ₂	47.59	52.89	49.61	63	62.22	74.25	69.44	68.9	64.9	69.89
CaO	9.78	10.1	9.28	6.51	6.13	9.14	7.32	8.7	9.7	11.65
MnO	0.81	0.49	0.94	0.3	0.54	0.53	0.38	0.42	0.41	0.36
FeO	31.25	23.43	28.93	17.03	18.10	2.54	13.81	9.9	11.05	3.83
CaO/SiO ₂	0.21	0.19	0.19	0.10	0.10	0.12	0.11	0.13	0.15	0.17

The EDX analysis of slag in 8 minute pellet showed (Table 4- 7) the formation of silicate slag with (~20-30%) FeO. The final slag composition in 10 minute pellet showed the final FeO to be about 10%. This means although reduction has taken place but there has been a barrier in further progress of reduction, this again maybe due to the formation of some iron-silicate phases such as fayalite and lowered activity of FeO in silicate slag as described for pellet 4 with the same CaO/SiO₂ ratio and 10 Wt% slag. By reduction of FeO in the slag to iron, the iron grains were coarser but iron still had a sponge structure highly wetted by slag.

In pellet 7 less grain coarsening occurred than pellet 4, this can be justified by the fact that, in pellet 7, more non-ferrous synthetic gangue was added to the composite.

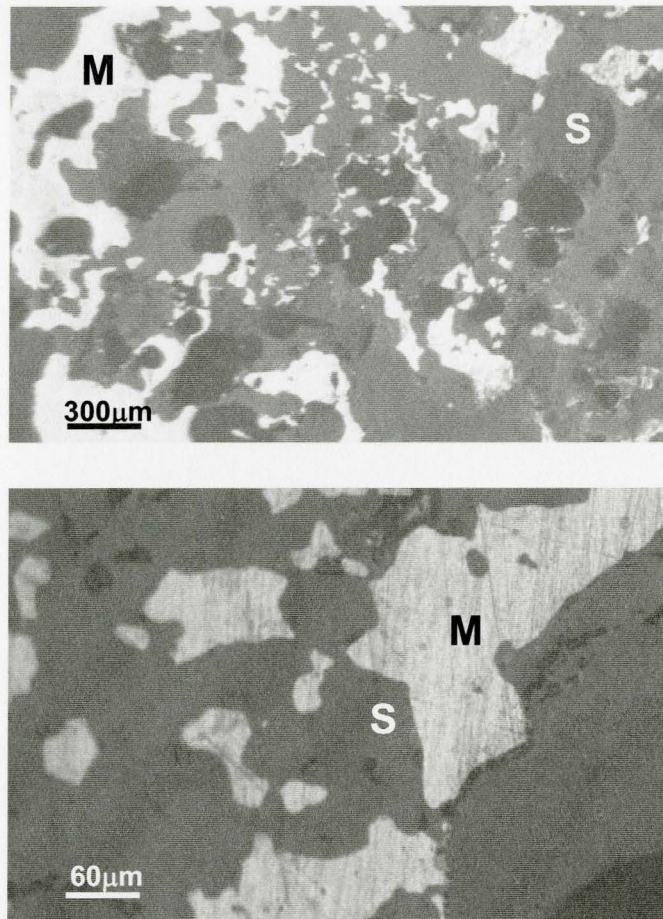


Figure 4- 25- Pellet 7, $\text{CaO/SiO}_2=0.13$, 15Wt% gangue and ash, 1310C, 10min

The microstructure of pellet 7 at 10 minutes is similar to the microstructure of 8 minute pellet except the grains are coarser in 10 minute pellet (Figure 4- 25). The steps considered in pellet 7 are similar to pellet 4.

The steps occurring are quite similar to pellet 4.

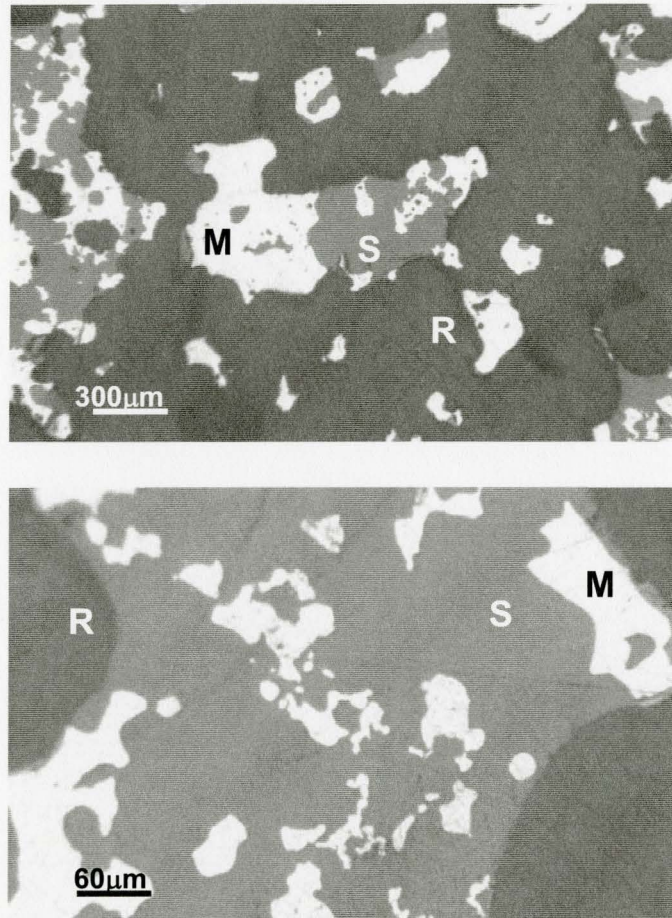
Pellet 8: $\text{CaO}/\text{SiO}_2=0.55$, 15Wt% gangue and ash, 1310C

Figure 4- 26-Pellet 8, $\text{CaO}/\text{SiO}_2=0.55$, 15Wt% gangue and ash, 1310C, 8min,

Cross-sectional image in pellet 8 at 8 minutes shows a few coarse iron grains wetted by coarse slag droplets as islands in the center surrounded by an empty region. Finer sintered iron highly wetted by slag is seen in the locations near the surface (Figure 4- 26).

Table 4- 8- EDX-results - pellet 8, CaO/SiO₂=0.55, 15Wt% gangue and ash, heated at 1310C

	8 minutes					10 minutes				
	Point1	Point2	Point3	Point4	Point5	Point1	Point2	Point3	Point4	Point5
MgO	1.9	2.36	2.65	1.28	0.81	1.36	1.32	1.51	1.59	1.4
Al ₂ O ₃	8.7	9.28	9.33	14.7	10.59	13.26	13.23	14.49	14.37	13.15
SiO ₂	36.36	40.01	40.07	54.39	41.98	53.41	52.41	53.18	52.85	53.38
CaO	29.85	31.5	32.41	24.03	15.85	29.97	29.03	29.27	21.68	30
MnO	0.68	0.51	0.51	0.52	0.13	0.52	0.66	0.37	0.24	0.61
FeO	22.41	16.34	15.03	5.08	30.64	1.48	3.35	1.18	1.27	1.47
CaO/SiO ₂	0.82	0.79	0.81	0.44	0.38	0.56	0.55	0.55	0.41	0.56

The EDX analysis of slag in 8 minutes pellets (Table 4- 8) showed high FeO content in slag near the surface and lower quantities of FeO in slag in central locations. Also the final slag in 10 minute pellet had very low quantities of FeO (~<2%).

Pellet 8 showed a behavior similar to pellet 2 with the same CaO/SiO₂ ratio (5 wt% slag) and can be described the same.

It was interesting to see that although pellet 2 and pellet 8 after 8 minutes showed less densification than pellet 5.

Once FeO reduction is near completion, the interfacial tension of the remaining would increases and the slag layer forms low-wetting droplets on the surface of iron as shown in Figure 4- 27.

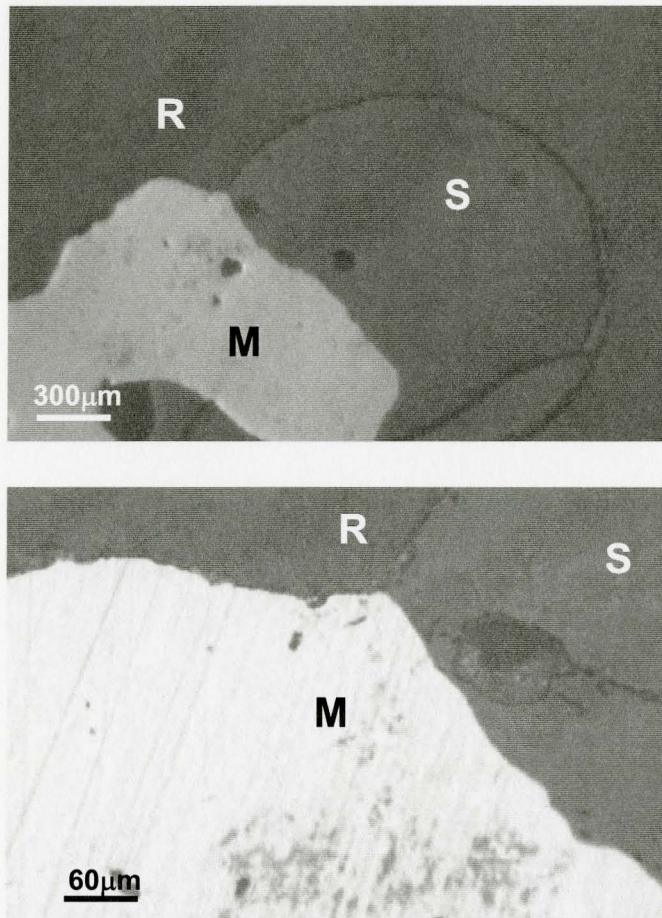


Figure 4- 27- Pellet 8, $\text{CaO/SiO}_2=0.55$, 15Wt% gangue and ash, 1310C, 10min

The steps occurring are quite similar to pellet 2.

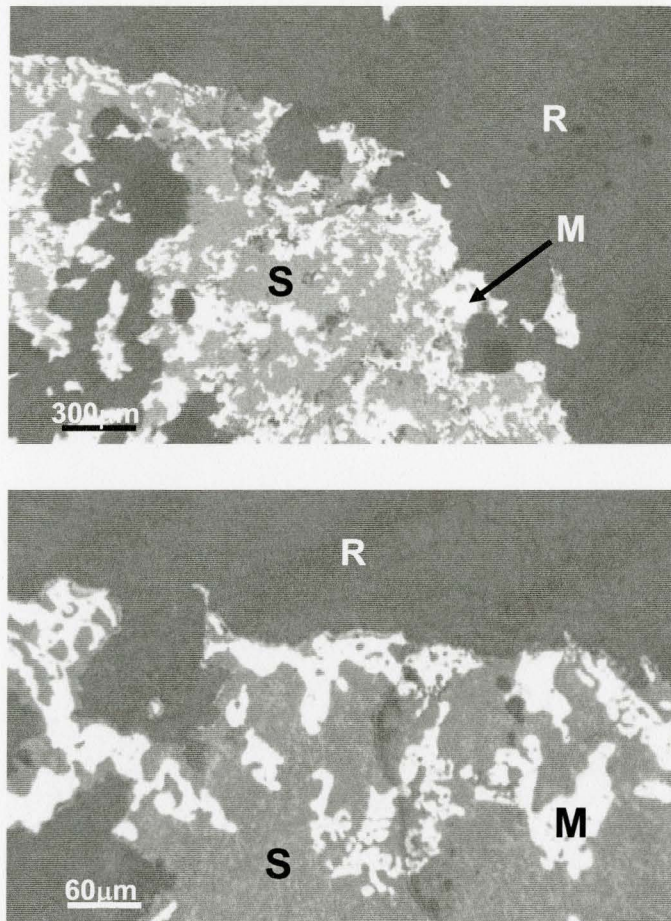
Pellet 9: $\text{CaO}/\text{SiO}_2=1.42$, 15Wt% gangue and ash, 1310C

Figure 4- 28-Pellet 9, $\text{CaO}/\text{SiO}_2=1.42$, 15Wt% gangue and ash, 1310C, 8min

Pellet 9 shows a densification and melting behavior similar to pellets 3 and 6 (both with the same CaO/SiO_2 ratio but lower amount of slag). The only major difference between this pellet and pellets 3 and 6 is that the formation of a shell and evacuation of central regions took longer time.

It can be seen in the images taken that while in pellets 3 and 6 a shell has been fully formed and the central regions completely depleted, in pellet 9, as seen in Figure 4- 28, a shell is formed by the highly wetting slag near the surface and central regions near depletion due to interfacial force near the surface.

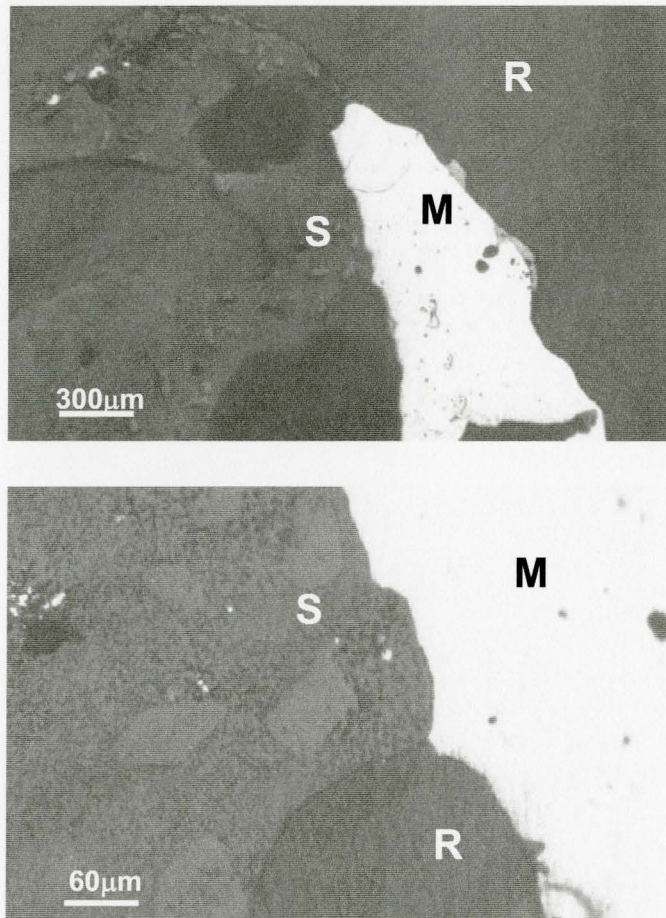


Figure 4- 29- Pellet 9, $\text{CaO/SiO}_2=1.42$, 15Wt% gangue and ash, 1310C, 10min

Table 4- 9- EDX-results - pellet 9, CaO/SiO₂=1.42, 15Wt% gangue and ash, heated at 1310C

	<i>8 minutes</i>					<i>10 minutes</i>				
	Point1	Point2	Point3	Point4	Point5	Point1	Point2	Point3	Point4	Point5
MgO	0.56	1.08	0.79	1.38	0.53	0.01	0.31	0.54	1.18	1.16
Al ₂ O ₃	6.65	11.46	8.54	8.37	47.27	49.47	10.1	11.48	11.58	12.1
SiO ₂	14.42	31.94	24.26	19.74	19.03	14.7	39.8	37.19	38.58	37.26
CaO	11.92	33.43	22.59	20.49	28.34	34.91	46.88	48.43	45.46	47.11
MnO	0.49	0.07	0.3	0.44	0.02	0.04	0.63	0.54	0.73	0.48
FeO	65.95	22.03	43.51	49.58	4.81	0.87	2.28	1.81	2.47	1.89
CaO/SiO ₂	0.83	1.05	0.93	1.04	1.49	2.37	1.18	1.30	1.18	1.26

The first liquid contains a large amount of FeO and forms in the unreduced core that later will be reduced and densify the iron structure. The EDX results for pellet 9 (Table 4- 9) also show a trend similar to pellet 3 and 6.

The steps occurring are quite similar to pellet 3.

Pellet 10: $\text{CaO}/\text{SiO}_2=0.26$, 3.17Wt% gangue and ash,(no oxide addition), 1310C

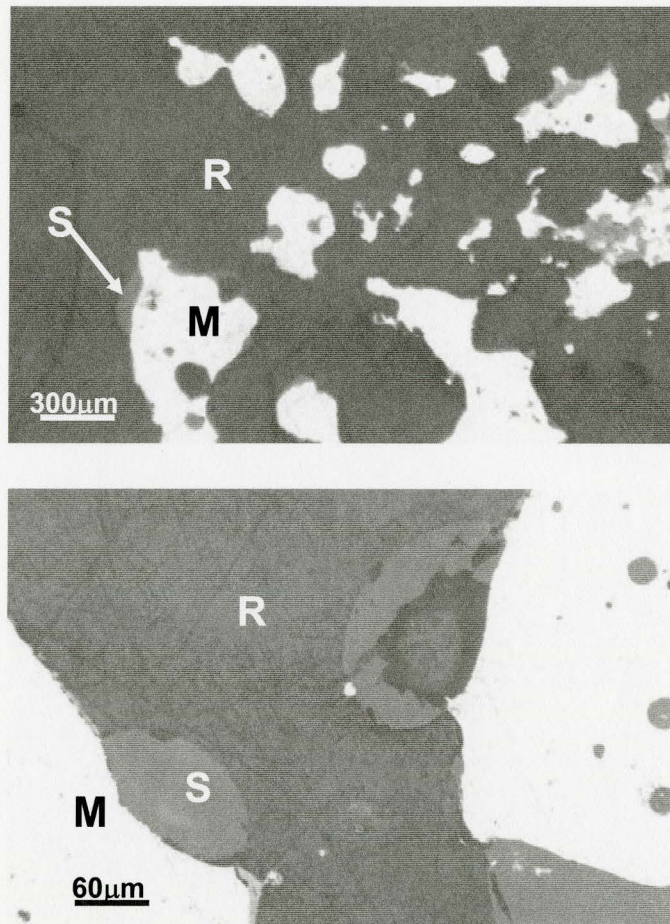


Figure 4- 30- Pellet 10, $\text{CaO}/\text{SiO}_2=0.26$, 3.17Wt% gangue and ash, 1310C, 8min

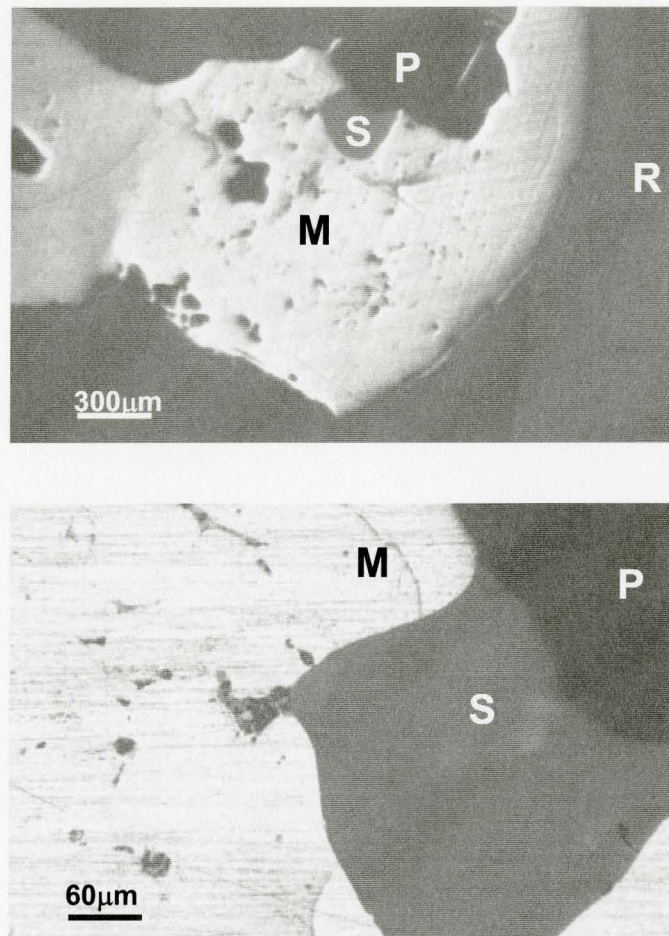


Figure 4- 31- Pellet 10, $\text{CaO/SiO}_2=0.26$, 3.17Wt% gangue and ash, 1310C, 10min

Table 4- 10- EDX-results - pellet 10 (with no addition), CaO/SiO₂=0.26, 3.17Wt% gangue and ash, heated at 1310C

	8 minutes					10 minutes				
	Point1	Point2	Point3	Point4	Point5	Point1	Point2	Point3	Point4	Point5
MgO	8.53	7.49	7.14	6.9	6.79	7.58	2.67	2.6	8.65	3.03
Al ₂ O ₃	21.88	22.14	16.74	16.74	16.52	17.49	34.69	34.59	1.13	35.27
SiO ₂	53.51	53.38	58.95	58.43	58.45	48.39	45.85	46.42	2.64	44.93
CaO	13.81	13.81	13.81	11.12	11.2	16.19	9.94	9.85	4.13	9.23
MnO	1.52	1.44	1.15	2.37	2.34	2.72	1.61	1.7	1.95	1.49
FeO	0.76	1.74	2.21	4.44	4.71	7.64	5.24	4.84	81.5	6.06
CaO/SiO ₂	0.26	0.26	0.23	0.19	0.19	0.33	0.22	0.21	1.56	0.21

In pellet 10, (pellet with no addition), no oxide addition was made to the stoichiometric coal and ore composite. The gangue from ore and ash formed a silicates slag.

The EDX results and comparison of FeO content of slag in 8 and 10 minutes shows that the initial slag was very rich in silica and contained a small amount of FeO. It can be seen that FeO instead of being reduced has been highly dissolved in the slag and the final slag is rich in FeO.

4.2. Leco Carbon and Sulfur Analysis

Leco carbon and sulfur analysis was performed by Leco carbon and sulfur analyzer model CS444 on fully melted pellets, heated at 1310C for 15 minutes. Longer time was intentionally given in order to separate slag and metal completely.

Table 4- 11-The results of leco Carbon and Sulfur test on the final melted iron

Pellet No.	CaO/SiO ₂	Wt %Slag	Percent C in iron	Percent S In iron
1	0.13	5	2.67	0.28
2	0.55	5	3.23	0.25
3	1.42	5	3.54	0.11
4	0.13	10	1.9	0.34
5	0.55	10	3.31	0.38
6	1.42	10	3.03	0.26
7	0.13	15	1.72	0.22
8	0.55	15	1.81	0.14
9	1.42	15	2.84	0.08

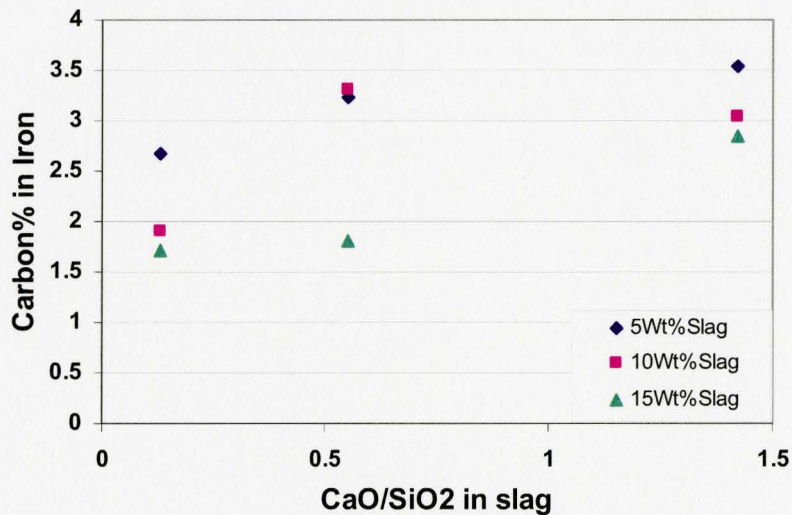


Figure 4- 32-Carbon content of the final melted iron versus CaO/SiO₂ in slag for different slag weight percents

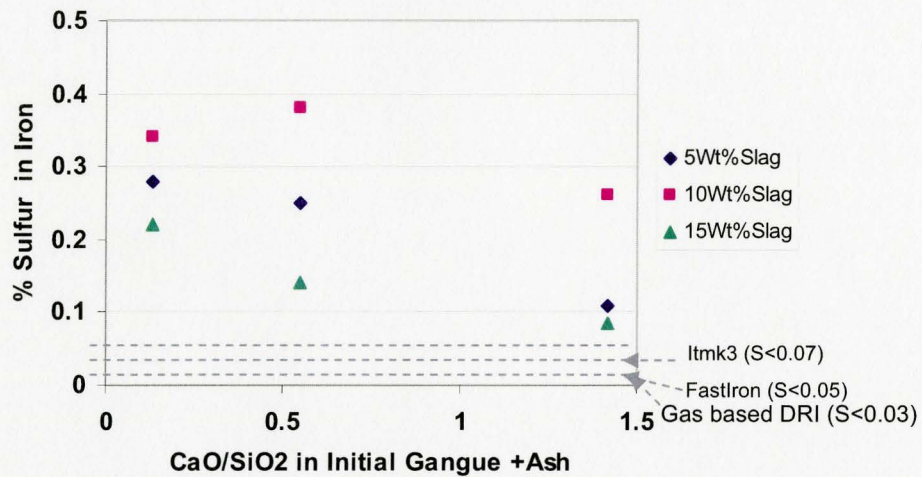


Figure 4- 33- Sulfur content of the final melted iron versus CaO/SiO₂ in slag for different slag weight percents

The results from Figure 4- 32 and Figure 4- 33, show that except in case of CaO/SiO₂=0.5 for 10 wt% slag:

- Increase in CaO/SiO₂ ratio, increases the carbon content and lowers sulfur content in iron.
- Carbon content of iron is lowered when the slag content increases.
- More sulfur removal takes place when higher slag content is present.

The increase in carbon content with increase in CaO/SiO₂ ratio may be due to the fact that, higher lime to silica ratio increases the fluidity of the slag and therefore the reduction takes place more rapidly due to more efficient mass transfer of FeO in slag. As the reduction is completed faster, there would be more time available to C/CO to be in contact with reduced iron and carburize it.

Figure 4- 33 shows that amount of sulfur in iron is lowered in case of more basic slags and also when slag content is higher.

Similar behavior was reported in Kobayashi et al's patent [40], where they confirmed higher sulfur removal took place when more lime was added to the slag. According to Kobayashi et al, [40], when iron is still solid during the formation of the liquid slag from gangue and ash, sulfur is transferred with ash to the liquid slag phase. According to Kobayashi the practice is different from typical desulphurization of hot metal with CaO-containing slag where metal is liquid.

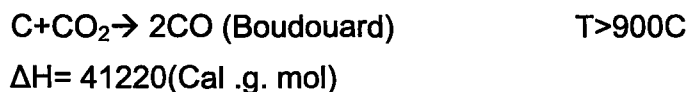
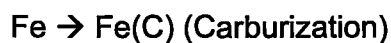
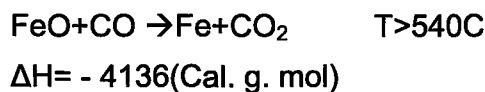
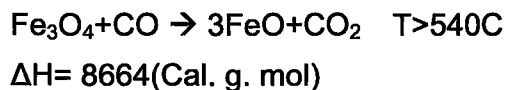
Higher degree of desulphurization in more basic pellets can be attributed to lowered viscosity and therefore higher fluidity of more basic slags which increases sulfur capture by slag.

4.3. Simultaneous Differential Thermal Analysis and Thermo - Gravimetric Analysis (DTA/TGA)

Simultaneous Differential Thermal Analysis and Thermo-Gravimetric Analysis (DTA/TGA), was performed on 200 mg samples of the same powder mixes from which pellets 1 to 10 were made. The test was done under Argon atmosphere and heating rate of 20C/min. The equipment used was NETZSCH STA 409 PC.

In the following section the results from simultaneous DTA/TGA are shown and discussed.

The reactions are considered to take place in the system of coal and magnetite ore composite are as follows:



Superimposing of the DTA results revealed general range of temperatures in endothermic and exothermic reactions taking place in the system.

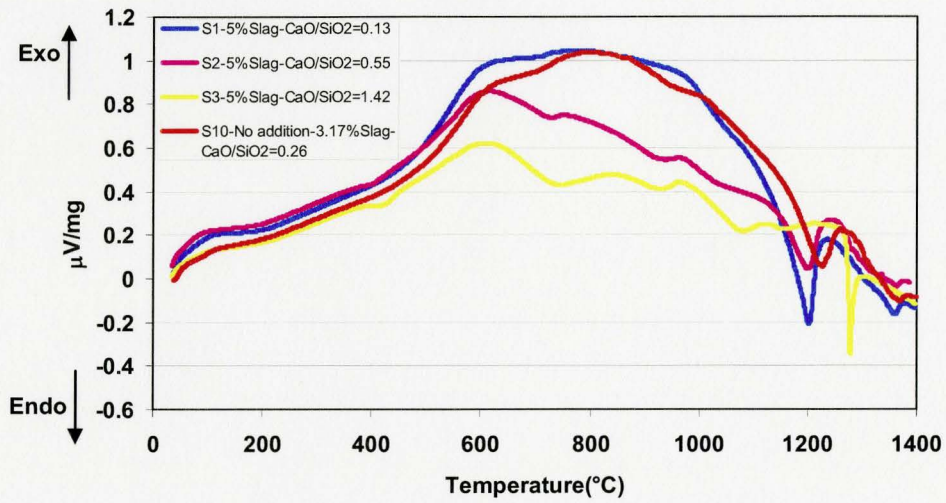


Figure 4- 34-Superimposed DTA curves of samples 1-3 and 10 as reference

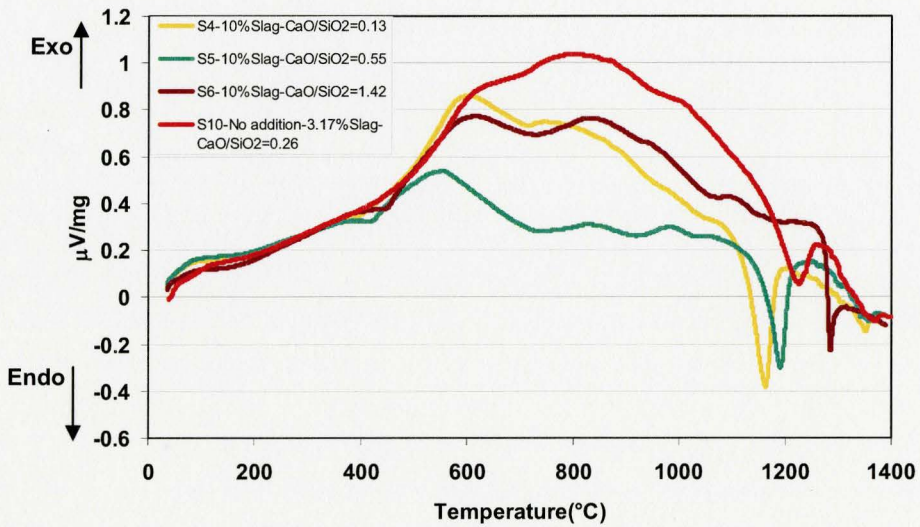


Figure 4- 35-Superimposed DTA curves of samples 4-6 and 10 as reference

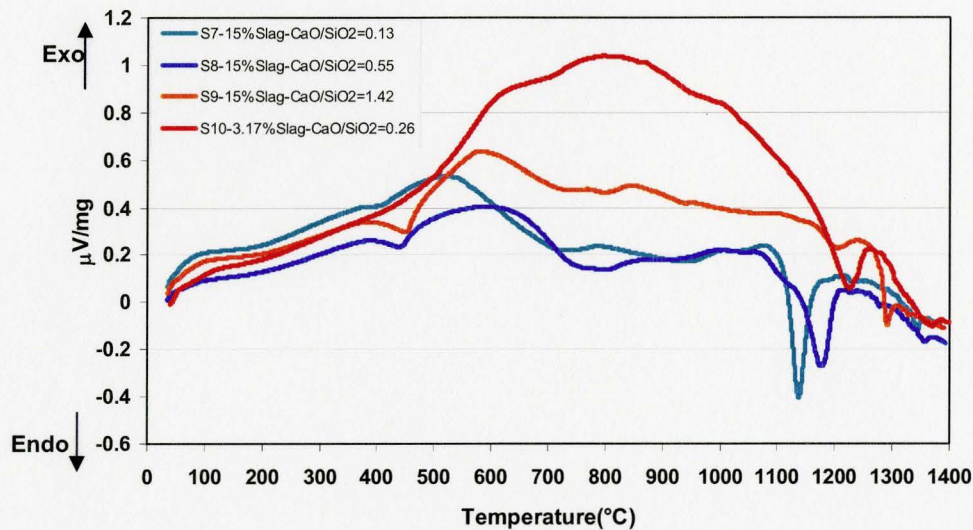


Figure 4- 36-Superimposed DTA curves of samples 7-9 and 10 as reference

A small endothermic peak due to coal devolatilization can be seen in the temperature range between $400^{\circ}\text{C} < T < 500^{\circ}\text{C}$ and the second more endothermic event $T > 540^{\circ}\text{C}$, which can be attributed to the reduction of magnetite to wustite. Following the reduction of magnetite, the exothermic reduction of wustite occurs.

The next endothermic event is the carbon gasification by Boudouard reaction and generation of CO gas. This reaction takes place at $900^{\circ}\text{C} < T < 1000^{\circ}\text{C}$.

After 1000°C , other endothermic events can be observed corresponding to the stage at which first liquid slag is forming from gangue and ash particles. In samples 1,2,4,5,7,8,10, with the $\text{CaO/SiO}_2 = 0.13$ and 0.5 , two sharp endothermic peaks can be observed. First sharp peak occurs in the range of $1150^{\circ}\text{C} < T < 1220^{\circ}\text{C}$, which shows the melting of slag. This range is lower than predicted melting points of $\text{CaO-SiO}_2\text{-Al}_2\text{O}_3$ slag system which could show the contribution of FeO in formation of the slag phase. The second peaks appear at $1350^{\circ}\text{C} < T < 1385^{\circ}\text{C}$ which show the melting points of iron with 2-2.5% carbon. (See figure 1-18). In samples 3, 6, 9 with $\text{CaO/SiO}_2 = 1.42$, slight endothermic curves can be seen at $1000^{\circ}\text{C} < T < 1200^{\circ}\text{C}$ followed by a distinct sharp peak at $1278^{\circ}\text{C} < T < 1297^{\circ}\text{C}$.

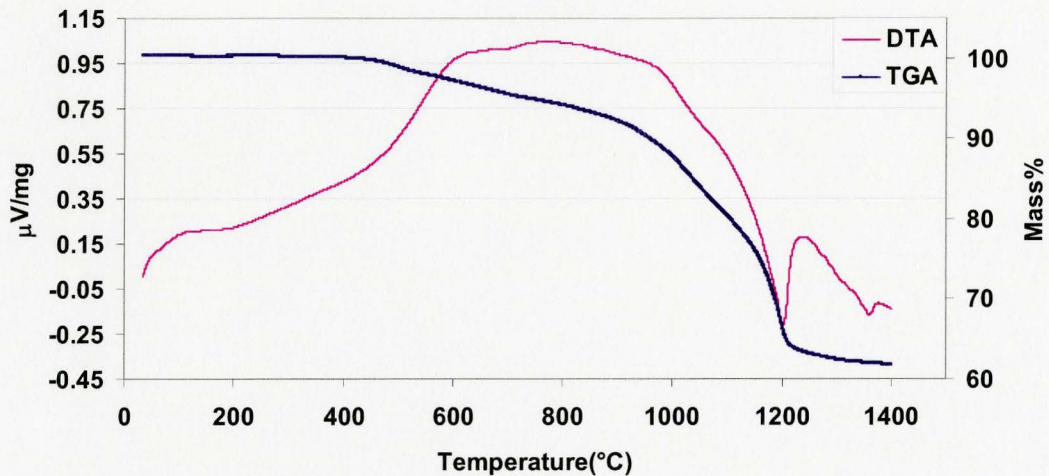


Figure 4- 37-Simultaneous DTA/TGA curves for sample 1 with $\text{CaO/SiO}_2=0.13$, 5Wt%Slag

In Figure 4- 37 for sample 1, it can be seen that melting peak of slag occurred at 1205C and initiated at about 1080C. It can also be seen that at temperature range where the melting peak of slag appears in the DTA curve, TGA curve shows very rapid mass loss. This means reduction at the presence of liquid slag was much faster than solid state. It suggests that slag contained FeO and smelting reduction of FeO took place. In this sample at 1365C, a small peak appears. As the last peak occurring in this system this should be attributed to melting of iron resulted from localized carburization.

Similar behavior can be seen in Figure 4- 38 for sample 2. Again in this sample it can be seen that when melting peak of slag appears, TGA curve finds sharper slope or in other words rapid reduction takes place when liquid slag forms which can be again related to rapid FeO reduction from slag. The melting peak of Fe-C alloy for this sample appears at 1378C.

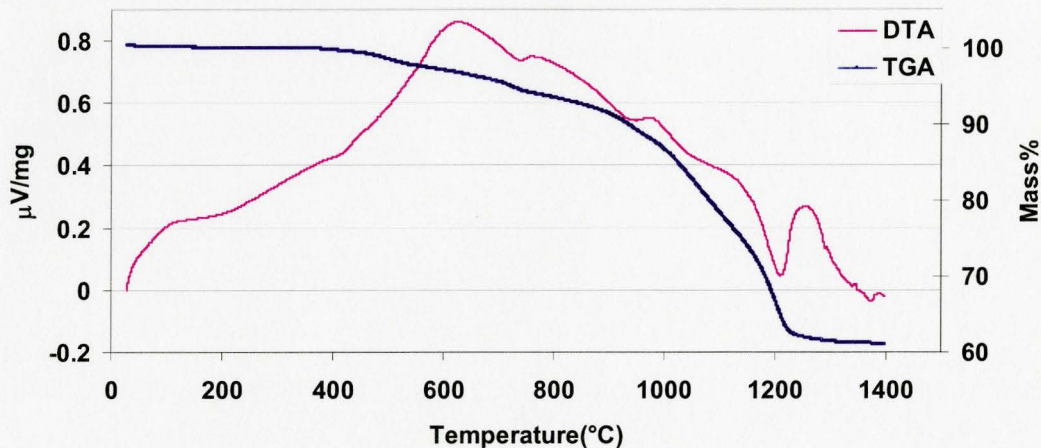


Figure 4- 38- Simultaneous DTA/TGA curves for sample 2 with $\text{CaO/SiO}_2=0.55$, 5Wt% gangue and ash

Figure 4- 39 shows simultaneous DTA/TGA curves for sample 3 with $\text{CaO/SiO}_2=1.42$. In this sample with higher lime/silica ratio in slag, the behavior seem to be different from sample 1 and 2.

After 1000C, two small peaks can be seen in DTA curve. The temperature of the first peak is 1088C and the second 1167C. For this reason there is uncertainty in determining the melting point of slag. However it can also be seen that, TGA line is not affected when these two curves occur. This could mean that because of presence of more flux (CaO) and reaction of lime with other gangue particles especially SiO_2 , more unreacted and free FeO was available for solid state reduction and reduction is almost complete before melting of iron as seen in Figure 4- 39. In this sample there is no distinct peak for slag and only small curves can be seen. The amount of slag being formed, must have been small as melting point of the $\text{SiO}_2\text{-CaO-Al}_2\text{O}_3$ slag was predicted to be very high (>1500C).

This result is in contrast with the results from rapid heating of pellet made from the same sample batch. As it was seen before in Table 4- 3, slag contained FeO which appeared as dendrites after solidification as seen in Figure 4- 11 . The difference between these two results is contributed to major difference in heating rates. In the previous experiments where rate was faster than chemical reaction, the temperature of the sample rose rapidly and melting started including molten gangue and unreduced iron oxide.

In this sample, it can be seen that when reduction is completed, the last melting peak which should be the melting point of iron appears at 1280C. The relatively low melting point of iron shows carburization has been efficient in this sample. This may be caused by extensive solid state reduction which permits solid iron to be in contact with CO/C for longer times.

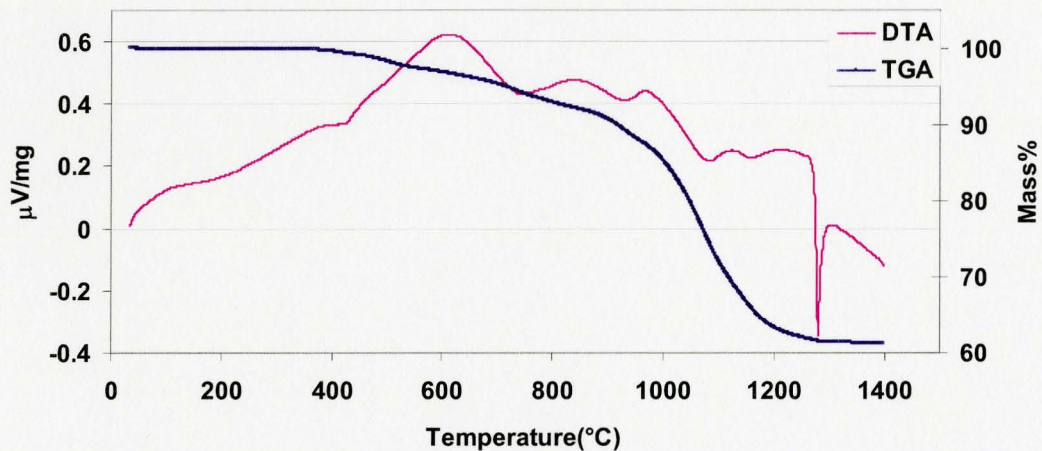


Figure 4- 39- Simultaneous DTA/TGA curves for sample 3 with $\text{CaO}/\text{SiO}_2=1.42$, 5Wt% gangue and ash

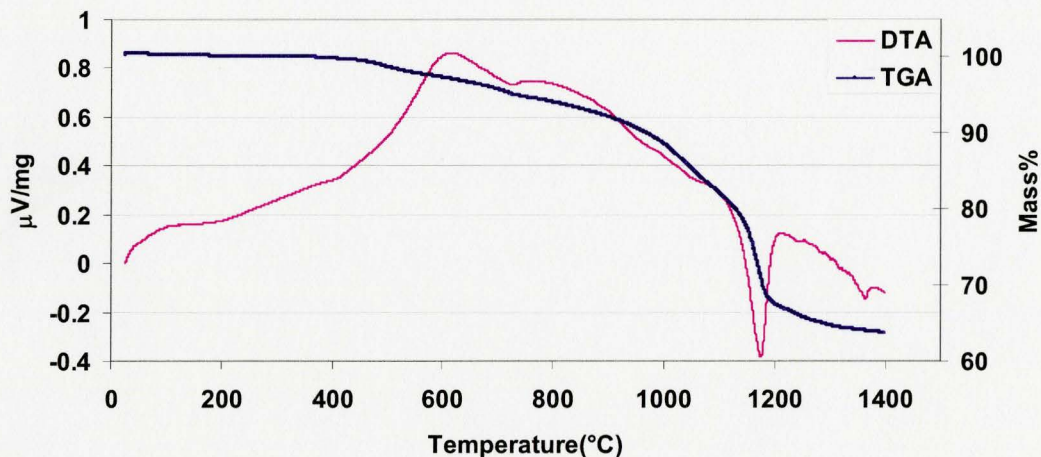


Figure 4- 40- Simultaneous DTA/TGA curves for sample 4 with $\text{CaO}/\text{SiO}_2=0.13$, 10Wt% gangue and ash

The general behavior seen for samples 4, ($\text{CaO}/\text{SiO}_2=0.13$) and 5 with $\text{CaO}/\text{SiO}_2=0.54$ shown in Figure 4- 40 and Figure 4- 41, is similar to sample 1 and 2 with same ratios of lime to silica but lower amount of slag.

It can be seen that rapid reduction takes place when liquid slag forms which means FeO is reduced in slag.

In sample 4 the temperature of melting peak of slag is 1177C, this peak started at 1080C. In sample 5 this peak appears at 1203C and started at 1105C. Formation of more iron-silicate intermediate compounds in sample 4 with higher silica may be responsible for lowered melting point compared to sample 5.

Similarly as seen in Figure 4- 37 and Figure 4- 38 melting point of slag in sample 1 with higher amount of silica is lower than sample 2.

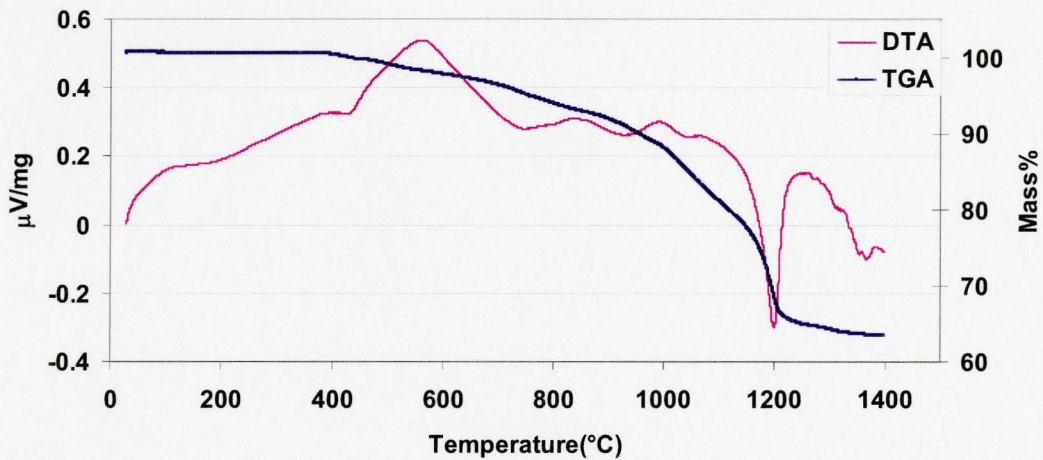


Figure 4- 41-Simultaneous DTA/TGA curves for sample 5 with $\text{CaO}/\text{SiO}_2=0.55$, 10Wt% gangue and ash

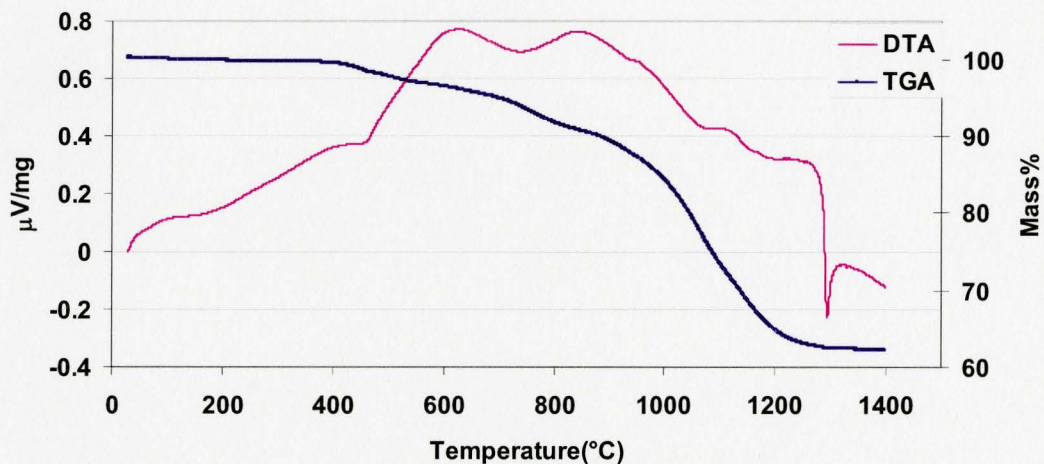


Figure 4- 42- Simultaneous DTA/TGA curves for sample 6 with $\text{CaO}/\text{SiO}_2=1.42$, 10Wt% gangue and ash

The general behavior of DTA and TGA curves in sample 6 is similar to sample 3 and can be explained in the same way. In this sample distinct peaks of slag can not be seen. The melting peak of iron appears at 1294C.

The DTA/TGA lines for sample 7,(Figure 4- 43) and sample8,(Figure 4- 44),with 15wt% gangue and ash, shows a melting behavior similar to samples 1,2,4 and 5 with $\text{CaO}/\text{SiO}_2 \leq 0.54$.

It can again be seen that by melting of slag, rate of reduction increase which shows rapid reduction of FeO in slag. In sample 7, the melting peak of slag begins at 1100C and the temperature of peak is 1152C. In sample 8 the start of melting peak is 1085C and the melting peak 1186C.

The peak for melting of iron appears at 1358C for sample 7, and at 1366C for sample 8.

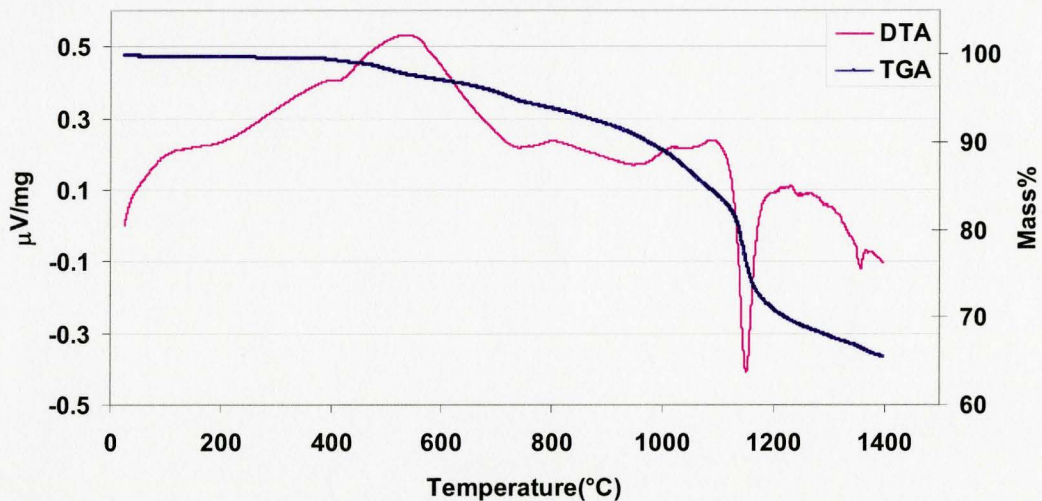


Figure 4- 43- Simultaneous DTA/TGA curves for sample 7 with $\text{CaO/SiO}_2=0.13$, 15Wt% gangue and ash

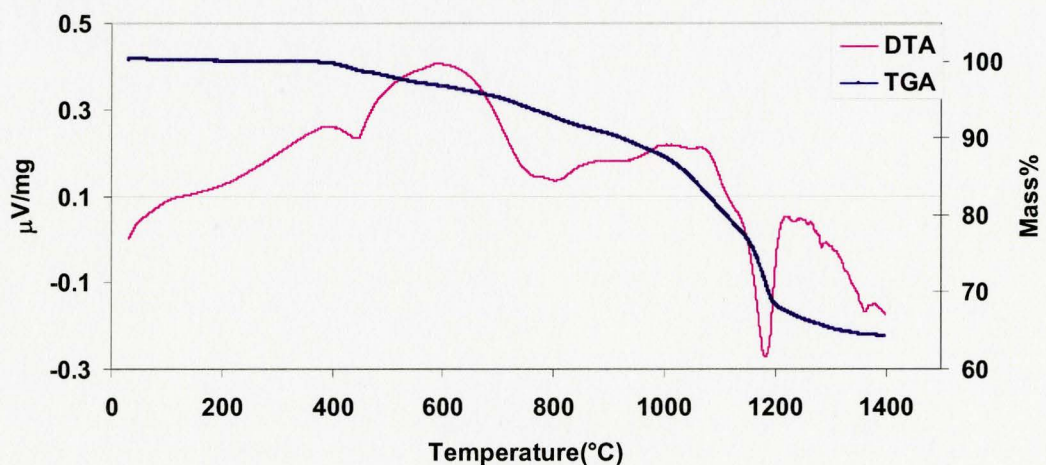


Figure 4- 44- Simultaneous DTA/TGA curves for sample 8 with $\text{CaO/SiO}_2=0.55$, 15Wt% gangue and ash

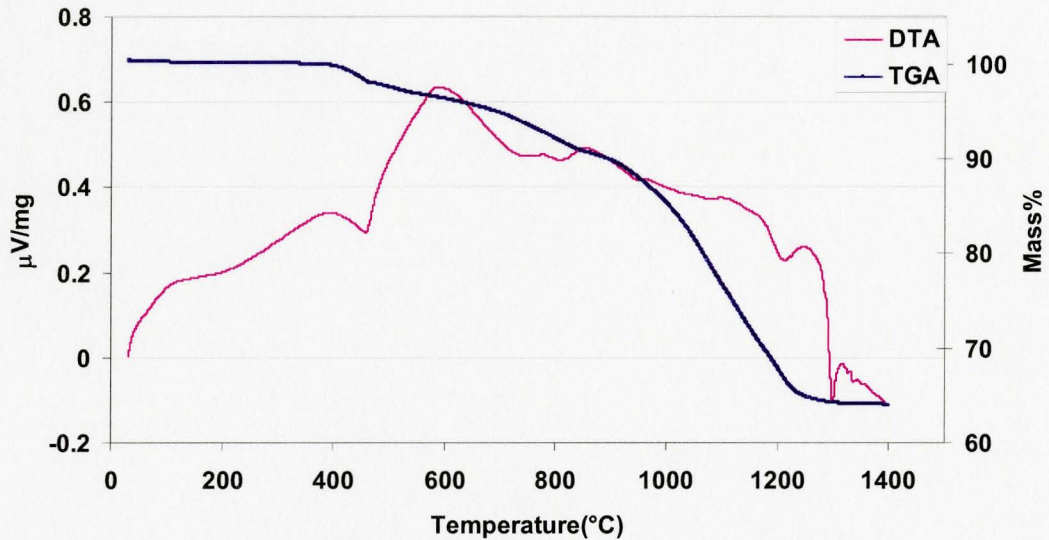


Figure 4- 45- Simultaneous DTA/TGA curves for sample 9 with $\text{CaO/SiO}_2=1.42$, 15Wt% gangue and ash

According to Figure 4- 45 for sample 9, similar to samples 3 and 6 with same lime to silica ratio, minor melting of slag did not influence the trend of reduction as seen in TGA curve. In other words slag did not include much FeO and reduction continued in solid state. A small peak of slag can be seen at 1218C and melting peak of iron can be seen at 1305C.

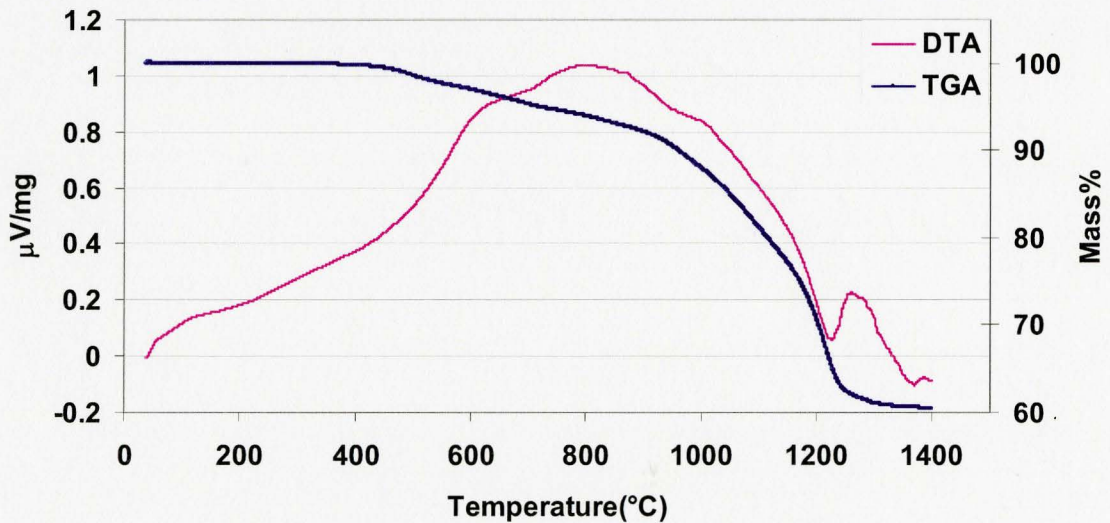


Figure 4- 46- Simultaneous DTA/TGA curves for no addition sample with $\text{CaO/SiO}_2=0.26$, 3.17Wt% gangue and ash

In sample with no addition of flux (Figure 4- 46), the general behavior is similar to samples with lower amount of lime. In this sample it can be seen that reduction takes place more rapidly when liquid slag forms and shows smelting reduction with higher rate than solid state reduction. The peaks of melting point of slag (1216C) and iron (1375C) are both higher than melting points of other samples as sample was not fluxed.

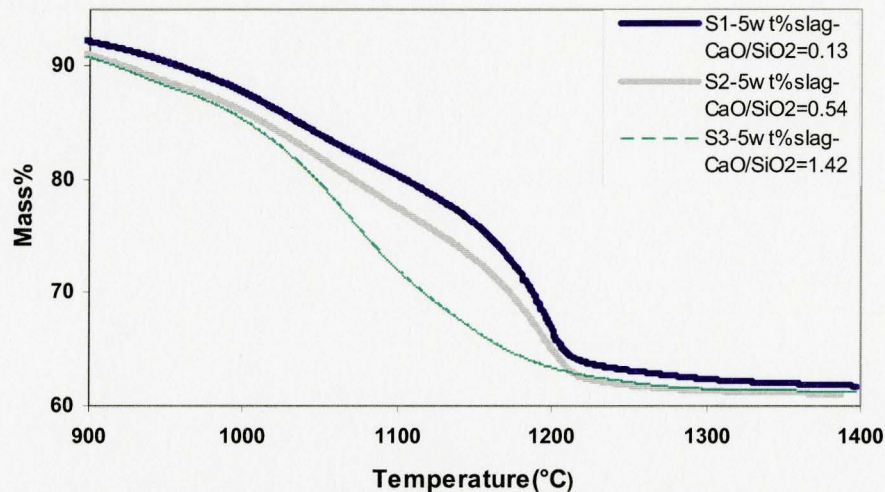


Figure 4- 47-TGA curves for samples 1-3

In Figure 4- 47, TGA curves for samples 1 to 3 with 5wt% initial gangue and ash, from 900C to 1400C are superimposed in one diagram for comparison. Similarly the TGA curves for samples 4-6 with 10 wt% gangue and ash is shown in Figure 4- 48 and TGA curves for samples 7-9 with 15 wt% gangue and ash is shown in Figure 4- 49.

In Figure 4- 47, it can be seen that samples 1 and 2 have very similar trends. Sample 2 with higher amount of lime shows higher degree of reduction compared to sample 1, also sample 3 showed highest degree of reduction compared to all three samples. It can also be seen that slightly before 1000C, TGA curve for sample 3 deviates from the other two curves to much lower masses. This suggests that added lime reacted with silica and FeO was free to be reduced. Also the heating rate was so low that FeO did not dissolve much in slag.

The higher masses of two other samples with lower CaO/SiO_2 shows that before the formation of liquid slag (1080-1203C in sample 1 and 1140-1216C in sample 2) there was lower free FeO available for reduction due to formation of iron-silicate intermediate compounds. However in these samples melting helped FeO to be more free and be reduced more rapidly. The same trends can also be seen in Figure 4- 48 for samples 4-6, and in Figure 4- 49 for samples 7-9.

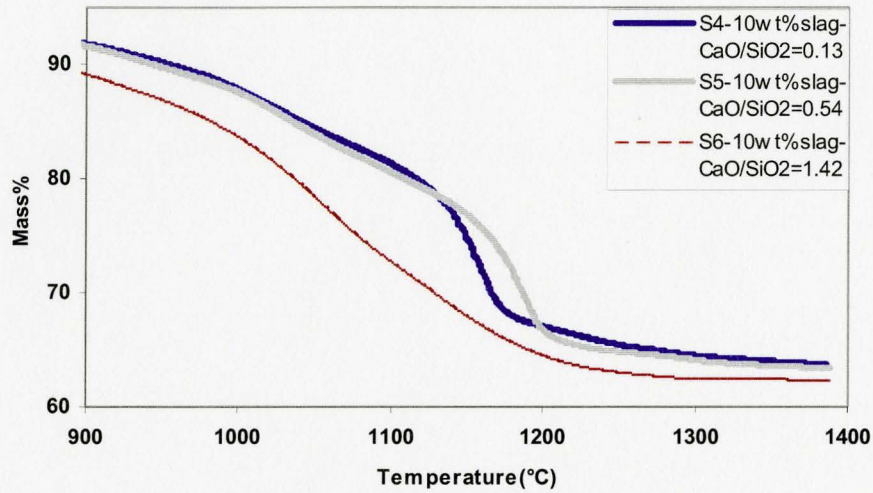


Figure 4- 48- TGA curves for samples 4-6

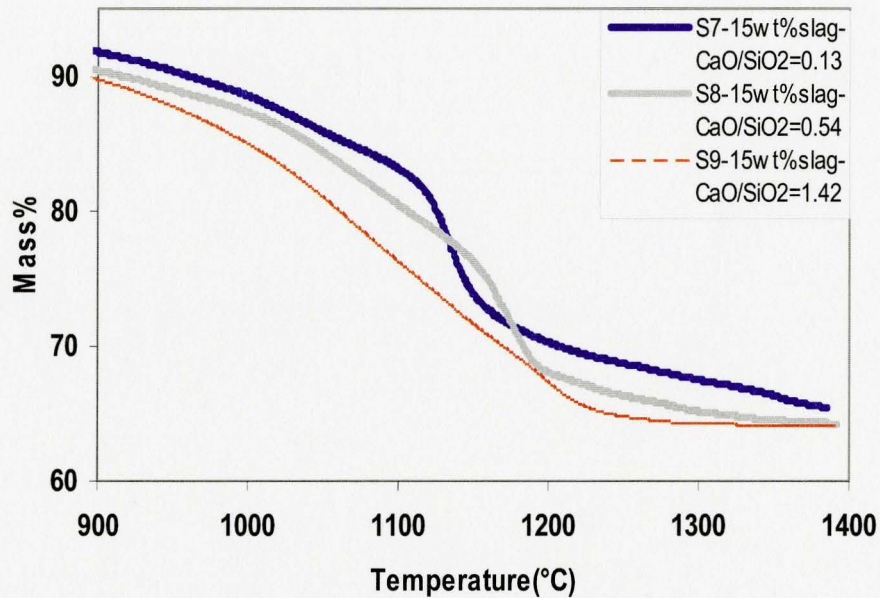


Figure 4- 49- TGA curves for samples 7-9

It can not be concluded that when the curve reaches the constant level, reduction is 100% completed. There may still be a small amount of FeO left in the sample. For this reason, relative degrees of reduction are calculated relative to lowest mass achieved at 1400C among samples with the same content of slag. Relative reduction degrees can be seen in Table 4- 12.

Table 4- 12-Relative reduction degrees at 1200C, 1300C and 1400C derived from DTA/TGA curves

5Wt%gangue+ash			
	S1-CaO/SiO ₂ =0.13	S2-CaO/SiO ₂ =0.54	S3-CaO/SiO ₂ =1.42
1200C	86.55	92.16	94.96
1300C	97.76	99.16	99.16
1400C	98.32	100	100
10Wt%gangue+ash			
	S4-CaO/SiO ₂ =0.13	S5-CaO/SiO ₂ =0.54	S6-CaO/SiO ₂ =1.42
1200C	86.61	87.57	94.58
1300C	94.49	94.61	99.40
1400C	96.09	96.39	100.00
15Wt%gangue+ash			
	S7-CaO/SiO ₂ =0.13	S8-CaO/SiO ₂ =0.54	S9-CaO/SiO ₂ =1.42
1200C	81.64	87.66	91.39
1300C	89.35	96.45	99.25
1400C	95.43	100.00	100.00

It can generally be seen from the table above that by increasing the amount of gangue and ash in samples the reduction degrees are less which can be caused by more distance between carbon particles and FeO and therefore less rapid reduction. For this reason higher reduction degrees are not recommended.

4.4. Current Understanding

Solid iron oxide reduction progresses from the surface towards the core of the coal ore composite pellets tested as the direction of heat transfer is from surface to the core. Therefore a certain thickness of porous iron sinter phase is formed (iron sintered shell). After certain degree of solid iron oxide reduction, in fluxed pellets, unreduced FeO in the core starts to form liquid slag with other present oxides, in fluxed pellets the initial droplets have low viscosity and can coalesce rapidly. The slag formed in the core would then be exuded to solid iron sinter shell due to the strong capillary forces caused by the porous iron shell. In non fluxed pellets the initial droplets of slag are so viscous and sticking to other particles that before their coalescence, the solid state reduction continues towards the core and therefore the sponge iron structure is achieved.

The amount of liquid FeO (depending on the degree of pre-reduction in solid state), formed together with the composition and content of gangue oxides determines the melting point and physical properties of the initially formed slag. These physical properties such as surface tension, viscosity and density would influence the rate of FeO mass transfer in the slag and therefore rate of smelting reduction of liquid FeO in slag.

Rapid reduction of FeO leads to densification and thickening of the iron shell as seen in pellets with more basic slags which have lower viscosity ($\text{CaO/SiO}_2=1.42$). It was very interesting to see that by further reduction of FeO, interfacial tension of the remaining slag with iron increased so much that slag was separated from the iron structure. In these types of pellets, complete separation of iron from slag was possible when iron melted given enough time. The reduction progressed rapidly so that after 10 minutes the average FeO content of the slag based on the EDX analysis was less than 2 percent indicating a high recovery of iron units. The slag separation only took place when reduction was near completion and while slag contained higher amounts of FeO it remained in the shell and did not exude out which minimizes the risk of FeO attack to the refractory. For this reason, also rapid densification, slag separation and high reduction degree, this type of pellets are most recommended among the pellets tested in this study.

In less basic fluxed pellets ($\text{CaO/SiO}_2=0.55$), the rate of reduction was less, slag was also very rapidly exuded out to the slag surface. The reduction of liquid FeO in slag continued. The shell densified and remaining slag was separated from the surface by forming droplets on the surface. But as the slag exudation to the surface takes place when still containing appreciable amount of FeO, this type of pellet is not recommended due to possible refractory attack.

Observations showed that for the clean separation of slag from iron, while liquid slag is melted and separated, iron could be softened and densified but not necessarily fully melted.

The case where a dense iron structure did not form was when slag forming oxides were highly acidic ($\text{CaO}/\text{SiO}_2=0.13$). In this case a sponge iron structure was seen in all the pellet cross section, this means that solid oxide reduction continued through the pellet center. There was also some FeO in the liquid slag. In these pellets smelting reduction could not progress sufficiently due to lowered activity of FeO by formation of iron-silicate slag phases such as fayalite.

Several other factors can influence the amount of FeO in liquid slag; such as furnace heating rate, sample size, particle size distribution, bulk density and crucible type. These parameters were kept constant in the main experiments of this study with rapid heating of pellets but studying the influence of them on the melting behavior of coal ore composite pellets would be among the future work of this research.

The results from Differential Thermal Analysis and Thermo Gravimetric Analysis (DTA/TGA) with very low heating rate of 20C/min, showed that the degree of reduction (Table 4- 12), not only depends on the heating rate, but also on the chemical reactions taking place due to composition of the gangue and ash and availability of FeO to solid state reduction. It was seen that in samples with highest amount of lime ($\text{CaO}/\text{SiO}_2=1.42$), FeO was free to be reduced in solid state. However with less fluxed samples ($\text{CaO}/\text{SiO}_2 \leq 0.54$), less reduction took place even before melting of slag as iron oxide had reacted with gangue minerals and it was less free. The slag in these samples contained iron oxide and smelting reduction was faster than solid state reduction.

Chapter 5

5. Summary, Conclusions and Recommendations for future work

5.1. Summary

In this study the objective was to investigate the melting behavior of coal ore composites. Two series of experiments were performed. In the initial series of experiments, coal ore composites were made from one ore type and three coal types. Each composite type was made in 2 batches of stoichiometric and under stoichiometric ratios. In the second series of experiments, composites were made from 1 coal type and ore based on the stoichiometric carbon for reduction. By addition of synthetic gangue oxides of CaO, SiO₂, Al₂O₃, composites were prepared. Optical microscopy was used to study the morphological changes, densification and phases present. Energy dispersed X ray analysis (EDX) was done on several points on slag phase both on quenched samples after 8 and 10 minute pellets. Also Leco carbon test was done on the final melted product being heated for 15 minutes. Simultaneous Differential Thermal Analysis (DTA) and Thermo Gravimetric Analysis (TGA) were performed on pellets at the heating rate of 20C/min under argon gas the results were studied and discussed.

5.2. Conclusions

1. The melting behavior of coal ore composites is a complex process involving:
 - Slag of variable composition (including various contents of FeO).
 - Metal with variable carbon content.
 - Phase separation driven by surface-interfacial tension
 - Densification by solid state diffusion and reduction of iron oxide in liquid phase.
2. Clean phase separation of slag from metal was observed at the micro scale and subsequently at the macro scale.
3. More densification and slag separation takes place at higher temperatures and more heating time.
4. Coal type influences the melting, coalescence and phase separation.
5. The melting coalescence and phase separation is dependent on coal/ore ratios and requires stoichiometric coal for a minimum of 10 minutes at 1300C and 5 minutes at 1350C for 1g samples.
6. In samples held at temperature for 10 minutes, different CaO/SiO₂ ratios caused different melting behaviors and different levels of slag separation.
 - For pellets with silica rich slags, CaO/SiO₂=0.13, pellet kept its sponge shape for the longest time. The iron sintered skeleton became coarser with FeO reduction. Iron and slag did not separate due to high wettability and high viscosity of silica rich slag.
 - The dense hollow iron shell was formed in samples with more basic slags, (CaO/SiO₂=1.42). High wettability of sintered reduced iron with slag, lowered viscosity of slag, also high rate

of FeO reduction in slag are the reasons behind the densification of iron shell in these samples.

- The average remaining FeO in slags with ($\text{CaO}/\text{SiO}_2 \geq 0.55$) was seen to be less than 2% which would give excellent recovery of iron.
7. The clean separation of iron from slag in more basic slags, ($\text{CaO}/\text{SiO}_2 \geq 0.55$), takes place by increase in iron and slag interfacial tension when FeO is reduced.
 8. Higher slag content did not change the overall melting and phase separation behavior but could retard them.

5.3. Recommendations for future work

1. Use of a tube furnace with controlled atmosphere (reducing and inert), cooling zone, and flexibility to change heating rate, and in situ pellet temperature measurement and analysis of the exit gas is strongly recommended.
2. More DTA tests, quenching from different temperatures and EDX analysis of the slag in quenched pellets.
3. In the experiments for studying melting behavior of coal ore composites , the effect of following parameters be investigated:
 - Other CaO/SiO₂ ratios
 - Slag components other than (SiO₂ and CaO)
 - Addition of pre-melted slag instead of powder oxides
 - Coal/Ore ratios
 - Particle size distribution of raw materials (carbon , ore , gangue minerals)
 - Pellet size
 - Effect of crucible type and substrates
 - Effect of heating rate
 - Effects of layered charges
 - Effect of different slags on sulfur and phosphorous removal
 - Atmosphere (comparing results in reducing and inert atmosphere)
4. Other thermal analysis methods such as Dilatometry
5. In situ observations of the reactions and physical changes during reduction and melting by use of more advanced techniques such as confocal laser microscopy and X-ray video cameras.

6. References

- [1]-Robert Klawonn, *Direct form Midrex 2nd quarter*, (2002):2
- [2]-Isao Kobayashi, Yasuhiro Tanigaki, Akira Uragami, *www.Midrex.com*
- [3]-Honggyu Gou, W-K.Lu, *ISIJ International*, Vol.32, No.6, (1992): 733
- [4]-W-K.Lu,D.F.Haung, *ISIJ International*, Vol.33, No.10,(1993):1055-1061
- [5]-S.Sun,W-K.Lu, *ISIJ International*,Vol.33, No.10,(1993):1062
- [6]-S.Sun,W-K.Lu, *ISIJ International*, Vol.39, No.2,(1999):123-129
- [7]-S.Sun,W-K.Lu, *ISIJ International*,Vol.39, No.2 ,(1999):130-138
- [8]-W-K.Lu,D.F.Haung , *ISIJ International*, Vol. 41, No.8,(2001):807
- [9]-Wakelin,D., *Making shaping and Treating of steel* ,11th ed, Pittsburgh, Pa., The AISE Steel Foundation,(1999)
- [10]-*Ironmaking Processes Alternatives Screening Study*, Vol.2, Department of Energy, US, Lockwood Greene, Aug 2000
- [11]- Kuwata, Yasuo, *Direct from Midrex4th quarter*, (1998):3
- [12]-<http://www.midrex.com>
- [13]-W-K.Lu,http://www.steel.org/mt/projects/hearth_furnace/desc.htm
- [14]-R.J.Dry, R.J.Batterham, *ATSE Focus*, No.123, 2002
- [15]-Osamu, T. et al, *Direct from Midrex , 2nd quarter*,(2002): 8
- [16]- Negami, Takuya ,*Direct from midrex , 1st quarter*, (2001): 7
- [17]-Tanigaki,Kobayashi, *Kobelco technology review* ,No.23,(Apr.2000):3
- [18]-Tsuge, Osamu; Kikuchi, Shoichi, *61th Ironmaking Conference Proceedings*, Nashville, TN, United states, Iron and Steel Society, (Mar10, 2002): 511
- [19]-Matsumura,T.,Takenaka,Y.,Shimizu,M.,*La Revue de Metallurgie*,(1998):341
- [20]- S.Meissner, *Ironmaking and Steelmaking*, Vol.30, No.2, (2003):170
- [21]-Randall M.German, *liquid phase sintering*, New York, Plenum press, (1985)

- [22]-Randall M.German, *Sintering Theory and Practice*, New York, Willey-Inter Science Publication,(1996)
- [23]-W.Kehl, H.F. Fischmeister, *Powder Metallurgy*, No.3, (1980):113
- [24]-HyO-Hoon Park, *Metallurgical Transactions A*, Vol.15A, (1984):1075
- [25]-Murakami,T., Fukuyama,H. *ISIJ International*,Vol.41,(2001) :416
- [26]-Taichi Murakami, Kazuhiro Nagata, *Mineral Processing & Extractive Metallurgical Review*, Vol.24, (2003):253
- [27]-Sasaki,Y.,Asano,R., *ISIJ International*,Vol.41,(2001): 209
- [28]-Asano,R.,Sasaki,Y.and Ishii,K., *ISIJ International*, Vol.42,(2002):121
- [29]-Ko-ichiro Ohno, *Steel Research*, Vol.74, No.1, (Jan2003):5
- [30]-Ko-ichiro Ohno,*Yazawa International Symposium*,San Diego,California, ,Vol.1,(2003):815
- [31]-Th.Courtney, *Metallurgical Transactions A*, Vol.15A, (1984):1065
- [32]-PennyK.Iwamasa, *ISIJ International*, Vol.36, No.11 (1996):319
- [33]-Itaro Jimbo, A.W.Cramb. *ISIJ International*, Vol.32, No.1, (1992): 26-35
- [34]-V.F.Chevrier, A.W.Cramb, *Metallurgical and Materials Transactions B*, Vol.31B, (2000):537
- [35]-C.Dumay and A.W.Cramb, *Metallurgical and Materials Transactions B*, Vol.261B, (1995):174
- [36]-Kunihiko Nakashima, Katsumi Mori, *ISIJ International*, Vol.32,No.1,(1992):11
- [37]-L.A.Girifalco, R.J.Good, *Journal of Physical Chemistry*, Vol.61, (1957):904
- [38]-Y.Chung ,A.W.Cramb, *Metallurgical And Materials Transactions B* ,Vol. 31b,(Oct 2000):957
- [39]-Verein Deutscher, *Slag Atlas*, Dusseldorf,Verlag Stahleisen GmbH,1995
- [40]-Kobayashi et al, *United States patent*, Patent No. 6630010, (Oct7, 2003)

7. Appendix

Table 7- 1-Experimental conditions, final weights in primary series of experiments

No.	Coal type	Temp. (C)	Time (min)	Initial Weight (g)	Bulk Density (g/cm ³)	%fixed carbon in coal	%ash in coal	% Coal/Ore	final weight(g)
1	A	1300	5	1	2.5	73.9	6.7	27.2	0.6
2	A	1300	5	1	2.5	73.9	6.7	21.76	0.61
3	B	1300	5	1	2.5	67.15	9.03	30	0.58
4	B	1300	5	1	2.5	67.15	9.03	24.01	0.6
5	C	1300	5	1	2.5	57.15	7.8	35.1	0.56
6	C	1300	5	1	2.5	57.15	7.8	28.07	0.57
7	A	1300	10	1	2.5	73.9	6.7	27.2	0.58
8	A	1300	10	1	2.5	73.9	6.7	21.76	0.57
9	B	1300	10	1	2.5	67.15	9.03	30	0.58
10	B	1300	10	1	2.5	67.15	9.03	24.01	0.55
11	C	1300	10	1	2.5	57.15	7.8	35.1	0.55
12	C	1300	10	1	2.5	57.15	7.8	28.07	0.49
13	A	1300	15	1	2.5	73.9	6.7	27.2	0.56
14	A	1300	15	1	2.5	73.9	6.7	21.76	0.56
15	B	1300	15	1	2.5	67.15	9.03	30	0.59
16	B	1300	15	1	2.5	67.15	9.03	24.01	0.54
17	C	1300	15	1	2.5	57.15	7.8	35.1	0.54
18	C	1300	15	1	2.5	57.15	7.8	28.07	0.53
19	A	1325	5	1	2.5	73.9	6.7	27.2	0.6
20	A	1325	5	1	2.5	73.9	6.7	21.76	0.49
21	B	1325	5	1	2.5	67.15	9.03	30	0.59
22	B	1325	5	1	2.5	67.15	9.03	24.01	0.56
23	C	1325	5	1	2.5	57.15	7.8	35.1	0.53
24	C	1325	5	1	2.5	57.15	7.8	28.07	0.48
25	A	1325	10	1	2.5	73.9	6.7	27.2	0.56
26	A	1325	10	1	2.5	73.9	6.7	21.76	0.55
27	B	1325	10	1	2.5	67.15	9.03	30	0.57
28	B	1325	10	1	2.5	67.15	9.03	24.01	0.55
29	C	1325	10	1	2.5	57.15	7.8	35.1	0.54
30	C	1325	10	1	2.5	57.15	7.8	28.07	0.57
31	A	1325	15	1	2.5	73.9	6.7	27.2	0.56
32	A	1325	15	1	2.5	73.9	6.7	21.76	0.53
33	B	1325	15	1	2.5	67.15	9.03	30	0.53
34	B	1325	15	1	2.5	67.15	9.03	24.01	0.55
35	C	1325	15	1	2.5	57.15	7.8	35.1	0.56
36	C	1325	15	1	2.5	57.15	7.8	28.07	0.53
37	A	1350	5	1	2.5	73.9	6.7	27.2	0.54

38	A	1350	5	1	2.5	73.9	6.7	21.76	0.46
39	B	1350	5	1	2.5	67.15	9.03	30	0.58
40	B	1350	5	1	2.5	67.15	9.03	24.01	0.54
41	C	1350	5	1	2.5	57.15	7.8	35.1	0.54
42	C	1350	5	1	2.5	57.15	7.8	28.07	0.54
43	A	1350	10	1	2.5	73.9	6.7	27.2	0.56
44	A	1350	10	1	2.5	73.9	6.7	21.76	0.48
45	B	1350	10	1	2.5	67.15	9.03	30	0.56
46	B	1350	10	1	2.5	67.15	9.03	24.01	0.56
47	C	1350	10	1	2.5	57.15	7.8	35.1	0.54
48	C	1350	10	1	2.5	57.15	7.8	28.07	0.54
49	A	1350	15	1	2.5	73.9	6.7	27.2	0.59
50	A	1350	15	1	2.5	73.9	6.7	21.76	0.53
51	B	1350	15	1	2.5	67.15	9.03	30	0.55
52	B	1350	15	1	2.5	67.15	9.03	24.01	0.55
53	C	1350	15	1	2.5	57.15	7.8	35.1	0.54
54	C	1350	15	1	2.5	57.15	7.8	28.07	0.47

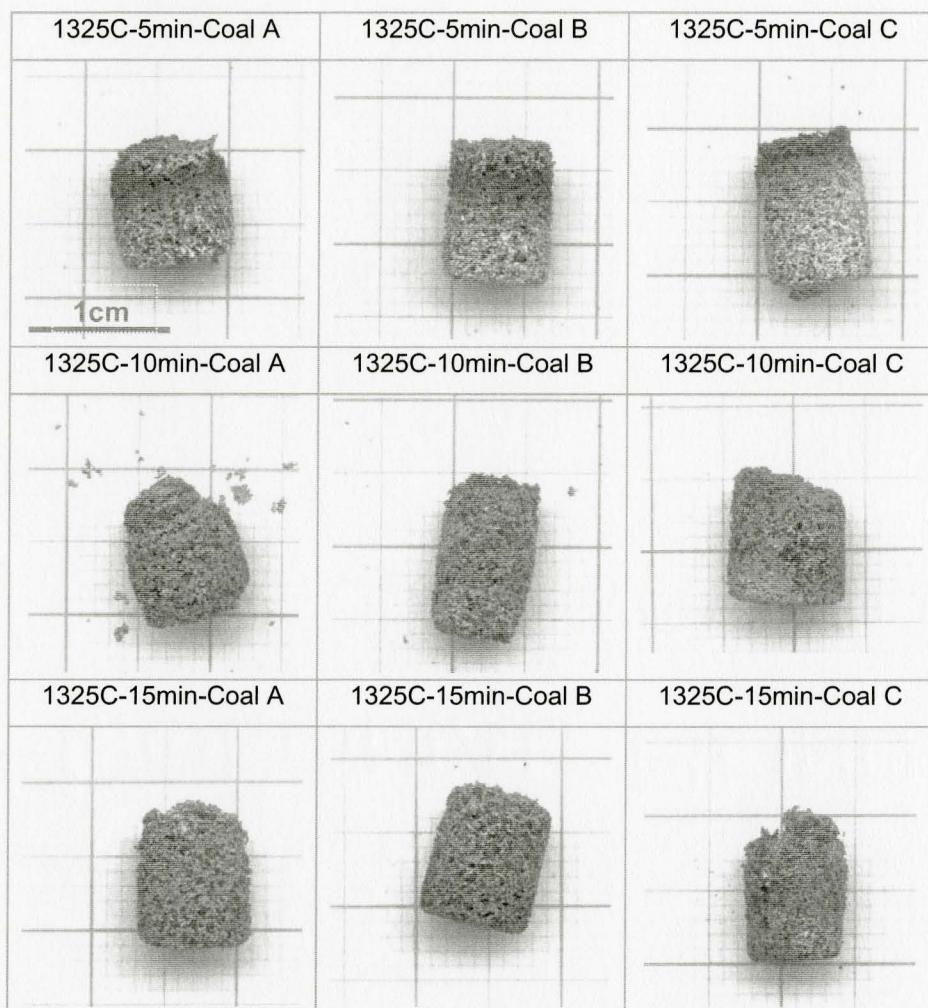


Figure 7- 1- Scanned images, samples with sub-stoichiometric coal at 1325C

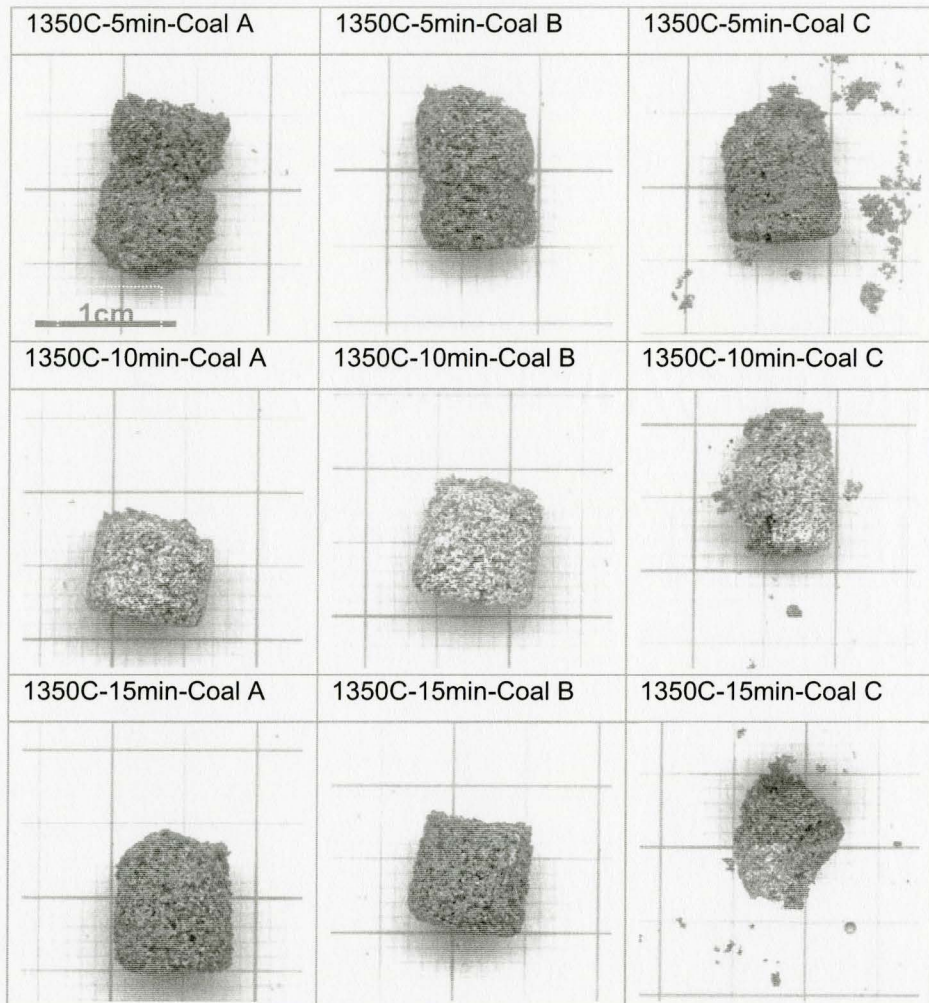


Figure 7- 2- Scanned images, samples with sub-stoichiometric coal at 1350C

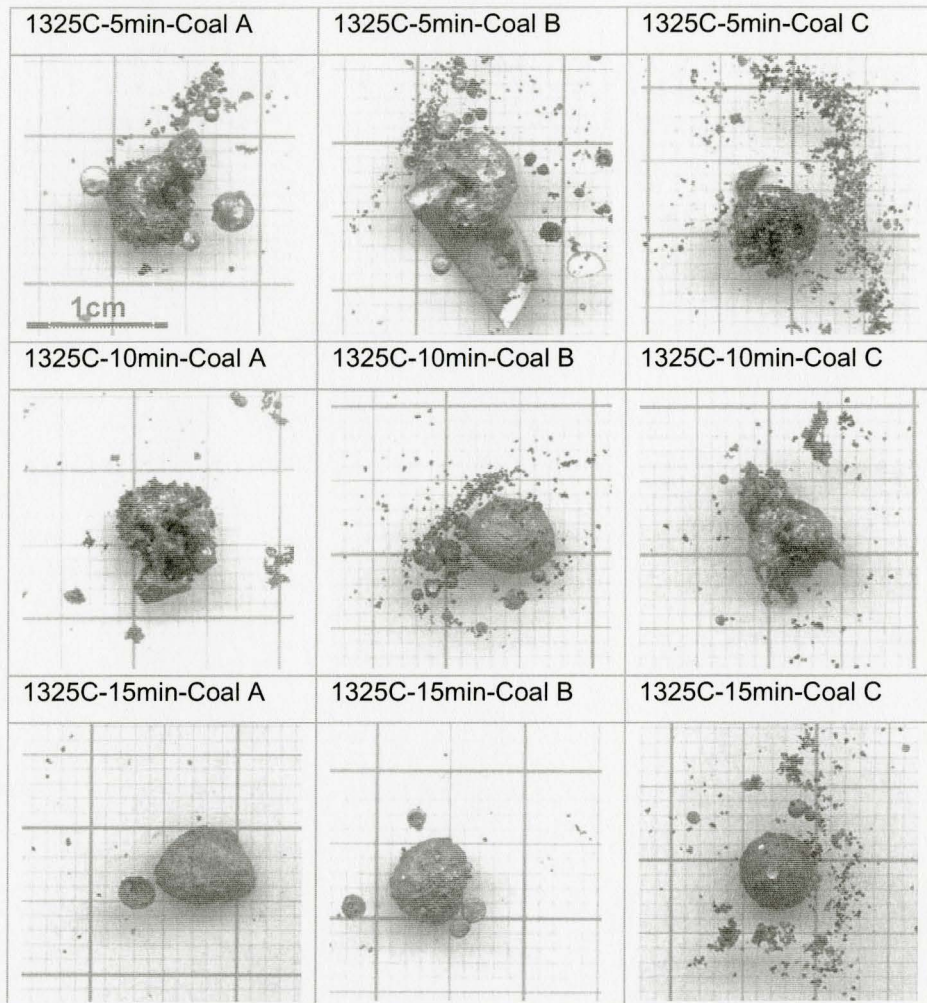


Figure 7- 3- Scanned images, samples with stoichiometric coal at 1325C

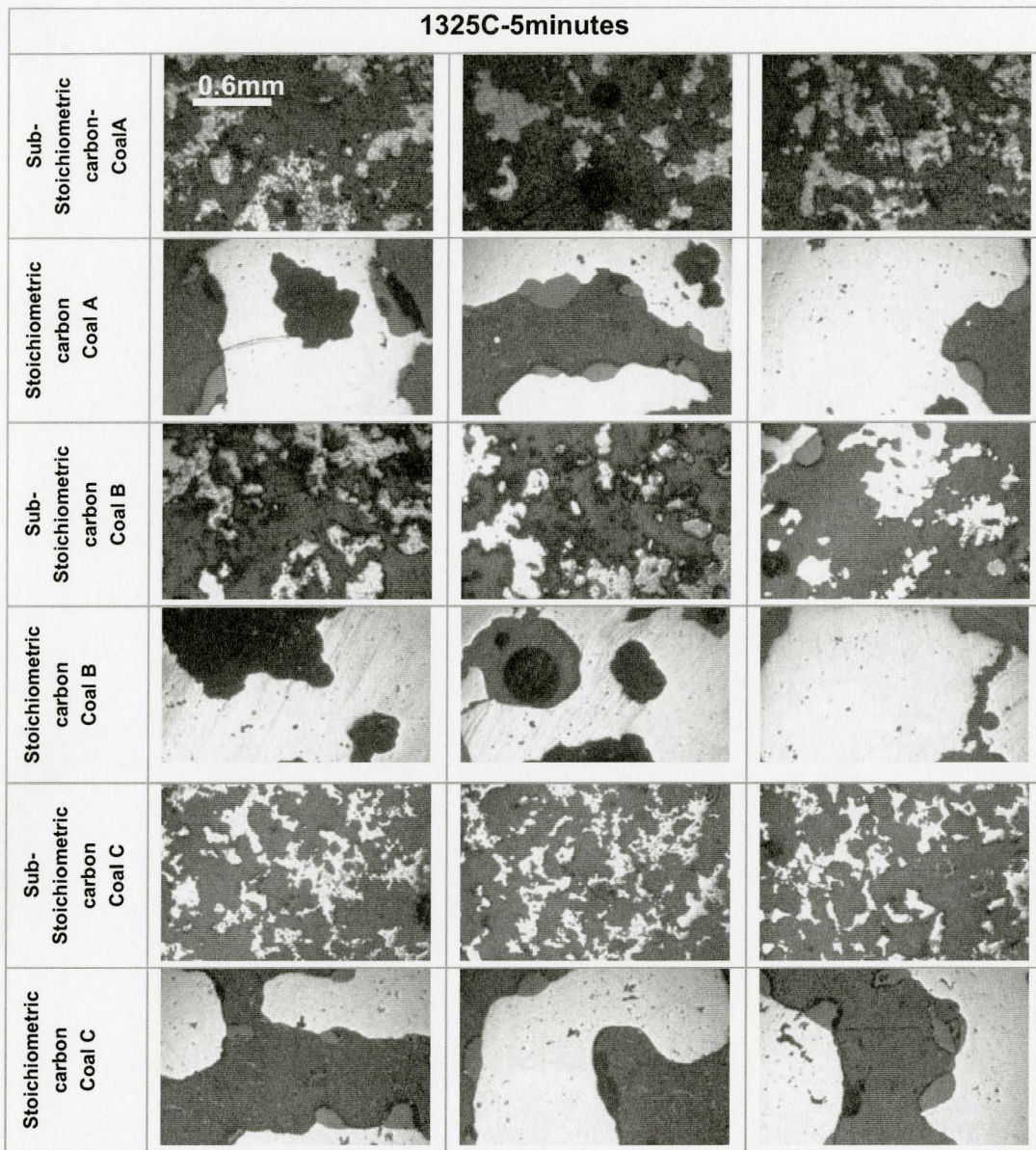


Figure 7- 4- Samples reacted at 1325C for 5 min

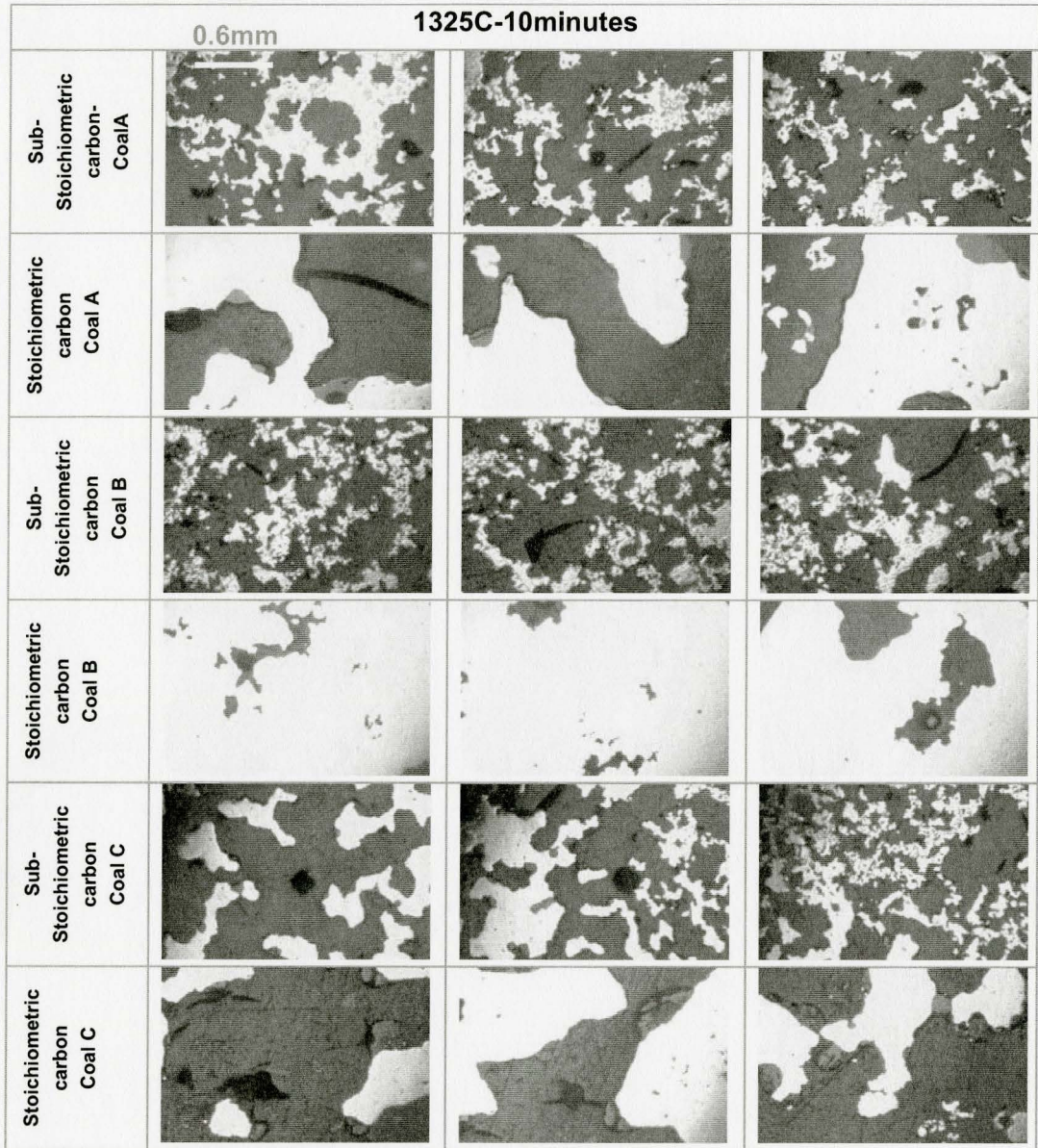


Figure 7- 5- Samples reacted at 1325C for 10 min

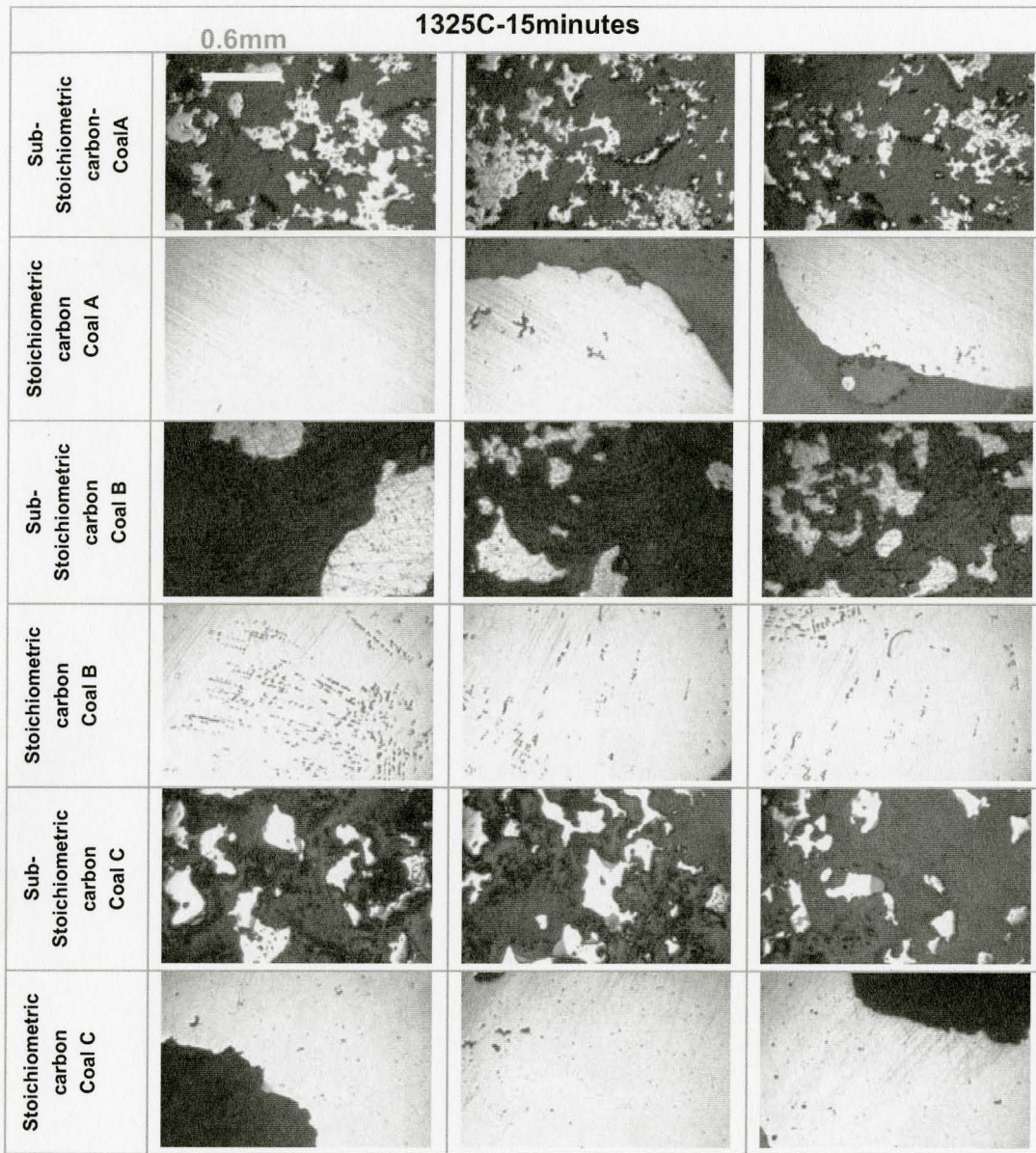


Figure 7- 6- Samples reacted at 1325C for 15 min

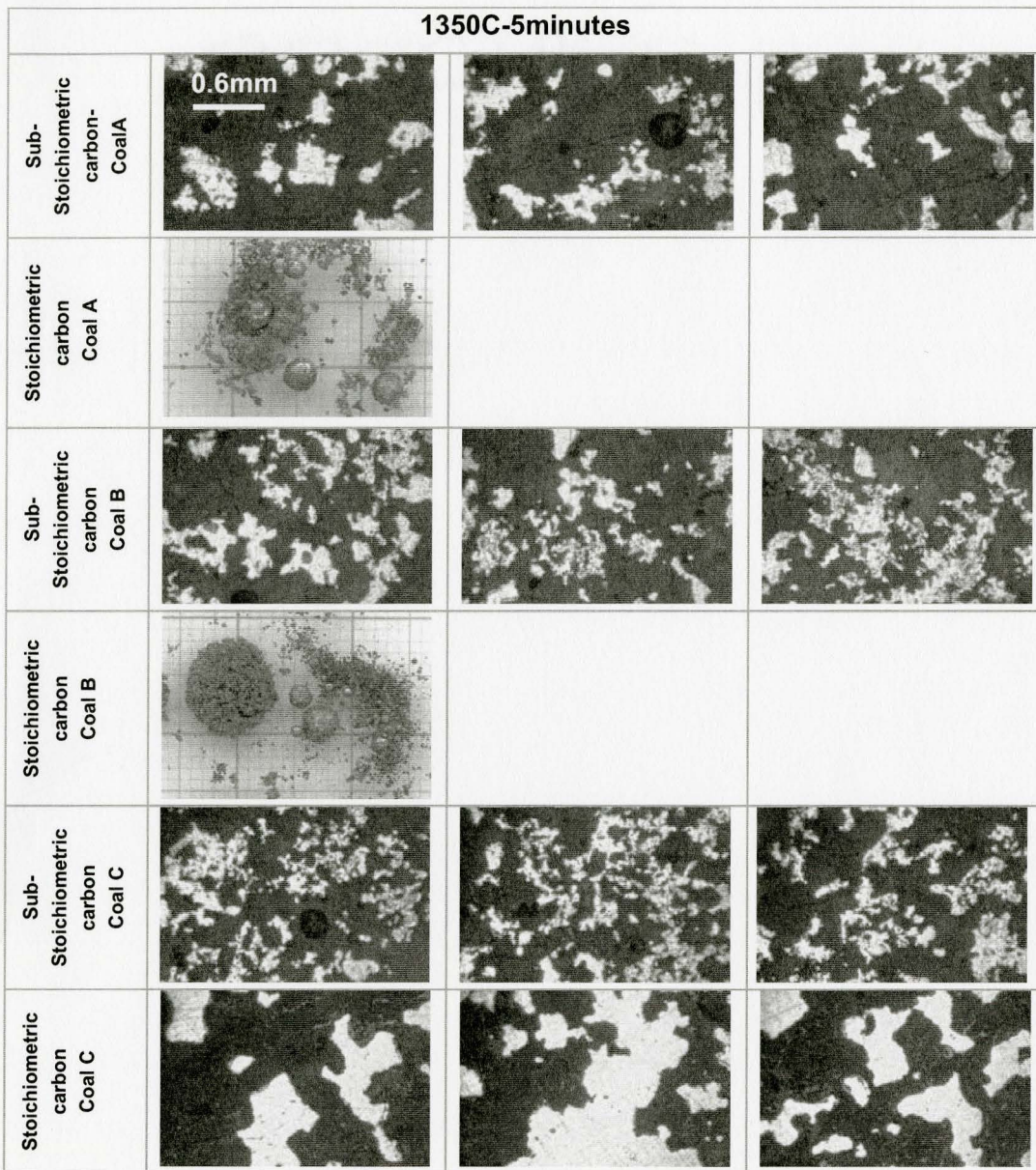


Figure 7- 7- Samples reacted at 1350C for 5 min

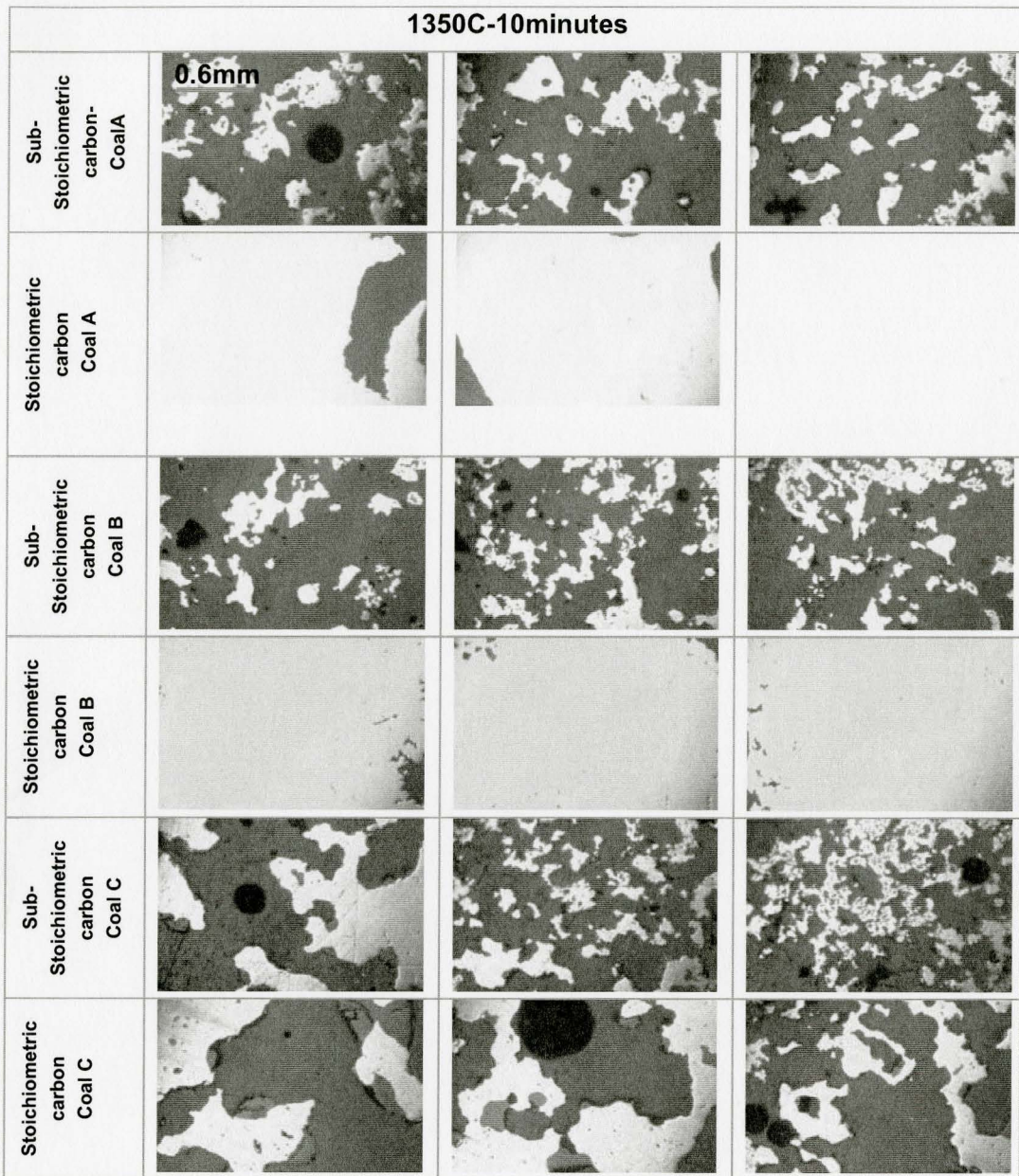


Figure 7- 8- Samples reacted at 1350C for 10 min

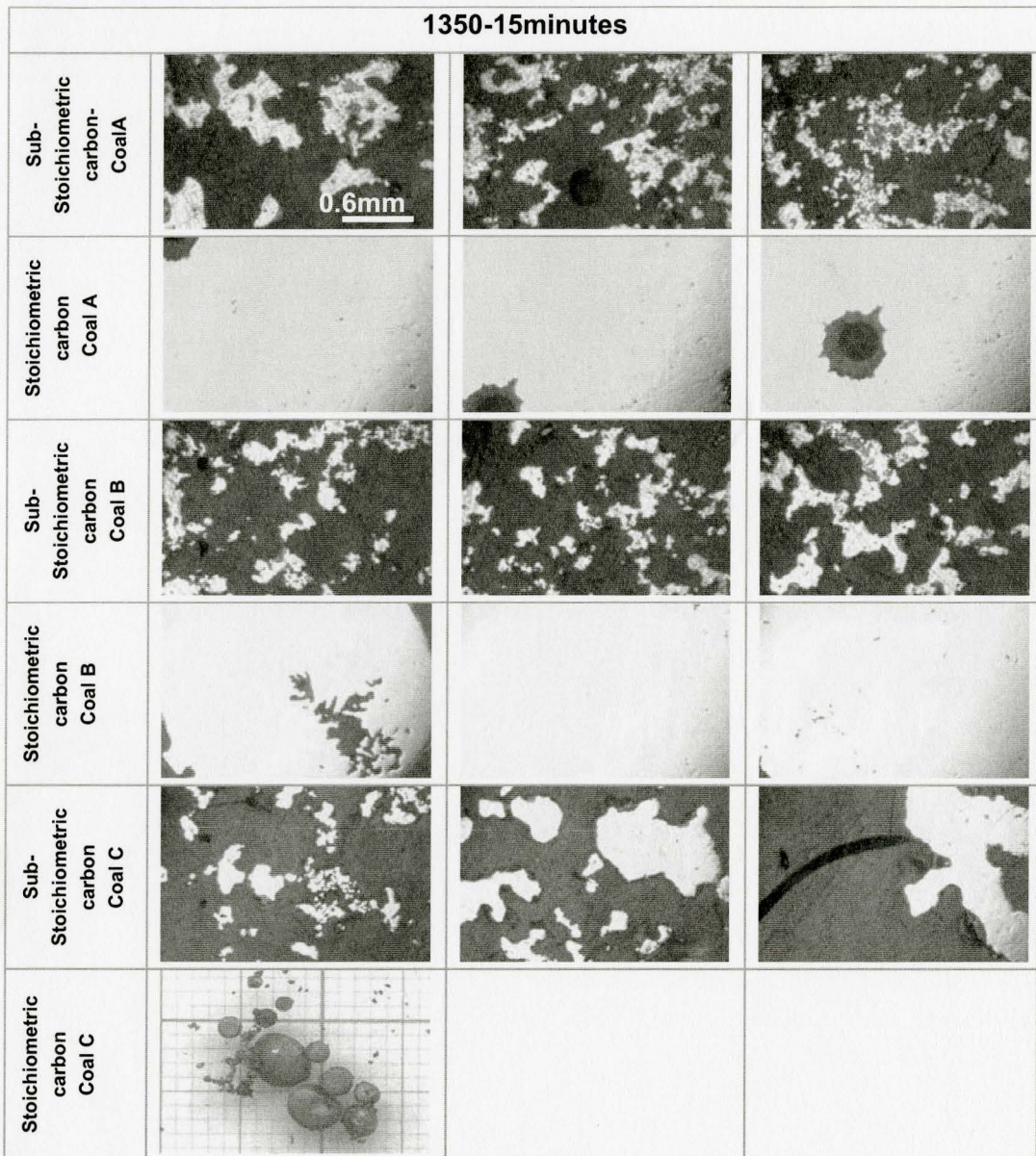


Figure 7- 9- Samples reacted at 1350C for 15 min

Table 7- 2- Experimental conditions, final weights, second series of experiments

No.	Coal type	%Coal/ (coal .ore)	Wt%slag	CaO/SiO2 in slag	Temp.(C)	Time(min)	Bulk Density (g/cm3)	Initial weight(g)	Final weight(g)
1	A	21.4	5	0.13	1310	8	3.8	1	0.64
2	A	21.4	5	0.13	1310	8	3.8	1	0.63
3	A	21.4	5	0.13	1310	8	3.8	1	0.62
4	A	21.4	10	0.55	1310	8	3.8	1	0.69
5	A	21.4	10	0.55	1310	8	3.8	1	0.67
6	A	21.4	10	0.55	1310	8	3.8	1	0.67
7	A	21.4	15	1.42	1310	8	3.8	1	0.76
8	A	21.4	15	1.42	1310	8	3.8	1	0.72
9	A	21.4	15	1.42	1310	8	3.8	1	0.73
10	A	21.4	3.17	0.26	1310	8	3.8	1	0.65
1	A	21.4	5	0.13	1310	10	3.8	1	0.63
2	A	21.4	5	0.13	1310	10	3.8	1	0.63
3	A	21.4	5	0.13	1310	10	3.8	1	0.64
4	A	21.4	10	0.55	1310	10	3.8	1	0.68
5	A	21.4	10	0.55	1310	10	3.8	1	0.67
6	A	21.4	10	0.55	1310	10	3.8	1	0.67
7	A	21.4	15	1.42	1310	10	3.8	1	0.73
8	A	21.4	15	1.42	1310	10	3.8	1	0.72
9	A	21.4	15	1.42	1310	10	3.8	1	0.73
10	A	21.4	3.17	0.26	1310	10	3.8	1	0.63